Unified charge transport in disordered organic field-effect transistors and light-emitting diodes

Cristina Tanase

Unified charge transport in disordered organic
field-effect transistors and light-emitting diodes

Cristina Tanase
Ph.D. thesis
University of Groningen, The Netherlands

MSC Ph.D. thesis series 2005-06
ISSN 1570-1530

The work described in this thesis has been carried out at the Materials Science Center in Groningen, and is part of the research programme of the Dutch Polymer Institute (DPI), Technology Area - Functional Polymer Systems, project ♯276.

Printed by: Optima Grafiche Communicatie, Rotterdam

Rijks*universiteit* Groningen

Unified charge transport in disordered organic field-effect transistors and light-emitting diodes

Proefschrift

ter verkrijging van het doctoraat in de
Wiskunde en Natuurwetenschappen
aan de Rijks*universiteit* Groningen
op gezag van de
Rector Magnificus, dr. F. Zwarts,
in het openbaar te verdedigen op
vrijdag 27 mei 2005
om 13.15 uur

door

Cristina Tanase

geboren op 16 april 1975
te Bacau, Roemenië

Promotor:	Prof. dr. ir. P. W. M. Blom
Copromotor:	Dr. D. M. de Leeuw
Beoordelingscommissie:	Prof. dr. R. H. Friend
	Prof. dr. J. W. H. Hofstraat
	Prof. dr. T. T. M. Palstra

ISBN: 90-8559-055-8

Contents

Chapter 1

Introduction

Summary

Since the 1990's, after field-effects and electroluminescence were discovered in conjugated polymers, substantial effort has been devoted to the use of these materials in electronic devices. In this chapter we present a brief overview regarding the field of conjugated polymers and describe the operation principles of two (opto)electronic devices comprising semiconducting polymer films as the active component, namely light-emitting diodes and field-effect transistors. Finally, a short outline of the thesis is given.

1.1 Organic semiconductors

Electrical conduction in organic materials has been reported for the first time in the 1950's and early 1960's, when photoconductivity and electroluminescence were detected in organic crystals, such as naphthalene and anthracene [1–4]. Although the crystals showed high charge carrier mobility, their processability was very poor with little potential for applications. In the mid-1960's molecularly doped polymers formed by small organic pigments dispersed in an insulating polymer matrix were developed for xerographic applications [5]. They possessed the semiconducting properties of small organic molecules and the mechanical properties of polymers. A breakthrough in the field of conducting polymers was made in 1977, when the first highly conductive polymer, chemically doped polyacetylene, was reported [6]. In the 1980's electroluminescence was reported from double layer vacuum-sublimed molecular thin film devices [7], and from conjugated polymers such as poly(*p*-phenylene vinylene) (PPV) [8]. Since then, a new perspective has been opened on the applicability of organic molecules and semiconducting polymers into (opto)electronic devices.

Beside the research in the field of polymer light-emitting diodes (LEDs), several other research fields based on polymer semiconductors have been developed in the past decade, such as field-effect transistors (FETs) [9–11] and photovoltaics [12–14]. The polymers used in these applications are processed from solution, using spin coating, film casting or inkjet printing techniques, being able to provide large-area, flexible, lightweight displays and integrated circuits. Their low cost production, resulting mainly from the ease of processing, make them interesting for the electronic industry. But in order to be competitive, organic displays must provide comparable device performance with the already existing inorganic ones. These organic displays combine the mechanical properties of solution-processable organic materials with the electrical properties of semiconductors. Nowadays, the synthesis of new solution-processable polymers has shown that different color emission, high mobility and increased efficiency can be achieved in (opto)electronic devices. Some commercial application based on semiconducting polymers have already become available, such as a Philips shaver (2002) and a Philips mobile phone (2004), both featuring a polymer LED display.

In this thesis we focus on the charge transport through undoped (unintentionally doped) conjugated polymers that are used as active materials in LEDs and FETs. Conjugated polymers are organic macromolecules which have a framework of alternating single and double carbon-carbon bonds. Single bonds are referred to as σ-bonds and are associated with a highly localized electron density in the plane of the molecule, and double bonds contain a σ-bond and a π-bond, where the π-bond is the overlap between p_z orbitals of neighboring atoms along the conjugation path. The conjugation of single and double bonds establishes a delocalization of the electrons situated above and below the plane of the molecule. π-bands are either empty (called the Lowest Unoccupied Molecular Orbital - LUMO) or filled with electrons (called the Highest Occupied Molecular Orbital - HOMO). The band gap of these materials determined from optical measurements is within the semiconductor range of 1–4 eV, which covers the whole range from infrared to ultraviolet region. A well-known ex-

ample of a conjugated polymer is polyacetylene, which consists only of a single chain of alternating single- and double-bonds (Figure 1.1). The polyacetylene has a degenerated ground state. But most of the molecules studied throughout this thesis do not have this ground state. In Figure 1.2 some examples of the most commonly used conjugated polymers are presented.

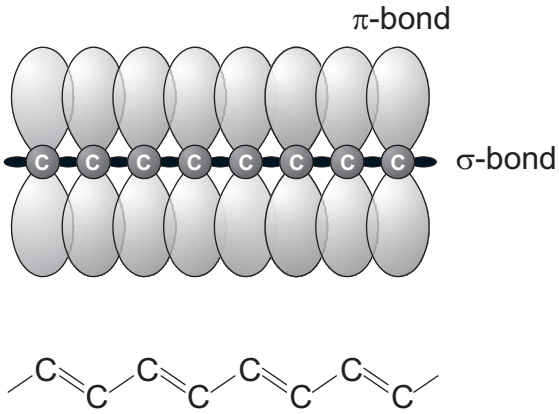

Figure 1.1: Schematic representation of the electronic bonds between carbon atoms (above) in polyacetylene (below).

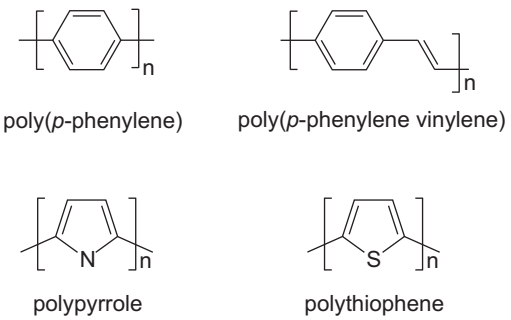

Figure 1.2: Chemical structure of some commonly used conjugated polymers. Hydrogen atoms are not shown and can be replaced by different sidegroups.

1.2 Polymer light-emitting diodes

Since the discovery of electroluminescence in poly(*p*-phenylene vinylene) (PPV) in 1990 [8] extensive research has been carried out to understand and develop polymer light-emitting diodes (LEDs). A typical single-layer polymer LED is presented in Figure 1.3a. A thin polymer film is spin-coated from solution on a semitransparent bottom electrode, normally indium-tin-oxide (ITO), which forms the anode. A low

work-function metal (calcium or barium) is evaporated on top of the polymer and serves as cathode.

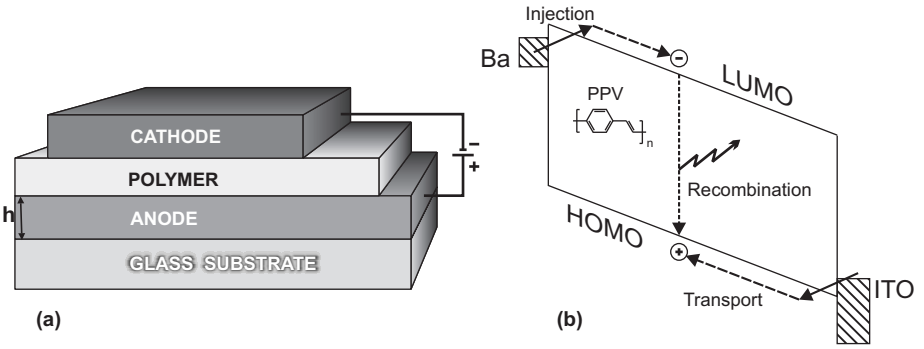

Figure 1.3: Schematic representation of a polymer LED (a) and energy-band diagram of a PPV-based LED (b).

The main processes that govern the operation of the polymer LED are: charge injection, charge transport and recombination (Figure 1.3b) [15]. Under forward bias, holes and electrons are injected from the anode and cathode, respectively. The charge carriers move through the polymer film and recombine. The energy released upon recombination is emitted as a photon through the semitransparent electrode. The emitted light can be tuned from red to blue, depending on the band gap of the polymer. In order to be injected from the electrodes, the charges must surmount or tunnel through a barrier at the polymer/electrode interface, which is determined by the position of the highest occupied molecular orbital (HOMO or π orbital) and the lowest unoccupied molecular orbital (LUMO or π^* orbital) and the position of the electrode metal work-functions. In the case of PPV, which has the HOMO level at 5.2 eV and the LUMO level at 2.9 eV, a good choice for the hole injecting electrode is ITO due to its work-function of ≈ 5 eV, resulting in a small injection barrier for holes [16]. In order to have a small interface energy barrier for electrons, low work-function metals such as calcium (Ca) or barium (Ba) ($\phi_M \approx 3$ eV) must be used in the case of PPV. A schematic band diagram of a PPV-based LED under forward bias using ITO as a hole injector and Ba as an electron injector is shown in Figure 1.3b. In this case the injection does not limit the device performance. However, the control of the anode/polymer and polymer/cathode interfaces is important, since it controls the charge injection process. A consequence is that it may influence the electronic structure and luminescence properties of the polymers [17,18]. The chemistry involved at these interfaces is always related to the nature of the polymer and the metal in question, the cleanliness of the materials and the evaporation process [19]. Despite these chemical interactions between the polymer and the metal, measurements of the built-in electrical field showed that the electrode-polymer interfaces still scale with the work-functions of the electrodes [20].

Besides injection, the charge transport in disordered organic semiconductors has been studied extensively. From current-voltage measurements, it has been demon-

strated that the current flow in the LED is limited by the bulk transport and not by injection for contacts barriers smaller than 0.4 eV [21–23]. Due to relatively low mobility in these disordered semiconductors, the charges build up in the device and space-charge effects occur in polymer LEDs. To achieve high efficiency, a balanced electron and hole transport is required. In that case, the recombination of the charges takes place close to the middle of the semiconductor. But when the charge transport is not balanced, the recombination moves toward one of the electrodes, where the luminescence is quenched by the electrode. The origin of this effect is dipole quenching and leads to a reduced efficiency [24].

One way to overcome this problem is to introduce a number of active layers, each optimized for its own functionality [7,25]. For example, in the case of a trilayer diode, the highly emissive layer is sandwiched between a hole- and electron-transporting layers. The hole transporting layer adjacent to the anode must have high mobility for holes, whereas the electron transporting layer adjacent to the cathode must have high mobility for electrons. In this way, the holes and electrons meet each other in the highly emissive layer and the recombination zone can be shifted away from the cathode, where excitons are quenched. As a result, high efficiencies and low operating voltages can be simultaneously achieved. This approach has been successfully applied in small molecule devices [26] and polymer-based devices [27]. Recently, a record efficiency of 110 lm/W was reported for doped small molecules LEDs, which is over 50% higher than for inorganic LEDs [28].

1.3 Polymer field-effect transistors

The concept of the field-effect transistors (FET), first proposed by Lilienfield in 1930 [29] and later studied by Shockley and Pearson in 1948 [30], started to be used as a practical application only in 1960 [31]. The most popular FET is the metal-oxide-semiconductor FET (MOSFET), also known as the metal-insulator-semiconductor FET (MISFET), in which the gate electrode is electrically insulated from the conducting channel by an insulating oxide layer (Figure 1.4). The basic idea of a field-effect transistor is to modulate the current that flows between two ohmic contacts, the source and the drain electrodes, by applying a voltage to a third contact, the gate electrode. In this way charge carriers can be accumulated or depleted in the semiconductor close to the semiconductor/insulator interface. In fact, this device can be considered as a capacitor, where one plate is the conductive channel in the semiconducting layer and the other is the gate electrode.

The operation of an unintentionally doped p-type MISFET can be explained by analyzing the energy band diagram which is schematically presented in Figure 1.5 [32]. In equilibrium the Fermi levels of the gate metal and the semiconductor align due to the charge carriers, which move to or from the semiconductor/insulator interface. When a voltage, called flat-band voltage, V_{fb}, equal to the difference between the Fermi levels of the materials is applied no band bending will be present in the semiconductor at the semiconductor/insulator interface (Figure 1.5a). The charges that are present in the device under biasing conditions are those in the semiconductor and

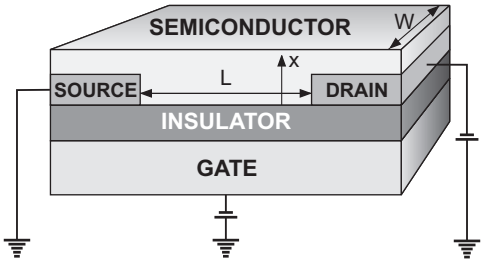

Figure 1.4: Schematic representation of a polymer FET

those with equal opposite sign on the gate. By applying positive or negative gate voltages, induced charge carriers electrostatically accumulate or deplete in the semiconductor close to the semiconductor/insulator interface giving rise to band bending in the semiconductor. If a negative bias is applied to the gate, the voltage drop across the insulator will accumulate holes at the semiconductor/insulator interface and the energy bands are bent upwards (Figure 1.5b). The additional positive charges accumulated in this region are supplied by the drain- and source-ohmic contacts. These charges are mobile and under a small drain bias will give rise to the field-effect current. If a positive voltage is now applied to the gate, the positive charges are depleted from the semiconductor/insulator interface and the energy bands bend downwards. In this case the transistor is biased in the depletion mode (Figure 1.5c). In this way the field-effect current is varied in the source-drain channel.

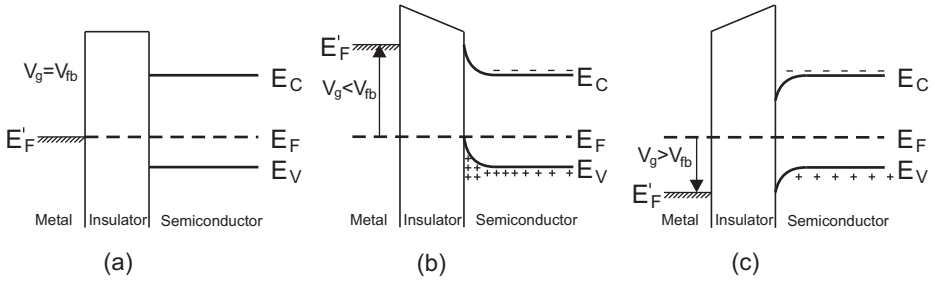

Figure 1.5: Energy-band diagram of a p-type MIS FET working in: a) flat-band ($V_g = V_{fb}$); b) accumulation ($V_g < V_{fb}$); c) depletion ($V_g > V_{fb}$).

1.4 Scope and outline of this thesis

Charge transport in conjugated polymers is regarded as a hopping process between localized states, which are thought to consist of individual conjugated segments. Due to different orientations of the conjugated segments with respect to each other and to

their different lengths, a distribution of localized energy states will be present in the polymer. In this way the charge carrier transport through the semiconductor bulk material is related to the order in the system. Considering the amount of disorder, three classes of organic semiconducting polymers are distinguished: amorphous, crystalline and partially-ordered (or partially crystalline). The scope of this thesis is to study the charge transport in amorphous conjugated polymers in various device configurations. Different transport parameters, such as charge carrier density and charge carrier mobility are analyzed in: field-effect transistors, single and double layer light-emitting diodes, in-plane diodes and ambipolar transistors. In order to relate the transport characteristics to the morphological and energetic disorder present in the polymer films, a number of different polymers are analyzed.

In *Chapter 2*, the relevant charge transport models for disordered organic semiconductors are presented. Then, we present two theoretical models frequently used to analyze the charge transport in polymer based LEDs and FETs: hopping in a Gaussian DOS is applied to explain the field and temperature dependence of the carrier mobility in LEDs, while the hopping in an exponential DOS explains the gate voltage and temperature dependence in FETs. Because the polymers characterized in these devices belong to the same class of disordered π conjugated systems, one unified description should be used to describe their electrical transport characteristics. But this will be discussed in *Chapter 4*.

Chapter 3 describes the polymers used in this thesis, the device preparation and the procedures used to measure the devices.

A fundamental process in the charge transport in disordered polymer FETs and LEDs, the dependence of the charge mobility on the charge density, is addressed in *Chapter 4*. In order to determine the local mobility in FETs, the charge carrier density distribution perpendicular to the semiconductor/insulator interface is calculated. It is shown that a major part of the charge carriers is located close to the interface and they have the highest mobility. In a space charge-limited (SCL) diode based on disordered polymers the enhancement of the hole current at high bias was attributed in the earlier reports to the field dependence of the mobility. We demonstrate that the charge carrier density dependence of the mobility is dominant at room temperature, while at low temperatures the field dependence of the mobility must be considered. Then one polymer is used as active material in a LED and a FET in order to understand why fundamentally different properties such as charge transport and mobility values are reported for these devices. We demonstrate that the strong increase of the mobility with increasing charge density is responsible for the observed large mobility differences obtained from the LEDs and FETs. The exponential density of states, which consistently describes the field-effect transport measurements, is shown to be a good approximation of the tail states of the Gaussian density of states used to describe the LED transport measurements.

To relate the transport characteristics to the morphological and energetic disorder present in the polymer film, in *Chapter 5* the charge transport for different disordered polymers is studied. Optimization of chemical structure, annealing, and solvent lead

to high mobility of 9×10^{-10} m^2/Vs in a hole-only diode and 1×10^{-6} m^2/Vs in a FET. Comparison of the electrical measurements in planar metal-polymer-metal devices with those of field-effect transistors demonstrates that the enhanced current measured in planar devices originates from a high surface charge carrier density at the polymer/substrate interface. The presence of such a conducting channel due to charging of the surface obscures the intrinsic in-plane conducting properties of PPV.

In *Chapter 6* the electrical properties of a dual-layer PPV LED are discussed. We combine two PPV layers, one with high mobility and the other with high luminescence. As a result, high light output efficiencies and low operating voltages are simultaneously achieved with relatively thick active layers. Another advantage of this dual-layer LED is that both polymers emit light. This means that a short-circuit in the luminescent layer does not lead to a catastrophic failure of the diode.

PCBM is a soluble C_{60} derivative which is used as electron acceptor in bulk heterojunction solar-cells. Recently, PCBM started to be used as active organic material in FETs. In *Chapter 7* it is demonstrated that a methanofullerene based FET exhibits ambipolar transport characteristics. The devices operate in hole or electron accumulation, depending on the biasing conditions. The characteristics of PCBM ambipolar FETs are also analyzed in CMOS-like inverters.

Bibliography

[1] H. Mette, *Z. Physik* **134**, 566 (1953).

[2] R. G. Kepler, *Phys. Rev.* **119**, 1226 (1960).

[3] O. H. Le Blanc, *J. Chem. Phys.* **33**, 626 (1960).

[4] M. Pope, H. P. Kallmann, P. Magnante, *J. Chem. Phys.* **38**, 2042 (1963).

[5] H. Hoegl, *J. Phys. Chem.* **69**, 755 (1965).

[6] C. K. Chiang, C. R. Fincher Jr., Y. W. Park, A. J. Heeger, H. Shirakawa, E. J. Louis, S. C. Gau, A. G. MacDiarmid, *Phys. Rev. Lett.* **39**, 1098 (1977).

[7] C. W. Tang, S. A. Van Sylke, *Appl. Phys. Lett.* **51**, 913 (1987).

[8] J. H. Burroughes, D. D. C. Bradley, A. R. Brown, R. N. Marks, K. Mackay, R. H. Friend, P. L. Burns, A. B. Holmes, *Nature* **347**, 539 (1990).

[9] H. Koezuka, A. Tsumura, Y. Ando, *Synth. Met.* **18**, 699 (1987).

[10] A. R. Brown, A. Pomp, C. M. Hart, D. M. de Leeuw, *Science* **270**, 972 (1995).

[11] H. Sirringhaus, P. J. Brown, R. H. Friend, M. M. Nielsen, K. Bechgaard, B. M. W. Langeveld-Voss, A. J. H. Spiering, R. A. J. Janssen, E. W. Meijer, P. Herwig, D. M. de Leeuw, *Nature* **401**, 685 (1999).

[12] G. Yu, K. Pakbaz, A. J. Heeger, *Appl. Phys. Lett.* **64**, 3422 (1994).

[13] S. E. Shaheen, C. J. Brabec, N. S. Sariciftci, F. Padinger, T. Fromherz, J. C. Hummelen, *Appl. Phys. Lett.* **78**, 841 (2001).

[14] P. Schilinsky, C. Waldauf, C. J. Brabec, *Appl. Phys. Lett.* **81**, 3885 (2002).

[15] D.D.C. Bradley, A. R. Brown, P. L. Burn, R. H. Friend, A. B. Holmes, A. Kraft, *Solid State Science* **107**, Springer, Heidelberg, 304 (1992).

[16] A. R. Brown, D.D.C. Bradley, J. H. Burroughes, R. H. Friend, N. C. Greenham, P. L. Burn, A. B. Holmes, and A. Kraft, *Appl. Phys. Lett.* **61**, 2793 (1992).

[17] W. R. Salaneck, S. Stafström, J. L. Brédas, *Conjugated polymer surfaces and interfaces*, Cambridge Univ. Press (1996).

[18] N. Johansson, F. Cacialli, K. Z. Xing, G. Beamson, D. T. Clark, R. H. Friend, W. R. Salaneck, *Synth. Met.* **92**, 207 (1998).

[19] R. H. Friend, R. W. Gymer, A. B. Holmes, J. H. Burroughes, R. N. Marks, C. Taliani, D. C. C. Bradley, D. A. Dos Santos, J. L. Brédas, M. Lögdlund, W. R. Salaneck, *Nature* **397**, 121 (1999).

[20] I. H. Campbell, T. W. Hagler, and D. L. Smith, J. P. Ferraris, *Phys. Rev. Lett.* **76**, 1900 (1996).

[21] P. W. M. Blom, M. J. M. de Jong, J. J. M. Vleggaar, *Appl. Phys. Lett.* **68**, 3308 (1996).

[22] G. G. Malliaras, J. C. Scott, *J. Appl. Phys.* **85**, 7426 (1999).

[23] I. H. Campbell, P. S. Davids, D. L. Smith, N. N. Barashkov, J. P. Ferraris, *Appl. Phys. Lett.* **72**, 1863 (1998).

[24] P. W. M. Blom, M. C. J. M. Vissenberg, *Mat. Sc. and Engineering* **27**, 53 (2000).

[25] S. A. Jenekhe, J. A. Osaheni, *Science* **265**, 765 (1994).

[26] B. W. D'Andrade, M. A. Baldo, C. Adachi, J. Brooks, M. E. Thompson, and S. R. Forrest, *Appl. Phys. Lett.* **79**, 1045 (2001).

[27] R. H. Friend, *Pure Appl. Chem.* **73**, 425 (2001).

[28] NOVALED Press Release *A new OLED world record set in Dresden*, 16 February 2005.

[29] J. E. Lilienfield, U. S. Patent 1745175 (1930).

[30] W. Shockley, G. L. Pearson, *Phys. Rev.* **74**, 232 (1948).

[31] D. Kahn, M. M. Atalla, *IRE Solid-State Device Research Conference*, Carnegie Institute of Technology, Pittsburgh (1960).

[32] S. M. Sze, *Physics of semiconductor devices*, 2^{nd} Ed., John Wiley & Sons, New York (1981).

Chapter 2

Charge transport models for disordered organic systems

Summary

The charge carrier mobility in organic optoelectronic devices remains by far lower than that of conventional inorganic devices.[1] This must be ascribed to the specific charge transport mechanism present in organic materials. We present two theoretical models which are frequently used to analyze the charge transport in polymer based LEDs and FETs: the hopping in a Gaussian DOS is applied to explain the field and temperature dependence of the carrier mobility in LEDs, while the hopping in an exponential DOS explains the gate voltage and temperature dependence in FETs. In fact, because the polymers characterized in these devices belong to the same class of disordered π conjugated systems, one unified description should be used to describe their electrical transport characteristics.

[1] However, as argued in *Chapter 1* organic semiconductors possess a number of characteristics which make it worthwhile to study them.

2.1 Introduction

An ideal crystal has a three-dimensional architecture characterized by the infinite repetition of identical structure units in space. Its structure can be described in terms of a lattice characterized by long-range order and strongly coupled atoms [1]. For silicon or germanium this strong coupling results in the formation of long-range delocalized energy bands separated by a forbidden energy gap [1]. Charge carriers added to the semiconductor move in these energy bands with a relatively large mean free path. Carrier scattering significantly affects the carrier mobility, which depends on the conductivity effective mass of electrons and the temperature. Carrier mobility in the order of 10^{-1} m^2/Vs is reported for pure inorganic semiconducting crystals such as silicon or germanium. In organic crystals, such as pentacene, the molecules are held together by weak van der Waals or London forces. This weak coupling results in a narrow width for the valence and conduction bands and the band structure can be easily disrupted by introducing disorder in the system. Although organic molecular crystals still exhibit band conduction, excitations and interactions localized on individual molecules play a dominant role. Their mobility, in the order of 10^{-3} m^2/Vs, is significantly lower than those of their inorganic counterparts.

By contrast, conjugated polymers do not have a well-ordered structural configuration as crystals. The conjugation of the polymer backbone is disrupted by chemical or structural defects, such as chain kinks or twists. Experimentally, it has been found that the charge carrier mobility in these materials is in the range of $10^{-12} - 10^{-10}$ m^2/Vs for polymer light-emitting diodes and $10^{-8} - 10^{-5}$ m^2/Vs for polymer field-effect transistors. This is orders of magnitude lower than the mobility determined for organic crystals. Over the past decades intense research has been carried out in order to explain the transport of charge carriers in disordered polymer semiconductors which would justify such low mobility. There are several transport models showing good agreement with the electrical measurements for some particular systems, but no complete solution is available due to the diversity and complexity of these systems. Here, we present the most common transport models.

Disorder induced localized states

The absence of an ideal 3D periodic lattice in disordered polymer semiconductors complicates the description of charge transport processes in terms of standard semiconductor models. Because of their spatial and energetically disordered configuration, these systems have no translation symmetry. The concept of band conduction by free charges does not apply. Instead, the formation of localized states, $N = N(E)$, is enhanced and a different theoretical approach is required. In order to participate to the transport, the charge carriers must hop between these localized states (inter- or intra-chain transitions). This usually leads to a very low carrier mobility. To overcome the energy difference between two localized states, the carriers absorb or emit phonons. This process of phonon-induced hopping was suggested by Conwell [2] and Mott [3] in connection with metallic conduction in inorganic semiconductors, and later by Pines, Abrahams and Anderson [4] for electron relaxation processes in sili-

con. Mott discusses the hopping transport in a constant density of states (DOS), in which he argues that the hopping over long distances and hopping to high energies are equally important. In such a system the conductivity varies with temperature according to $\sigma \propto \exp\left[-\left(T_1/T\right)^{1/4}\right]$, where $T_1 = 128/9\pi a^3 N_F k_B$, N_F is the density of states at the Fermi level and a the size of the localized states [5]. Later, Miller and Abrahams proposed a hopping model based on a single-phonon jump rate description [6]. Their evaluation was made in the case of a lightly doped semiconductor at a very low temperature. The localized states were shallow impurity levels. The energy of these levels stands in a narrow range so the probability for an electron on one site to find a phonon to jump to the nearest site is high. The hopping rate of carriers from occupied i to unoccupied j localized donor states depends on the height of the energetic barrier $E_j - E_i$ and the distance R_{ij} between the states i and j:

$$\nu_{i\to j} = \nu_0 \exp\left(-2\gamma R_{ij}\right) \begin{cases} \exp\left(-\frac{E_j - E_i}{k_B T}\right) & \text{for } E_j > E_i \\ 1 & \text{for } E_j < E_i \end{cases} \tag{2.1}$$

where the pre-factor ν_0 is the attempt-to-hop frequency, γ is the inverse localization length, a is the average lattice distance, and k_B is the Boltzmann constant. The first exponential term from Eq. 2.1 represents the tunneling probability and the second exponential term accounts for the temperature dependence of the phonon density. When this model is applied to polymer semiconductors, the following assumptions are made: the conjugated segments of the polymer play the role of nearly isolated states and Eq. 2.1 is still valid at high temperatures [6].

The polaron model

The polaron model was first introduced in the case of inorganic crystals [7], and has later been used to explain the charge transport in molecular crystals [8] and conjugated polymers [9]. This transport model takes into account the strong electron-phonon interaction.

A polaron is basically a quasiparticle which results from the combination of a charge carrier with a lattice deformation induced by its charge. The transition rate for polarons as determined by Marcus is given by [10]:

$$\nu_{i\to j} \propto \frac{1}{\sqrt{E_r T}} \exp\left[-\frac{\left(E_j - E_i + E_r\right)^2}{4E_r kT}\right] \tag{2.2}$$

where E_r is the intramolecular reorganization energy. The charges moving by thermally activated hops between adjacent sites have a mobility which is field (F) and temperature (T) dependent [10, 11]:

$$\mu = \mu_0 \exp\left[-\frac{E_r}{4kT} - \frac{\left(aF\right)^2}{4E_r kT}\right] \frac{\sinh\left(aF/2kT\right)}{aF/2kT} \tag{2.3}$$

where μ_0 is slightly temperature dependent. However, using Marcus theory the polaron contribution to the activation of the mobility is insignificant. The activation of the mobility using this model amounts to 25-75 meV [12], while using the disordered model the activation energy amounts to 420 meV [13].

Another model that takes into account the strong coupling of charge carriers with the lattice is the Su-Schrieffer-Heeger (SSH) theory [14], which describes the electronic structure of conjugated polymers. This model is based on the concept of bond alteration along a perfect conjugated polymer chain with weak interchain coupling. Adding a charge to the polymer chain leads to a profound change in its geometrical structure characterized by a permutation of the bond alteration over a certain number ($\approx 3-5$) monomeric units. The π-electrons are treated in a tight-binding approximation. The main omission of the SSH model is that it does not consider the electron-electron and electron-hole interactions, which play an important role in the transport and recombination of charge carriers.

The multiple trapping and release model

Another model used to account for the low mobility in amorphous organic materials is the multiple trapping and release model. In this model a narrow band is associated with a high concentration of trap levels. Traps are levels localized at lattice defects or impurities in which the charge carriers are immobilized. These traps can be deep traps, which are located near the center of the band gap, or shallow traps, which are located close to the conduction or valence band. Developed for hydrogenated amorphous silicon (a-Si:H) by Le Comber and Spear [15], the multiple trapping and release model has been used more recently by Horowitz *et al.* [16] to explain the transport in sexithiophene FETs. This model assumes an exponential distribution of gap states. The charges injected or the charges which are already present in the organic semiconductor are trapped into localized states with a probability close to one and then released through a thermally activated process. The drift mobility D is given by:

$$\mu_D = \mu_0 \alpha \exp\left(-\frac{E_T}{k_B T}\right) \tag{2.4}$$

where μ_0 is the mobility at the band edge, α is the ratio between the effective density of states at the transport band edge and the density of traps, and E_T is the energy of the trap state. It has been demonstrated that the transport of carriers depends on the energy level of the trap states, the temperature and the voltage applied [16].

2.2 Charge carrier transport models for polymer LEDs and FETs

A semiconducting polymer is not a perfect conjugated system, because its twisted and kinked chains and chemical defects cause conjugation breaks (Figure 2.1). Due to the

variation in the conjugation lengths and in the interaction energies the semiconductor cannot simply have two delocalized energy bands separated by an energy gap. Instead, an energetic spread of the charge transport sites will be present, often approximated in shape by a Gaussian density of states (DOS). This shape is supported by the observation of Gaussian shaped absorption spectra of polymer materials [13]. The shape of the DOS is important for the description of the charge transport because it reflects the disorder of the system.

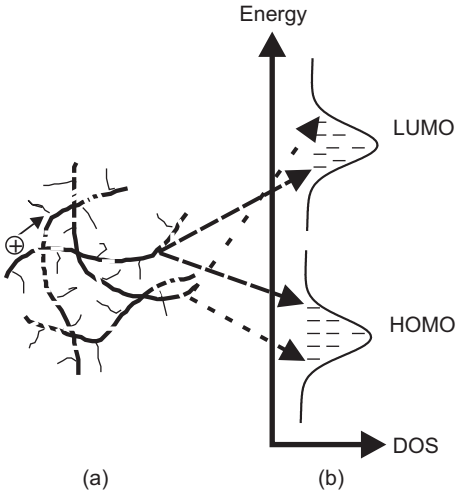

Figure 2.1: (a) Schematic view of polymer chain segments broken by defects, kinks between which the charge carriers hop. (b) Representation of the energy distribution of the localized states, which is approximated by a Gaussian distribution for the LUMO and HOMO levels.

2.2.1 Gaussian density of states

Bässler [13] proposed in 1993 a charge transport model for disordered organic systems. He assumes that electron-phonon coupling is sufficiently weak so that the polaronic effects can be neglected, and the hopping rates can be described by the Miller-Abrahams formalism (*Section 2.1*). The charges hop in a regular array of hopping sites. In this way both positional disorder (fluctuation in inter-site distance) and energetic disorder (fluctuation in site-energy) are introduced. In this model, the energy distribution of localized states can be approximated by a Gaussian function [13]:

$$DOS_{Gauss} = \frac{N_t}{\left(2\pi\sigma_{DOS}\right)^2} \exp\left(-\frac{\epsilon^2}{2\sigma_{DOS}^2}\right) \tag{2.5}$$

where N_t is the total density of sites, σ_{DOS} is the width of the Gaussian density of states (DOS) and the energy ϵ is measured relative to the center of the DOS. The choice for this particular DOS shape is supported by the observation that the

absorption spectra of disordered organic materials usually have Gaussian profiles [17] and by the fact that coupling between a charge carrier and a random distribution of static or induced dipoles leads to a Gaussian DOS function [18].

The charge transport in the Gaussian disorder model (GDM) cannot be solved analytically and therefore an alternative approach of Monte Carlo simulations has been applied [13,19,20]. Using the hopping rate from the Miller-Abrahams formalism, the Monte Carlo simulations revealed that carriers (in this case the electrons) with an arbitrary energy within a Gaussian DOS relax to an equilibrium level $-\sigma_{DOS}^2/k_BT$ below the center of the DOS distribution and the required energy to participate to the transport in the transport level located at $-(5/9)\sigma_{DOS}^2/k_BT$ (Figure 2.2). This gives rise to the dependence $\mu(T) = \mu_0 \exp\left[-\left(\frac{2\sigma_{DOS}}{3k_BT}\right)^2\right]$. But the hopping mobility must depend also on the electric field since the average barrier height for energetic uphill jumps in field direction is reduced [13]. On the basis of the Monte Carlo simulations, the charge carrier mobility is temperature- and field-dependent, and in the limit of high electric fields is given by [13]:

$$\begin{aligned} \mu_{GDM} &= \mu_0 \exp\left[-\left(\frac{2\sigma}{3k_BT}\right)^2\right] \\ &\times \begin{cases} \exp\left[C\left(\left(\frac{\sigma}{k_BT}\right)^2 - \Sigma^2\right)\sqrt{F}\right] & \text{for } \Sigma \geq 1.5 \\ \exp\left[C\left(\left(\frac{\sigma}{k_BT}\right)^2 - 2.5\right)\sqrt{F}\right] & \text{for } \Sigma < 1.5 \end{cases} \end{aligned} \tag{2.6}$$

where μ_0 is the mobility in the limit $T \to \infty$, with values between 10^{-6} and 10^{-5} m^2/Vs, C is a constant that depends on the site spacing, and Σ is the degree of positional disorder. A consequence of hopping in a Gaussian DOS is the non-Arrhenius behavior of the mobility [13].

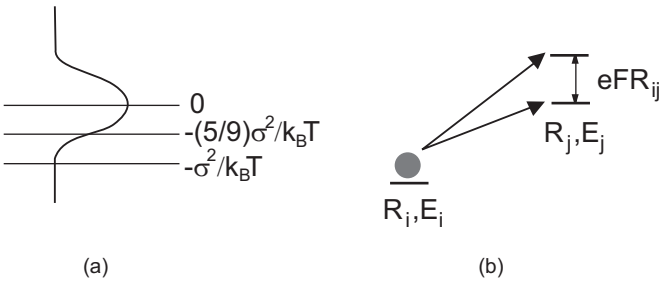

Figure 2.2: (a) The transport level located at $-(5/9)\sigma_{DOS}^2/k_BT$ and the equilibrium level located at $-\sigma_{DOS}^2/k_BT$ in a Gaussian DOS. (b) Representation of the energetic uphill jumps in the direction of the field. This representation is given for electrons.

Because the results of simulations performed within the frame of the standard Gaussian disorder model can explain the experimental results only at high fields ($> 10^8$ V/m), further improvement was necessary. A spatially correlated site-energy distribution was considered [21], which means that the energies are correlated over a greater length than the distance between hopping sites. Due to the correlation of energies of adjacent sites, the field dependence of the mobility extends to lower electric fields. Spatial correlations in site-energy may arise from long-range charge-dipole interactions in the material, where the disorder is determined by the random orientations of dipole moments of nearby molecules. In this correlated disordered model (CDM), the empirical expression for the mobility is given by [22, 23]:

$$\begin{aligned} \mu_{CDM} &= \mu_0 \exp\left[-\left(\frac{3\sigma_{DOS}}{5k_BT}\right)^2\right] \\ &\times \exp\left[C_0\left(\left(\frac{\sigma}{k_BT}\right)^{3/2} - \Gamma\right)\sqrt{\frac{eaF}{\sigma}}\right] \end{aligned} \tag{2.7}$$

where C_0=0.78, a is the intersite separation, and $\Gamma = 2$ for organic materials. The main difference between GDM and CDM is the predicted temperature dependent field dependence. Furthermore, in contrast with GDM, CDM simulations showed a better agreement with the experimental data at low fields [22, 24].

Over the last years the CDM hopping model of charge carriers in a Gaussian DOS has been used in order to explain the experimentally observed temperature and field dependence of the hole mobility in PPV based LEDs. In order to investigate the hole mobility, diodes with one hole injecting contact and one electron blocking contact have been fabricated. Such a structure is called hole-only diode. The experimentally measured current-voltage characteristics at low electric fields of hole-only diodes show a quadratic behavior, indicating that the current is space-charge limited. Injected from the contacts the charge carriers move slow in the polymer, which leads to the build-up of space charge in the semiconductor film. From the analysis of the transient measurements for PPV, it was demonstrated that in the steady-state the hole transport is "trap-free" [25], which means that the concentration of deep traps is small compared to the free carrier concentration [26, 27]. In this case the current density is characterized by Child's law [27]:

$$J = \frac{9}{8}\epsilon_0\epsilon_s\mu\frac{V^2}{L^3} \tag{2.8}$$

where ϵ_0 is the permittivity of vacuum, ϵ_s is the relative dielectric constant of the semiconductor, μ is the carrier mobility and L the thickness of the device. At high biases the current starts to increase more rapidly with voltage and Eq. 2.8 is no longer valid (Figure 2.3). This suggests that the mobility increases with the applied voltage. By changing the temperature, it is found that the mobility also depends on the temperature. The hole transport in PPV can be described by the combination of the SCL conduction model with a temperature and field-dependent mobility [28]:

$$J = ep\left(x\right)\mu_p\left(F\left(x\right),T\right)F\left(x\right) \tag{2.9}$$

$$\frac{\epsilon_0\epsilon_s}{e}\frac{dF\left(x\right)}{dx} = p\left(x\right) \tag{2.10}$$

$$\mu_p(F,T) = \mu(F=0)\exp\left(-\frac{\Delta}{k_BT}+\gamma\sqrt{F}\right) \tag{2.11}$$

where $p\left(x\right)$ is the density of holes at position x in the semiconductor film, $\mu(F=0)$ is the zero-field mobility, Δ is the zero-field activation energy, and γ is the field dependence parameter. The empirical equation which gives the temperature and field dependence of the mobility (Eq. 2.11) was noticed for the first time in poly(N-vinyl carbazole) by Gill in 1972 [29]. Since then this dependence was very often observed in disordered organic semiconductors [28, 30–32]. This equation system can be solved numerically for any given value of J. We present here the results obtained in Ref. [28]. We use the above described model to explain the J-V characteristics for a PPV derivative based hole-only diode (Figure 2.3).

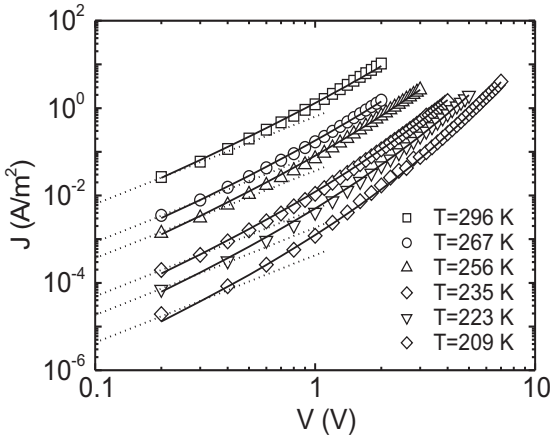

Figure 2.3: J–V characteristics of OC_1C_{10}-PPV hole-only diode for various temperatures. The polymer thickness is 125 nm. The dotted lines represent the prediction of the conventional SCLC model using Eq. 2.8. The solid lines represent the prediction of the SCLC model using the field-dependent mobility given by Eqs. 2.11 and 2.9 (data from Ref. [28]). The polymer is described in Chapter 3.

At low voltages the J-V characteristics are well described by the SCLC given by Eq. 2.8 (Figure 2.3 dashed lines), from which the zero-field mobility $\mu_p\left(0\right) = 5\times10^{-11}$ m^2/Vs is determined. At high voltages the SCL model with field-dependent mobility is used, giving an accurate description of the experimental data (Figure 2.3 solid lines). From the modeling the field coefficient $\gamma = 5.4\times10^{-4}$ $(m/V)^{1/2}$ and the activation energy of the mobility $\Delta = 0.48$ eV have been determined. In most experiments,

the temperature range is limited. Consequently it is difficult to discriminate between an $ln(\mu) \propto -(\sigma/k_BT)^2$ dependence (Eq. 2.6) and the Arrhenius behavior $ln(\mu) \propto -(\Delta/k_BT)$ (Eq. 2.11).

2.2.2 Exponential density of states

The hopping model proposed by Miller and Abrahams was further extended to the so-called variable range hopping model in which it is assumed that the localized states are spread over the entire energy gap [5]. This model suggests that charge carriers may either hop over a small distance with a high activation energy or hop over a long distance with a low activation energy. Subsequently, Monroe developed a transport model for the transport of photoexcited carriers within an exponential density of states (DOS) [33]. He describes the transport of charges in the band tail when hopping in addition to thermal excitation to the band edge is included.

The variable range hopping was further developed by Vissenberg and Matters in order to explain the charge transport in polymer FETs [34]. This transport model takes into account the filling of localized states with charge carriers in contrast to the one developed by Bässler which is a one particle model. The model predicts that at low carrier densities and low temperatures, the transport properties are determined by the tail states of Gaussian DOS, which is approximated by an exponential DOS [34]:

$$DOS_{expon} = \frac{N_t}{k_BT} \exp\left(\frac{\epsilon}{k_BT_0}\right) \tag{2.12}$$

where N_t is the number of states per volume unit, T_0 is the width of the exponential DOS, and ϵ the level energy. It is considered that the energy distribution of the carriers at equilibrium is given by the Fermi-Dirac distribution. If the system is filled with a charge carrier density, δN_t, which occupies a small fraction $\delta \in [0,1]$ of the localized states, the position of the Fermi level is fixed by the condition:

$$\delta \approx \exp\left(\frac{E_F}{k_BT_0}\right) \Gamma\left(1 - \frac{T}{T_0}\right) \Gamma\left(1 + \frac{T}{T_0}\right) \tag{2.13}$$

where approximation $-E_F >> k_BT_0$ has been used, meaning that most carriers occupy the sites with energy $\epsilon << 0$, and $\Gamma(a) = \int_0^\infty dx \exp(-x)\, x^{a-1}$. This condition is fulfilled when δ is low and $T < T_0$. For temperatures $T \geq T_0$ the function $\Gamma(1 - T/T_0)$ diverges and the assumption that only the tail of the DOS is important is no longer valid. The conductance of the system is given by the following equation:

$$G_{ij} = G_0 \exp(2\alpha R_{ij}) \exp\left(\frac{|E_i - E_F| + |E_j - E_F| + |E_i - E_j|}{2k_BT}\right) \tag{2.14}$$

where G_0 is a prefactor for the conductivity, α the effective overlap of electronic wave functions of the sites i and j and R_{ij} the distance between the sites.

Using the percolation theory [35], an expression for the conductivity can be derived as a function of the occupation fraction δ and the temperature T [34]:

$$\sigma(\delta, T) = \sigma_0 \left(\frac{\delta N_t \left(T_0/T\right)^4 \sin\left(\pi \frac{T}{T_0}\right)}{\left(2\alpha\right)^3 B_c} \right)^{T_0/T} \tag{2.15}$$

where σ_0 is a prefactor for the conductivity, and B_c is the critical number for the onset of percolation. For three-dimensional amorphous systems $B_c \approx 2.8$ [36]. The conductivity expressed by Eq. 2.15 has an Arrhenius-like temperature dependence $\sigma \propto exp\left[-E_a/k_BT\right]$ explained by the fact that in an exponential DOS the hopping can be described in terms of activation from the Fermi level to a specific transport level [33]. Moreover, the conductivity increases superlinearly with the charge carrier density $\sigma \sim \delta^{T_0/T}$. This is due to the fact that by increasing the carrier density the states are filled and an activated jump to the transport energy is facilitated.

When a small drain bias, V_d, is applied to the p-type organic FET, the current that flows in the conducting channel is small and ohmic and the conductivity of the semiconductor is [37]:

$$\sigma \cong \left(\frac{L}{Wh}\right) \frac{I_d}{V_d}\bigg|_{V_g=0, V_d \to 0} \tag{2.16}$$

where L and W are the channel length and width, respectively, and h is the thickness of the semiconductor. If now a negative gate voltage, V_g, is applied to the gate, the charges accumulate in the active semiconducting channel and the drain current increases due to the "field-effect". The total amount of induced charges in the accumulation channel is C_iV_g. By applying now a small drain voltage, V_d, the increase of the current in the accumulation channel is [38]:

$$\delta I_d = \frac{W}{L} C_i V_d \delta V_g \mu_{FET}(V_g) \tag{2.17}$$

Here the gradual channel approximation has been used, which means that $V_d << V_g$ such that the potential drop between source and drain can be neglected. Furthermore, it should be noted that the use of the total amount of induced charges (C_iV_g) in Eq. 2.17 is only valid when all charge carriers have the same mobility. But in disordered organic FETs the charge carrier density decreases from the semiconductor/insulator interface into the bulk (See Figure 1.4. According to Eq. 2.13, the occupation $\delta(x)$ depends on the gate induced potential $V(x)$ which depends on the distance:

$$\delta(x) = \delta_0 \exp\left(\frac{qV(x)}{k_BT_0}\right) \tag{2.18}$$

where δ_0 is the carrier occupation far from the semiconductor/insulator interface. In this situation the source-drain current must be calculated over the entire accumulation channel using the following expression [34]:

$$I_d = \frac{WV_d}{L} \int_0^d \sigma\left(\delta\left(x\right), T\right) dx \tag{2.19}$$

From Eqs. 2.15 and 2.19 the following expression for the field-effect current is determined [34]:

$$\begin{aligned} I_d &= \frac{WV_d\epsilon_s\epsilon_0\sigma_0}{Lq}\left(\frac{T}{2T_0-T}\right) \\ &\times\sqrt{\frac{2k_BT_0}{\epsilon_s\epsilon_0}}\left[\frac{\left(\frac{T_0}{T}\right)^4\sin\left(\pi\frac{T}{T_0}\right)}{(2\alpha)^3 B_c}\right]^{T_0/T} \\ &\times\left[\sqrt{\frac{\epsilon_s\epsilon_0}{2k_BT_0}}\left(\frac{C_i\left(V_g-V_{so}\right)}{\epsilon_s\epsilon_0}\right)\right]^{2T_0/T-1} \end{aligned} \tag{2.20}$$

where q is the elementary charge, ϵ_s is the relative dielectric constant of the semiconductor, ϵ_0 is the permittivity of vacuum, and V_{so} is the switch-on voltage of the transistor. For an unintentionally doped polymer V_{so} is determined by fixed charges in the insulator layer or at the semiconductor/insulator interface. In this case V_g becomes $V_g - V_{so}$. Eq. 2.20 has been used successfully to model the transfer characteristics of organic FETs [39].

Here we present the modeling of a polythiophene derivative FET (Figure 2.4). The transistor was measured in the linear regime ($V_d = -2$ V) and has the following dimensions: $W = 2500$ μm, $L = 10$ μm. The fit parameters are $T_0 = 425$ K, $\sigma_0 = 1.6 \times 10^6$ S/m and $\alpha^{-1} = 0.16$ nm [39]. We used $\epsilon_s = 3$. Good agreement between the experimental data and the model described here has been obtained.

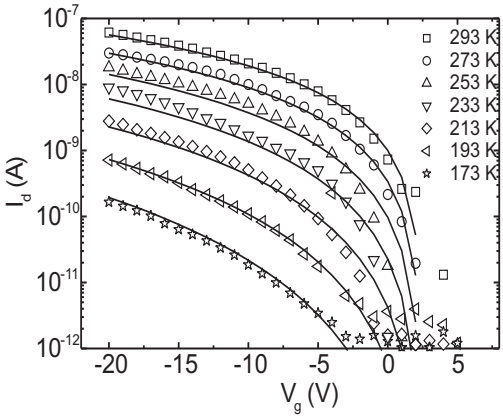

Figure 2.4: I_d versus V_g of P3HT field-effect transistor for various temperatures. The solid lines represent the prediction of the Vissenberg model using Eq. 2.20. The inset shows the chemical structure of P3HT.

2.2.3 Summary

We presented two theoretical models which are frequently used to analyze the charge transport in polymer based LEDs and FETs: hopping in a Gaussian DOS is applied to explain the field and temperature dependence of the carrier mobility in LEDs, while the hopping in an exponential DOS explains the gate voltage and temperature dependence in FETs. In fact, because the polymers characterized in these devices belong to the same class of disordered π-conjugated systems, one unified description should be used to describe their electrical transport characteristics. A detailed discussion of this matter will be presented in *Chapter 4*.

Bibliography

[1] C. Kittel, *Introduction to solid state physics*, 7^{th} Ed., John Wiley and Son, Inc. (1996).

[2] E. M. Conwell, *Phys. Rev.* **103**, 51 (1956).

[3] N. F. Mott, *Can. J. Phys.* **34**, 1356 (1956).

[4] D. Pines, *Can. J. Phys.* **34**, 1367 (1956).

[5] N. F. Mott, E. A. Davis, *Electronic processes in non-crystalline materials*, 2^{nd} Ed., Oxford University Press, London (1979).

[6] A. Miller, E. Abrahams, *Phys. Rev.* **120**, 745 (1960).

[7] J. Yamashita, T. Kurosawa, *J. Phys. Chem. Solids* **5**, 34 (1958).

[8] T. Holstein, *Ann. Phys* **8**, 325 (1959).

[9] K. Fesser, A. R. Bishop, D. K. Campbell, *Phys. Rev. B* **27**, 4804 (1983).

[10] R. A. Marcus, *J. Chem. Phys.* **81**, 4494 (1984).

[11] R. A. Marcus, N. Sutin, *Biochim. Biophys. Acta* **811**, 265 (1985).

[12] K. Seki, M. Tachiya, *Phys. Rev. B* **65**, 14305 (2001).

[13] H. Bässler, *Phys. Stat. Sol. B* **175**, 15 (1993).

[14] W. P. Su, J. R. Schrieffer, A. J. Heeger, *Phys. Rev. Lett.* **42**, 1698 (1979).

[15] P. G. Le Comber, W. E. Spear, *Phys. Rev. Lett.* **25**, 509 (1970).

[16] G. Horowitz, R. Hajlaoui, P. Delannoy, *J. Phys. III France* **5**, 355 (1995).

[17] K. D. Rockwitz, H. Bässler, *Chem. Phys.* **70**, 307 (1982).

[18] A. Dieckmann, H. Bässler, P. M. Borsenberger, *J. Chem. Phys.* **99**, 8136 (1993).

[19] P. M. Borsenberger, L. Pautmeier, H. Bässler, *J. Chem. Phys.* **94**, 5447 (1991).

[20] P. M. Borsenberger, L. Pautmeier, R. Richert, H. Bssler, *J. Chem. Phys.* **94**, 8276 (1991).

[21] Yu. N. Gartstein, E. M. Conwell, *Chem. Phys. Lett.* **245**, 351 (1995).

[22] D. H. Dunlap, P. E. Parris, V. M. Kenkre, *Phys. Rev. Let.* **77**, 542 (1996).

[23] S. V. Novikov, D. H. Dunlap, V. M. Kenkre, P. E. Parris, A. V. Vannikov, *Phys. Rev. Let.* **81**, 4472 (1998).

[24] P. W. M. Blom, M. C. J. M. Vissenberg, *Mat. Sci. Eng.* **27**, 53 (2000).

[25] J. C. Scott, S. Ramos, G.G. Malliaras, *J. Imaging Sci. Technol.* **43**, 234 (1999).

[26] P. M. Borsenberger, D. S. Weiss, *Organic photoreceptors for electrophotography*, Marcel Dekker, New York (1993).

[27] M. A. Lampert, P. Mark, *Current injection in solids*, Academic Press, New York (1970).

[28] P. W. M. Blom, M. J. M. de Jong, M. G. Van Munster, *Phys. Rev. B* **55**, R656 (1997).

[29] W. D. Gill, *J. Appl. Phys.* **43**, 5033 (1972).

[30] L. B. Schein, A. Peled, D. Glatz, *J. Appl. Phys.* **66**, 686 (1989).

[31] P. M. Borsenberger, *J. Appl. Phys.* **68**, 6263 (1990).

[32] M. A. Abkowitz, *Phil. Mag. B* **65**, 817 (1992).

[33] D. Monroe, *Phys. Rev. Lett.* **54**, 146 (1985).

[34] M. C. J. M. Vissenberg, M. Matters, *Phys. Rev. B* **57**, 12 964 (1998).

[35] V. Ambegaokar, B. I. Halperin, J. S. Langer, *Phys. Rev. B* **4**, 2612 (1971).

[36] G. E. Pike, C. H. Seager, *Phys. Rev. B* **10**, 1421 (1974).

[37] A. R. Brown, C. P. Jarrett, D. M. de Leeuw, M. Matters, *Synth. Met.* **88**, 37 (1997).

[38] S. M. Sze, *Physics of semiconductor devices*, 2^{nd} Ed., John Wiley & Sons, New York (1981).

[39] E. J. Meijer, C. Tanase, P. W. M. Blom, E. Van Veenendaal, B. -H. Huisman, D. M. De Leeuw, T. M. Klapwijk, *Appl. Phys. Lett.* **80**, 3838 (2002).

Chapter 3

Materials and experimental techniques

Summary

Here we present the conjugated organic materials used throughout this *Thesis*. In addition, we describe the device preparation, the design of the setup and the procedures used to characterize the devices.

3.1 Sample preparation

3.1.1 Materials

The general structure of conjugated organic materials is characterized by alternating single and double bonds between the atoms present in the backbone of the material. The presence of the π-bond orbitals in which electrons are delocalized give to these materials interesting electronic properties. Almost all conjugated polymers have an interrupted structure of the backbone. This can originate from chemical defects, such as the nonconjugated sp^3-hybridized carbon atom on the polymer backbone, structural defects, such as chain kinks or twists out of coplanarity, the presence of the side-groups, etc. In this way, the resulting polymer films from spin coating are usually amorphous or contain of small polycrystalline grains with the size of 5–20 nm. In general the films are highly disordered. Although long-range order is excluded in conjugated polymers, short-range order of a few lattice constants will generally be present. Chemical modification of conjugated polymers influences both the electronic and morphologic properties in terms of interchain distance, orientation and packing of the polymer chains. Different side chains attached to the polymer will lead to different structural configurations [1, 2] and, as a result, the conductive properties of the polymer can be modified. For example, in this *Thesis* we use different poly(*p*-phenylene vinylene) (PPV)-derivatives for different purposes: to increase the charge carrier mobility (*Chapter 5*), and to tune the solubility of the polymer in different organic solvents (*Chapter 6*).

The conjugated organic materials used throughout this thesis are presented in Figure 3.1. They have energy gaps ranging from 1.9 eV to 3.0 eV and are undoped or unintentionally doped.

P3HT is mainly used as active layer in FETs, but we will use it in LEDs as well. This polymer can have different configurations, head-to-tail (HT), tail-to-tail (TT), and head-to-head (HH) [3]. The regio-random P3HT consists of TT, HH and HT 3-alkylthiophene in a random pattern, while regio-regular P3HT consists of only HT 3-alkylthiophene. The difference in ordering and crystallinity between the two configurations has a huge effect on the electrical properties of the FETs in which P3HT is used [4–6]. Here, the processing conditions are not optimized in order to obtain the high mobility values reported in the literature [5, 6].

The most widely used semiconducting polymers for application in LEDs are PPV and its derivatives due to their excellent emissive properties [7–9]. They are very soluble, form a good film without spikes or irregularities by spin-coating, do not crystallize, and are now commercially available. Throughout this *Thesis* we will use some of the PPV derivatives in both LEDs and FETs. It has been demonstrated that the charge carrier mobility of PPVs can be increased by using symmetric side-chains polymers, such as $OC_{10}C_{10}$-PPV [1,10] or BEH-PPV [11] (Figure 3.1). Phase imaging Scanning Force Microscopy of these polymers has shown that the molecular structure of OC_1C_{10}-PPV is dominated by spiraling chains and a low degree of aggregation. For the symmetrical $OC_{10}C_{10}$-PPV aligned individual chains and strong aggregation was observed [2], leading to an enhancement of the charge transport. Similarly PPV

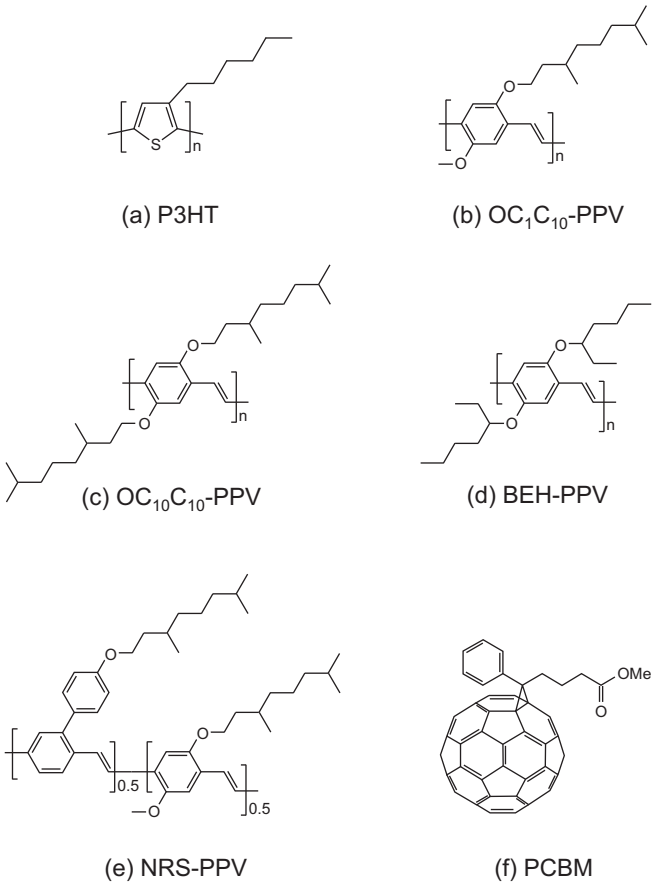

Figure 3.1: The molecular structures of the studied conjugated organic materials: (a) poly(3-hexyl thiophene) (P3HT); (b) poly[2-methoxy-5-(3′,7′-dimethyloctyloxy)-1,4-phenylene vinylene] (OC_1C_{10}-PPV); (c) poly[2,5-bis(3′,7′-dimethyloctyloxy)-1,4-phenylene vinylene] ($OC_{10}C_{10}$-PPV); (d) poly[2,5-bis(2′-ethylhexyloxy)-1,4-phenylene vinylene] (BEH-PPV); (e) poly [2-(4-(3′,7′-dimethyloctyloxyphenyl))-co-2-methoxy-5-(3′,7′-dimethyloctyloxy)-1,4-phenylene vinylene] (NRS-PPV); (f) [6,6]-phenyl-C_{61}-butyric acid methyl ester (PCBM).

copolymers with symmetric side-chains showed increased charge carrier mobility.

The random copolymer NRS-PPV does not exhibit a high charge carrier mobility but has the advantage of being easy to process. This is due to the asymmetrically branched side chains and the randomness of the copolymer backbone. Its high efficiency at low applied voltages makes this polymer suitable for applications.

PCBM is a soluble C_{60} derivative which is used as electron acceptor in bulk heterojunction solar-cells [12–15]. Recently, PCBM started to be used as active organic material in FETs [16, 17]. We demonstrate that this molecule presents high electron mobility and even ambipolar charge carrier transport when used in FETs.

3.1.2 Devices

LED preparation

All samples were prepared on square glass substrates covered with a patterned layer of indium-tin-oxide (ITO), which is transparent, so the light emitted by the LED can be collected.[1] ITO has a work-function of 4.8 eV. This matches relatively well with the HOMO of the PPVs (5.0–5.2 eV) in order to form a nearly Ohmic contact for the holes. Prior to spin coating of the organic layer(s) onto ITO, chemical and physical surface treatments were used to remove contaminants, smoothen the surface, and improve the ITO work function [18–20]. The cleaning steps were as follows: rubbing with demineralized water/soap solution, rinsing with demineralized water, ultrasonic treatment in acetone, rinsing with demineralized water, ultrasonic treatment in *iso*-propanol, blow-drying in a nitrogen flow, drying in oven at 120 °C, and finally UV-ozone treatment. Although ITO is widely used as an anode electrode, it has the disadvantage that oxygen diffuses in the organic active layer and contributes to the degradation of the device with time [21, 22]. In order to improve the device stability and performance, a conductive, transparent layer of PEDOT-PSS consisting of polyethylenedioxythiophene (PEDOT) doped with polystyrenesulfonate (PSS) was optionally spin-coated on top of the ITO [23]. After spin coating, the sample was baked at 140°C for several minutes in order to remove the remaining water that can cause degradation of the device [22, 24].

The active organic layer was spin coated from solution (spin speed rates of 1000–3000 rpm). The solvent used for most of the polymers was toluene, but other solvents, such as chlorobenzene, chloroform, and acetone have been used as well. The polymer solution was stirred overnight in the glove-box and optionally heated at 60–80°C. For double-layer LEDs, the bottom polymer layer was chemically modified in such a way that it could not be dissolved by the solvent used for spin coating the top polymer layer. The spin coating took place in a glove-box, under controlled nitrogen atmosphere in order to prevent contamination of the organic layer with water and oxygen. The polymer thickness varied between 50 nm and 300 nm. The layer thickness was measured using a Dektak profile analyzer.

[1] The LED substrates with patterned ITO electrodes were provided by Philips Research Laboratories Eindhoven.

The top-electrode was thermally evaporated on the sample inside a vacuum system at typically 10^{-7} mbar. Different metals were used, depending on the application: gold (80 nm) to prevent electron injection (work-function of 5.2 eV) for hole-only diodes, calcium (5 nm) or barium (5 nm), to inject electrons (work-function of 2.9 eV) and aluminum (100 nm) as protective layer for LEDs. The resulting sample consisted of four independent devices of different areas, from 10 mm^2 to 100 mm^2 (Figure 3.2a).

Planar diode preparation

For the planar devices, different substrates have been used, such as glass, Al_2O_3, quartz and SiO_2. Two types of device configuration have been used: single-contact configuration (Figure 3.2b), and finger configuration (Figure 3.2c). The devices were made as follows; a 5 nm titanium adhesion layer and 50 nm gold have been thermally evaporated through a shadow-mask. The pressure in the evaporation system was typically 10^{-7} mbar. The polymer layer was spin coated from solution at 1000–3000 rpm on top of the contacts in the glove-box in order to avoid contamination with water and oxygen. The solvent used was toluene. The polymer thickness varied from 50 nm to 400 nm, which was measured using a Dektak profile analyzer. The resulting sample consisted of four or five independent devices having the width W=1 mm and 5 cm, and the length L=1.25–100 μm. Finally the devices were transported to the measurement setup in order to be electrically characterized.

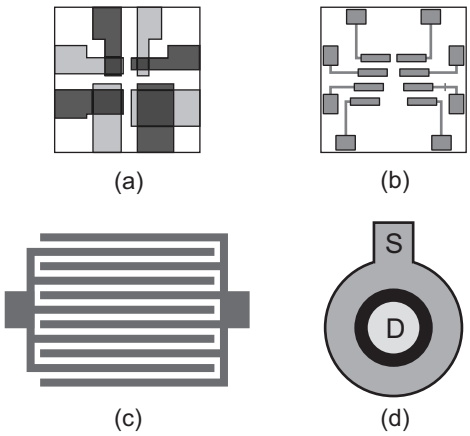

Figure 3.2: Schematic of LEDs (a), planar diodes (b,c), and FETs (c,d).

FET preparation

FETs were made using heavily doped silicon wafers as gate electrode, with a 200 nm thick layer of thermally oxidized SiO_2 as gate dielectric. By conventional photolithog-

raphy, gold drain and source electrodes were patterned on top of the SiO_2.[2] It was demonstrated that modification of the substrate surface prior to the deposition of the organic active layer made the substrate flat and influenced the film morphology [5, 6, 25]. In our experiments, the substrate was treated with the primer hexamethyldisilazane (HMDS) in order to make the surface hydrophobic.

The device was finished by spin coating the organic active layer from solution. The layer thickness, h, was typically 200 nm. The solvents used were toluene, chlorobenzene, and chloroform. Prior to spin coating, the solution was stirred overnight and optionally heated at 60–80 °C. To avoid contamination with water and oxygen, most of the polymers were spin-coated in the glove-box and then transported directly to the measurement set-up. Two FET configurations have been used: finger configuration with typical length, L=10 μm, and width, W=10 000 μm (Figure 3.2c); ring configuration with L=10–40 μm and W=1 000 μm (Figure 3.2d). The ring configuration has been used in order to minimize contributions by parasitic currents [26].

3.2 Experimental methods

3.2.1 SCL measurement techniques

The setup used to measure the polymer LEDs is presented in Figure 3.3. The sample holder and part of the setup were placed in a glove-box filled with dry nitrogen to avoid contamination of the sample with water and oxygen. In the sample holder, each of the four devices could be electrically addressed without moving the sample. The devices were then tested using several measurement units.

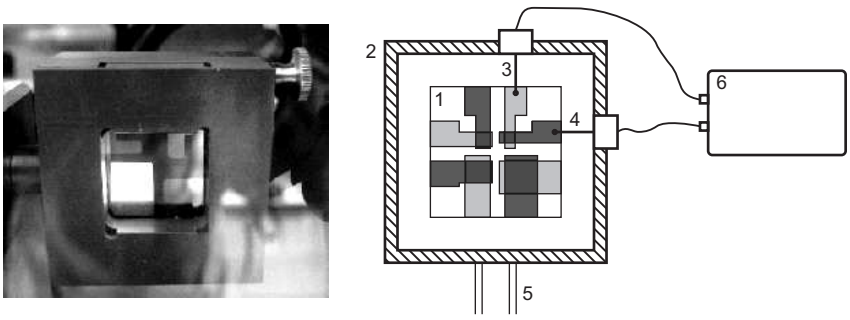

Figure 3.3: LED set-up. The measurement system consists of: (1) sample, (2) sample table, (3,4) electrical connectors, (5) cooling system, (6) Keithley 2400 Source Meter Unit.

Current-voltage (I-V) measurements were performed in dark or under yellow light using a Keithley 2400 Source Meter Unit. The light emitted by the LEDs was measured through the glass substrate using a photodiode placed on top of the device.

[2]The FET substrates with patterned gold electrodes were provided by Philips Research Laboratories Eindhoven.

Electroluminescence spectra were performed with an Ocean Optics Inc. Spectrometer placed on top of the device.

A typical example of the J–V characteristics of polymer hole-only diode and a LED is given in Figure 3.4a. From theory we expect three regimes: *i*) Ohmic J–V dependence at low voltages, *ii*) quadratic behavior at moderate voltages, and *iii*) stronger than quadratic behavior at high voltages. The steepness of the current is dependent on the material and thickness, and this increase is in most of the cases from one to six orders of magnitude. In Figure 3.4b, the photocurrent (PL) generated by the LED is presented. It should be noted that light starts to be observed from a built-in voltage V_{bi}=1.5–2 V, which represents the difference in work-function between the anode and the cathode. Temperature dependence measurements were performed under a permanent flow of cold dry nitrogen on the sample. The measurements were controlled using LabView and Ocean Optics Inc. OOIBase32 computer programs.

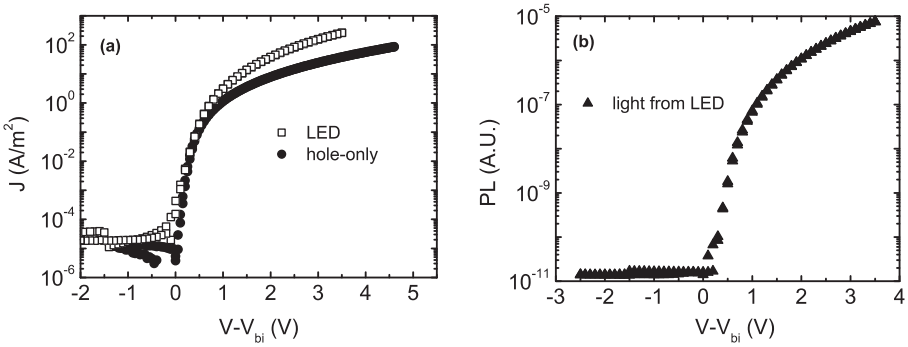

Figure 3.4: J–V characteristic of a polymer hole-only diode and a LED (a) and PL-V of polymer LED (b). In this particular example, OC_1C_{10}-PPV is sandwiched between ITO and Au electrodes for the hole-only diode and between ITO and Ba electrodes for the LED.

3.2.2 Field-effect measurements

The setup for the field-effect measurements is presented in Figure 3.5. The sample was placed in the characterization setup which was then pressurized at typically 10^{-6}–10^{-7} mbar. The electrical contacts for electrodes were connected afterwards. Two types of electrical measurements were performed: transfer characteristics (I_d–V_g) and output characteristics (I_d–V_d). All the measurements were performed in the dark. The data were controlled and recorded using a Keithley 4200 Semiconductor Characterization System. In order to perform the temperature measurements, the sample table was cooled using liquid nitrogen and a temperature controller was used.

A typical example of transfer and output characteristics of a polymer FET is presented in Figure 3.6.

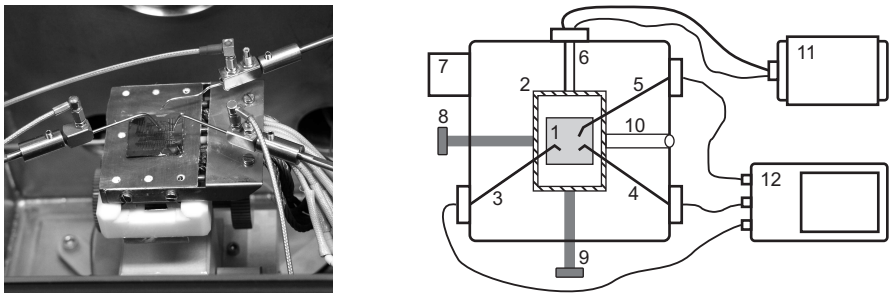

Figure 3.5: Field-effect measurement setup.The measurement system consists of: (1) sample, (2) sample table, (3-5) source, drain, gate connectors, (6) thermocouple+thermocouple wires, (7) vacuum pump, (8,9) x, y position adjusters, (10) cooling system, (11) temperature controller, (12) Keithley 4200 Semiconductor Characterization System.

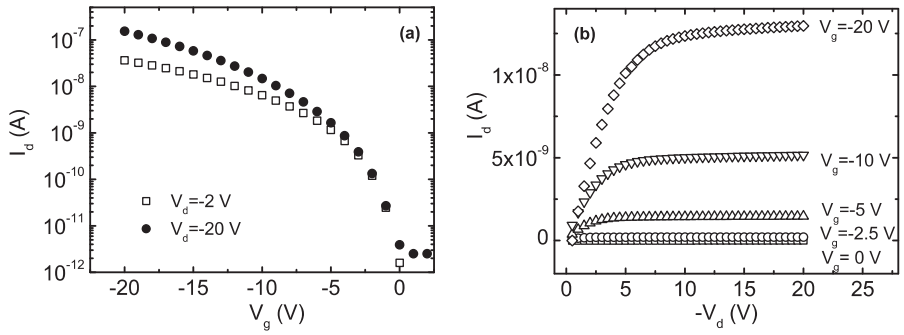

Figure 3.6: The transfer characteristics (I_d–V_g) (a) and output characteristics (I_d–V_d) (b) of OC_1C_{10}-PPV FET. The channel width is W=2 500 μm, and the channel length is L=10 μm.

3.2.3 Current–voltage planar measurements

The setup used to measure planar diodes is presented in Figure 3.7.

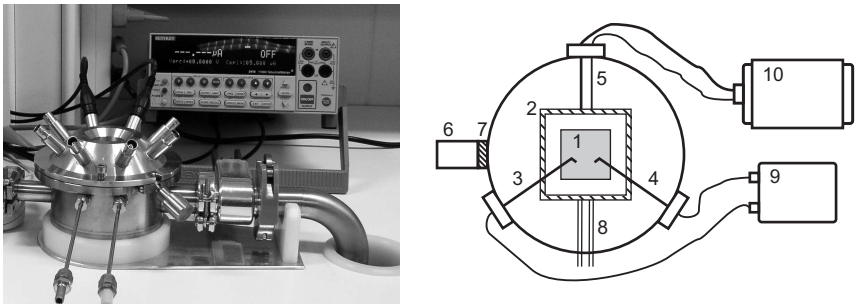

Figure 3.7: Planar diode setup. The measurement system consists of: (1) sample, (2) sample table, (3,4) electrical connectors, (5) thermocouple+thermocouple wires, (6) vacuum pump, (7) vacuum pump valve, (8) cooling system, (9) Keithley 2410 High Voltage Source Meter Unit, (10) temperature controller.

A typical example of the *I-V* characteristics of a polymer planar diode is presented in Figure 3.8. Because the distance between electrodes is at least 1.25 μm, large voltages in the order of kV are required to measure currents above the setup noise. Instead, a strongly enhanced current is measured for much lower voltages (Figure 3.8). We discuss this in *Chapter 5*.

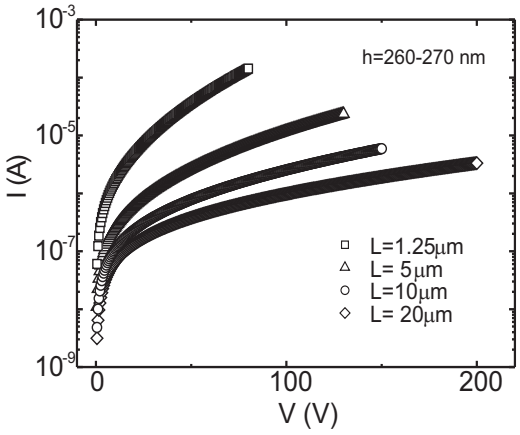

Figure 3.8: *I–V* characteristics of NRS-PPV planar diode.

Bibliography

[1] H. C. F. Martens, P. W. M. Blom, H. F. M. Schoo, *Phys. Rev. B* **61**, 7498 (2000).

[2] M. Kemerink, J. K. J. van Duren, P. Jonkheijm, W. F. Pasveer, P. M. Koenraad, R. A. J. Janssen, H. W. M. Salemink, J. H. Wolter, *Nano Lett.* **3**, 1191 (2003).

[3] Z. Bao, A. Dodabalapur, A. J. Lovinger, *Appl. Phys. Lett.* **69**, 4108 (1996).

[4] A. Assadi, C. Svensson, M. Willander, O. Ingans, *Appl. Phys. Lett.* **53**, 195 (1988).

[5] H. Sirringhaus, N. Tessler, R. H. Friend, *Science* **280**, 1741 (1998).

[6] H. Sirringhaus, P. J. Brown, R. H. Friend, M. M. Nielsen, K. Bechgaard, B. M. W. Langeveld-Voss, A. J. H. Spiering, R. A. J. Janssen, E. W. Meijer, P. Herwig, D. M. de Leeuw, *Nature* **401**, 685 (1999).

[7] J. H. Burroughes, D. D. C. Bradley, A. R. Brown, R. N. Marks, K. Mackay, R. H. Friend, P. L. Burns, A. B. Holmes, *Nature* **347**, 539 (1990).

[8] D. Braun, A. J. Heeger, *Appl. Phys. Lett.* **58**, 1982 (1991).

[9] P. W. M. Blom, M. J. M. de Jong, J. J. M. Vleggaar, *Appl. Phys. Lett.* **68**, 3308 (1996).

[10] P. W. M. Blom, M. C. J. M. Vissenberg, *Mat. Sci. Eng.* **27**, 53 (2000).

[11] C. Tanase, J. Wildeman, P. W. M. Blom, *Proc. of SPIE* **5464**, 351 (2004).

[12] G. Yu, J. Gao, J. C. Hummelen, P. Smith, A. J. Heeger, *Science* **270**, 1789 (1995).

[13] S. E. Shaheen, C. J. Brabec, N. S. Sariciftci, F. Padinger, T. Fromherz, J. C. Hummelen, *Appl. Phys. Lett.* **78**, 841 (2001).

[14] D. Chirvase, Z. Chiguvare, M. Knipper, J. Parisi, V. Dyakonov, J. C. Hummelen, *Synth. Met.* **138**, 299 (2003).

[15] V. D. Mihailetchi, P.W. M. Blom, J. C. Hummelen, M. I. Rispens, *J. Appl. Phys.* **94**, 6849 (2003).

[16] E. J. Meijer, D. M. de Leeuw, S. Setayesh, E. van Veenendaal, B. -H. Huisman, P. W. M. Blom, J. C. Hummelen, U. Scherf, T. M. Klapwijk, *Nature Mat.* **2**, 678 (2003).

[17] T. D. Anthopoulos, C. Tanase, S. Setayesh, E. J. Meijer, J. C. Hummelen, P. W. M. Blom, D. M. de Leeuw, to be published in *Adv. Mat.*

[18] J. S. Kim, M. Granström, R. H. Friend, N. Johansson, W. R. Salaneck, R. Daik, W. J. Feast, F. Cacialli, *J. Appl. Phys.* **42**, 6859 (1998).

[19] Th. Kugler, W. R. Salaneck, H. Rost, A. B. Holmes, *Chem. Phys. Lett.* **310**, 391 (1999).

[20] N. R. Armstrong, C. Carter, C. Donley, A. Simmonds, P. Lee, M. Brumbach, B. Kippelen, B. Domercq, S. Yoo, *Thin Solid Films* **445**, 342 (2003).

[21] J. C. Scott, J. H. Kaufman, P. J. Brock, R. DiPietro, J, Salem, J. A. Goitia, *J. Appl. Phys.* **79**, 2745 (1996).

[22] F. J. J. Janssen, J. M. Sturm, A. W. Denier van der Gon, L. J. van IJzendoorn, M. Kemerink, H. F. M. Schoo, M. J. A. de Voigt, H. H. Brongersma, *Org. Electr.* **4**, 209 (2003).

[23] L. Groenendaal, G. Zotti, P. H. Aubert, S. M. Waybright, J. R. Reynolds, *Adv. Mat.* **15**, 855 (2003).

[24] X. Crispim, S. Marciniak, W. Osikowicz, G. Zotti, A. W. Denier van der Gon, F. Louwet, M. Fahlman, L. Groenendaal, F. de Schryver, W. R. Salaneck, *J. Pol. Sci. B* **41**, 2561 (2003).

[25] M. L. P. da Silva, I. H. Tan, A. P. Nascimento Filho, E. Galeazzo, D. P. Jesus, *Sens. and Actuators B* **91**, 362 (2003).

[26] E. J. Meijer, C. Detcheverry, P. J. Baesjou, E. van Veenendaal, D. M. de Leeuw, T. M. Klapwijk, *J. Appl. Phys.* **93**, 4831 (2003).

Chapter 4

Charge carrier mobility in disordered organic FETs and LEDs

Summary

In conventional field-effect transistors, the extracted mobility does not take into account the distribution of charge carriers. However, in disordered organic field-effect transistors, the local charge carrier mobility decreases from the semiconductor/insulator interface into the bulk, due to its dependence on the charge carrier density. It is demonstrated that the experimentally determined field-effect mobility is a good approximation for the local mobility of the charge carriers at the interface.

Different theoretical descriptions and charge mobilities for disordered semiconductor FETs and LEDs are reported in literature. We demonstrate that the two device models can be unified and that the large mobility difference between FETs and LEDs originates from the strong dependence of the hole mobility on the charge carrier density.

In contrast with earlier reports, we demonstrate that the enhancement of the SCL current in PPV-based LEDs is determined by the dependence of the mobility on the charge density and electric field. From thickness dependence measurements the contribution of the electric field and of the charge carrier density to the hole mobility in LEDs can be disentangled.

4.1 Field-effect mobility

4.1.1 Introduction

In contrast with conventional monocrystalline silicon, the transport properties of disordered organic semiconductors are dominated by localized states [1,2]. By applying a gate voltage in a field-effect transistor, the charge carriers accumulate in the semiconductor close to the insulator. They fill the lower states of the organic semiconductor. Any additional charges in the system will occupy states at relatively high energies, which means that they will need less activation energy to jump to other sites. As a result the mobility will be enhanced and increases with charge carrier density. For the understanding of the transfer characteristics of organic semiconductors it is important to realize that in a FET the charge carrier density is not uniformly distributed in the accumulation channel, but decreases from the semiconductor/insulator interface into the bulk. The consequence is that for a given V_g distribution of charge carriers and mobility through the thickness of the accumulation layer is present. In literature, however, the field-effect mobility is determined assuming that all charge carriers have the same mobility. Experimentally, the field-effect mobility is calculated from the following equation [3]:

$$\mu_{FET}(V_g) = \frac{L}{WC_iV_d}\frac{\partial I_d}{\partial V_g}\bigg|_{V_d \to 0} \tag{4.1}$$

To determine how viable the latter approach is, a couple of questions arise. How applicable is Eq. 4.1 to disordered organic FETs? How does the field-effect mobility determined from Eq. 4.1 compare with the local mobility described by the variable range hopping model? To answer these questions the distribution of the charge carrier density in the accumulation channel is calculated. Then the distribution of the local mobility in the accumulation channel is determined for every gate voltage, and compared with the mobility values obtained from Eq. 4.1.

4.1.2 Charge carrier density distribution

The distribution of the charge carrier density in the accumulation channel is calculated using a numerical program in which an undoped system is considered. The gradual channel approximation is used, which means that the applied gate voltage is much greater than the drain voltage ($V_g >> V_d$). In this approximation variations along the source-drain channel can be neglected and the distribution of charge carriers is uniform along the interface and decreases away from the interface in the direction perpendicular to the semiconductor/insulator interface (x) (See inset Figure 4.1).

The total concentration of charges in the semiconductor layer is given by the formulas [4]:

$$p = \int_{\epsilon} DOS_{expon}(\epsilon) \cdot f_p(\epsilon)\, d\epsilon \tag{4.2}$$

$$n = \int_{\epsilon} DOS_{expon}(\epsilon) \cdot f_n(\epsilon)\, d\epsilon \tag{4.3}$$

where p, n represent the density of majority (holes) and minority (electrons) carriers, DOS_{expon} represents the exponential density of states which characterize the energy levels responsible for the charge transport, f_p, f_n represent the Fermi-Dirac distribution function for holes and electrons. The position of the Fermi level can be found from the preservation of the electrical charges $n + N_A^- = p$, where N_A^- is the number of ionized acceptors. By applying a negative gate voltage charges are induced into the channel. In this situation the Fermi level becomes $E_f(x) = E_f - qV(x)$, where x is the direction perpendicular to the semiconductor/insulator interface and $V(x)$ is the gate induced potential. Combining this with Eqs. 4.2 and 4.3, a relation between the charge concentration (p, n) and the potential (V) is obtained. From the Poisson equation and the relation between the electric field and the potential in the channel, the electric field distribution in the accumulation channel is [4]:

$$F_x(V) = \left[\left(\frac{2}{\epsilon_0 \epsilon_s} \right) \left| \int_0^V qp(V')\, dV' \right| \right]^{1/2} \tag{4.4}$$

where V' is the local potential, which varies from zero far away in the bulk to V in the accumulation channel, ϵ_s is the relative dielectric constant of the semiconductor and p is the density of charge carriers. The potential distribution is found from $x = \int_V^{V_0} (1/F_x(V'))dV'$, where V_0 is the surface potential at the semiconductor/insulator interface. The boundary conditions are given by: $F_x(V = 0) = F_x(V = V_0)$, which is the electric field at the semiconductor/insulator interface (x=0), and $\varphi_{ind} = \epsilon_0 \epsilon_s F_x(V_0)$, is the space charge density. The gate voltage is related to φ_{ind} as follows: $V_g = \varphi_{ind}/C_i + V_{fb}$, where V_{fb} is the flat-band voltage (See *Section 1.3*). In the calculations quantum mechanical effects are neglected, they become critical for doped semiconductors with charge concentration $> 10^{26}$ m^{-3}. Now the distribution of the charge carrier density in the accumulation layer can be calculated as function of distance x for every gate voltage [5]. Assuming $V_{fb} = 0$ the concentration of charge carriers as function of distance x is calculated for an undoped semiconductor with $C_i = 15.5 \times 10^{-5}$ F/m^2 and $\epsilon_s = 2.9$, for gate voltages of $V_g = -19$ V and $V_g = -10$ V at room temperature (Figure 4.1).

It appears that at $V_g = -19$ V the charge carrier density decreases from 3.5×10^{25} m^{-3} at the interface ($x = 0$) to 1.3×10^{24} m^{-3} at a distance of 2 nm from the interface. For $V_g = -10$ V, the total induced charge at the interface is about half to that at $V_g = -19$ V. It should be noted that the calculation of charge distribution applies to field-effect devices of undoped semiconductors in the linear operating regime (small source-drain voltage), where only details are different due to different values of C_i and ϵ_s.

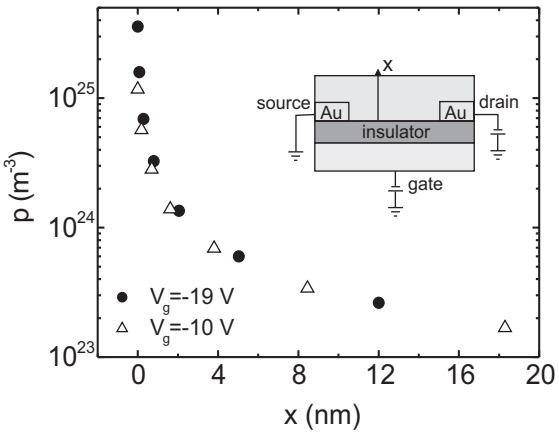

Figure 4.1: Numerically calculated distribution of charge carrier density in the accumulation channel perpendicular to the semiconductor/insulator interface for V_g= -19 V and -10 V. x describes the distance in the direction perpendicular to the semiconductor/insulator interface.

4.1.3 Local mobility versus field-effect mobility

In order to determine the dependence of the mobility on the charge carrier density, we use the hopping model developed by Vissenberg and Matters [1]. From the conductivity (Eq. 2.15), an expression for the local mobility as function of charge carrier density is derived:

$$\mu_{FET}(p) = \frac{\sigma_0}{e}\left[\frac{\left(\frac{T_0}{T}\right)^4 \sin\left(\pi\frac{T_0}{T}\right)}{(2\alpha)^3 B_C}\right]^{\frac{T_0}{T}} p^{\frac{T_0}{T}-1} \tag{4.5}$$

where σ_0 is a prefactor for the conductivity, α^{-1} is the effective overlap parameter between localized states and $B_c \cong 2.8$ is the critical number for the onset of percolation [6]. Taking into account the distribution of the charge carrier density perpendicular to the channel, the field-effect current is calculated using the integration over the accumulation channel $I_d = WV_d/L \int_0^t ep(x)\mu_{FET}(p(x))dx$, where t represents the total thickness of the accumulation channel. Using this formalism the *dc* transfer characteristics of disordered polymer FETs can be modeled as a function of T and V_g. In order to model the experimental data we use Eq. 2.20, which is the analytical expression for $I_d = WV_d/L \int_0^t ep(x)\mu_{FET}(p(x))dx$. In Figure 4.2, the experimental transfer characteristics of an OC_1C_{10}-PPV FET together with the modeled ones (Eq. 2.20) are presented in the temperature range from 206 K to 293 K. Good agreement is obtained between the experimental data and the model. The fit parameters T_0, σ_0 and α^{-1} are given in Table 4.1 for P3HT and OC_1C_{10}-PPV FET. The values obtained for σ_0 seem to exceed the theoretical calculated ones. The fact that the switch-on voltage, V_{so}, is not zero indicate the presence of fixed charges in

the insulator and/or in the semiconductor.

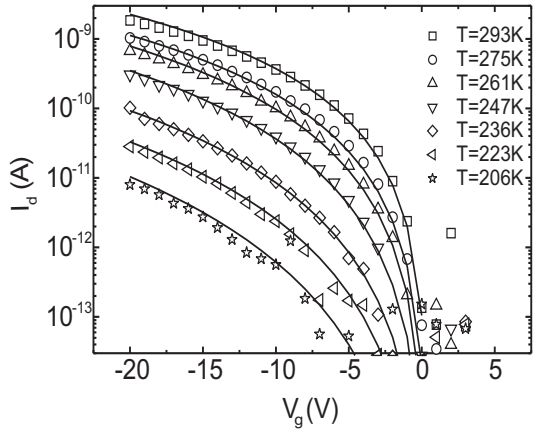

Figure 4.2: Transfer characteristics of an OC_1C_{10}-PPV FET. The solid lines are modeled with Eq. 2.20. $W = 2500$ μm, $L = 10$ μm, $V_d = -0.1$ V.

Polymer	T_0 (K)	σ_0 (10^6 S/m)	α^{-1} (Å)	$\mu_{FET}(V_g)$ (m^2/Vs)	V_{so} (V)
P3HT	425	1.6	1.6	6×10^{-8}	2.5
OC_1C_{10}-PPV	540	31	1.4	4.7×10^{-8}	0.5

Table 4.1: Fit parameters T_0, σ_0, α^{-1} and the field-effect mobility $\mu_{FET}(V_g)$ determined from Eq. 4.1 at $V_g = -19$ V at room temperature for a P3HT FET and a OC_1C_{10}-PPV FET.

Subsequently, by combining Eq. 4.5, using the parameters as determined from the modeled transfer characteristics, with the distribution of the charge carrier density as function of position x, the local mobility in the accumulation channel can be calculated, as also presented in Ref. [5]. In Figure 4.3, the distribution of the local mobility versus distance x is presented together with the experimental field-effect mobility from Eq. 4.1 for P3HT and OC_1C_{10}-PPV at a gate voltage $V_g = -19$ V.

We find that the local mobility decreases about one order of magnitude in the first 2 nm from the semiconductor/insulator interface into the bulk. Thus, due to the charge carrier density distribution in the accumulation channel, the local mobility is also strong dependent on the position in the accumulation channel. The local mobility of the charge carriers directly at the semiconductor/insulator interface for $V_g = -19V$ is roughly 9% larger for P3HT and 15% larger for OC_1C_{10}-PPV than the experimental field-effect mobility determined from Eq. 4.1. The reason for this relatively small difference is that not only a major part of the charge carriers is located close to the interface, but also that these charge carriers have the highest mobility. As a result, the field-effect current is mainly determined by the charge carriers directly at the interface. Consequently, the error due the approximation used in Eq. 4.1, namely

that all charge carriers have the same mobility, is relatively small.

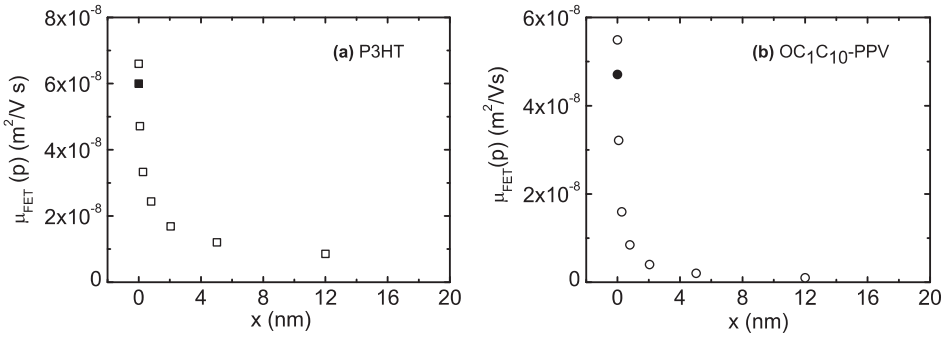

Figure 4.3: Distribution of local mobility $\mu_{FET}(p)$ as function of position in the accumulation channel for a P3HT FET (a) and an OC_1C_{10}-PPV FET (b) at $V_g = -19$ V (open symbols).The field-effect mobility as determined from Eq. 4.1 is given as a solid symbol.

4.1.4 Conclusion

In conclusion, in disordered organic transistors the dependence of the mobility on the gate voltage is determined by the charge carrier dependence of the local mobility. Taking into account the distribution of the charge carrier density in the active channel in the direction perpendicular to the insulator, the local mobility has been calculated as a function of position in the accumulation layer. It was demonstrated that for disordered organic FETs, in spite of the strong variations in the local mobility, the conventional field-effect mobility is a relatively good estimate for the local mobility of the charge carriers at the semiconductor/insulator interface.

4.2 Unification of the charge transport in disordered polymer LEDs and FETs

Two different groups of solution-processable conjugated polymers have been developed for LEDs (*e.g.* PPV derivatives) and FETs (*e.g.* poly(thienylene vinylene), polythiophene) which apparently have fundamentally different properties. The hole current in OC_1C_{10}-PLEDs is space-charge limited (SCL) and is governed by charge mobility, μ_{LED}, which is dependent on both the temperature, T, and the applied electric field, F [7]. At low electric fields, and at room temperature, the hole mobility amounts to 5×10^{-11} m^2/Vs [7]. Its field- and temperature dependencies are well described by hopping in a correlated Gaussian disordered system (*Section 2.2.1*) [8,9]. One of the most widely studied conjugated polymers in organic field-effect transistors is poly(3-hexyl thiophene) (P3HT) [10]. Typical field-effect mobilities, μ_{FET}, for spin-coated amorphous P3HT films are in the range of $10^{-9} - 10^{-8}$ m^2/Vs, whereas by ordering

the polymer in the film the field-effect mobility increased to about 10^{-5} m^2/Vs [11]. The transfer characteristics of amorphous P3HT are modeled as a function of temperature and gate bias with variable range hopping in an exponential density of states [1] and the field-effect mobility amounts to 6×10^{-8} m^2/Vs for a gate voltage $V_g = -19$ V [12].

The main question is why there is such a big difference in mobility and why different theoretical transport models for polymer LEDs and FETs are applied. First, the charge carrier density range in which polymer LEDs and FETs typically operate is determined. Then we establish the dependence of the charge mobility on charge carrier density and correlate the charge mobility obtained from LEDs and FETs.

We perform electrical measurements in LEDs and FETs using as active materials OC_1C_{10}-PPV and P3HT. Both polymers are highly disordered and the charge transport can be considered the same in all directions [13]. The experimental transfer characteristics of the OC_1C_{10}-PPV FET are presented for the temperature range from 206 K to 293 K in Figure 4.2. A field-effect mobility of 4.7×10^{-8} m^2/Vs at $V_g = -19$ V at room temperature has been obtained using Eq. 4.1. Surprisingly, this value for the field-effect mobility is approximately three orders of magnitude larger than the mobility value determined from hole-only diode [7]. The hole mobility of P3HT at low carrier densities is determined from J-V measurements of the hole-only diode (See Figure 4.4).

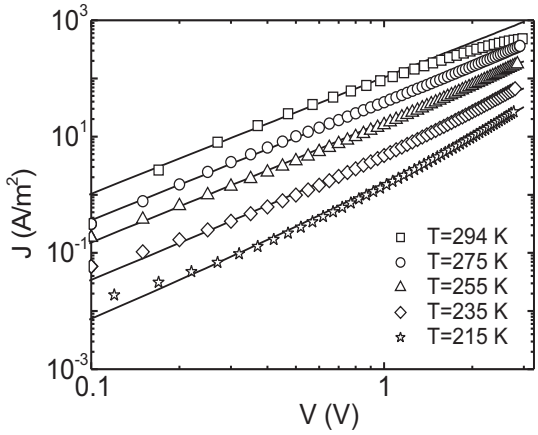

Figure 4.4: J–V of a P3HT hole-only diode for various temperatures. The polymer layer has a thickness of 95 nm. The solid lines represent the prediction of the SCLC model using the field-dependent mobility given by Eqs. 2.9 and 2.11

The current density at room temperature depends quadratically on the applied voltage, which is indicative of space-charge limited transport. The derived hole mobility at room temperature is 2.8×10^{-9} m^2/Vs, which is more than an order of magnitude lower than what is obtained in P3HT FETs [12]. In Tables 4.1 and 4.2 the parameters used to model the FETs and LEDs are presented. The question is why

Polymer	σ_{DOS} (meV)	$\mu_{LED}(F=0)$ (m^2/Vs)
P3HT	98	2.8×10^{-9}
OC_1C_{10}-PPV	110	5×10^{-11}

Table 4.2: Parameters $\mu_{LED}(F = 0)$ (zero-field mobility) at room temperature and σ_{DOS} (the width of the Gaussian density of states) for P3HT and OC_1C_{10}-PPV as determined from hole-only diode.

the experimental mobilities for the same polymer differ when measured in different device geometries (LEDs and FETs). In order to answer this question, we analyze the charge carrier density regime in which the two devices operate [13].

In a hole-only diode the current is space-charge limited for low electric fields. The experimental mobility is constant for low electric field and also independent of the charge carrier density. The lowest charge carrier density p_{LED} in a space charge-limited diode is found at the non-injecting contact and is given by [14]:

$$p_{LED} = \frac{3}{4}\left(\frac{\epsilon_0 \epsilon_s V}{qh^2}\right) \tag{4.6}$$

For P3HT for the voltage range applied of 0.1 V to 3 V the mobility is charge carrier and field-independent. This voltage range corresponds to hole density of 1.4×10^{21} to 4.1×10^{22} m^{-3}. For OC_1C_{10}-PPV for the voltage range applied of 1 V to 10 V (Figure 4.5) the mobility is charge carrier and field-independent.

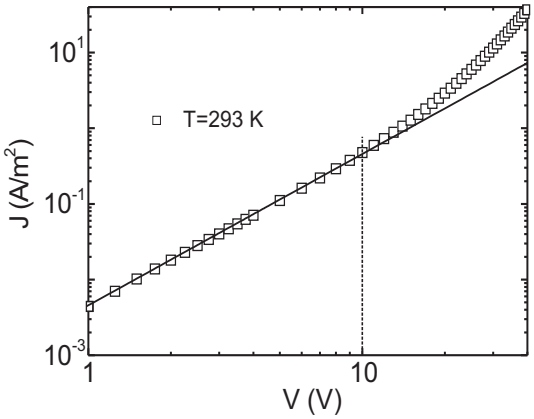

Figure 4.5: *J–V* of OC_1C_{10}-PPV hole-only diode at room temperature. The polymer layer thickness is 700 nm. The solid line represents the prediction of the conventional SCLC model using Eq. 2.8.

This voltage range corresponds to hole density of 2.5×10^{20} to 2.5×10^{21} m^{-3}. We note that for voltages higher than 3 V (carrier density $> 4.1 \times 10^{22}$ m^{-3}) for P3HT and 10 V (carrier density $> 2.5 \times 10^{21}$ m^{-3}) for OC_1C_{10}-PPV, the charge mobility

is not constant. In this case the carrier density dependence of mobility cannot be discriminated from the field dependence of mobility, due to the fact that in a space-charge limited diode both carrier density and field are simultaneously increased.

In FETs, the charge carrier density is calculated at the semiconductor/insulator interface as function of gate voltage. Furthermore, the experimental field-effect mobility is also determined from Eq. 4.1 as function of gate voltage.

The experimental mobilities obtained from the hole-only diode and the field-effect transistors are presented together in Figure 4.6, for both OC_1C_{10}-PPV and P3HT in the charge carrier density range from 10^{20} to 10^{25} m^{-3}. The combined results from the diode and field-effect measurements show‘ that the hole mobility is constant for charge carrier densities $< 10^{22}$ m^{-3} and increases with a power law for densities $> 10^{22}$ m^{-3}. The big differences in mobility values obtained from diodes and FETs, based on a single semiconducting disordered polymer, are due to the large differences in charge densities.

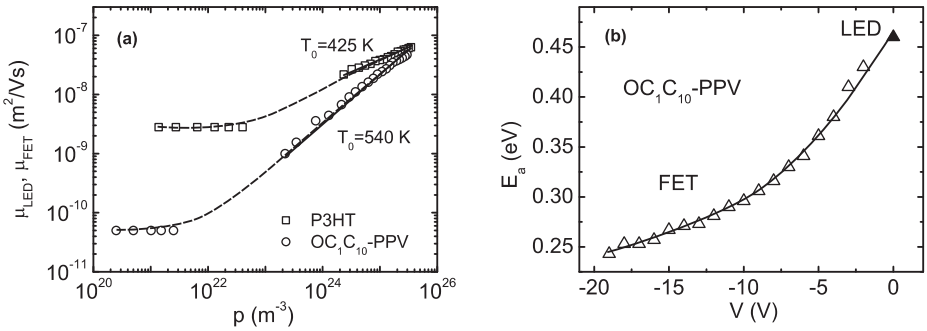

Figure 4.6: (a) Hole mobility as function of hole density p in hole-only diode and FET for P3HT and OC_1C_{10}-PPV (symbols). The solid lines represent the mobility as calculated from Eq. 4.5. The dashed lines are guides for the eye. (b) The activation energy of the mobility for OC_1C_{10}-PPV in both devices.

It has been reported that in OC_1C_{10}-PPV the optical properties exhibit a significant anisotropy [15]. But a possible anisotropy in the charge transport properties in direction perpendicular and parallel to the substrate would obscure a direct comparison between diodes and FETs. In a LED, the amount of energetic disorder is directly reflected in the thermal activation of the low-field mobility. For the (logarithm of) low-field mobility obtained from PPV-based LEDs it is difficult to discriminate whether its temperature dependence scales with $1/T$ or $1/T^2$ (Eqs. 2.7 and 2.11), due to the limited temperature range accessible in the experiments (150-300 K). When plotted against $1/T$ the mobility is also well described by $\mu \propto \exp(-E_a/k_BT)$, and an activation energy E_a of typically 0.48 eV for OC_1C_{10}-PPV has been reported [7]. Also for transistors the field-effect mobility is thermally activated by a gate-voltage dependent activation energy [16]. The activation energy E_a of the field-effect mobility is plotted for OC_1C_{10}-PPV as a function of gate voltage from -1 to -19 V in Figure 4.6b. Extrapolation towards $V_g = 0$ V yields an activation energy $E_a = 0.46$ eV, exactly

equal to the activation energy as obtained from the diode measurements. This is a strong indication for the absence of anisotropy in the charge transport properties.

The question that remains is whether the mobility description at low carrier densities, using a Gaussian DOS, is fundamentally different from the mobility description at high carrier densities, which employs an exponential DOS. In order to compare the two theoretical models used to explain the charge carrier transport in LEDs and FETs, we plotted together the Gaussian DOS (Eq. 2.5) and the exponential DOS (Eq. 2.12) as function of energy for our polymers. In Figure 4.7 the Gaussian DOS, as obtained from the temperature dependent diode measurements, is plotted as a function of energy for P3HT and OC_1C_{10}-PPV. For the total number of states per volume unit N_t we have used a value of 3×10^{26} m^{-3} for both P3HT and OC_1C_{10}-PPV, which corresponds to an average transport site separation $a = 1.4$ nm. Additionally, the exponential DOS of OC_1C_{10}-PPV and P3HT as obtained from the FET characteristics are shown, which are described by the characteristic temperature T_0. Both Gaussian and exponential DOS are presented on a semilogarithmic scale.

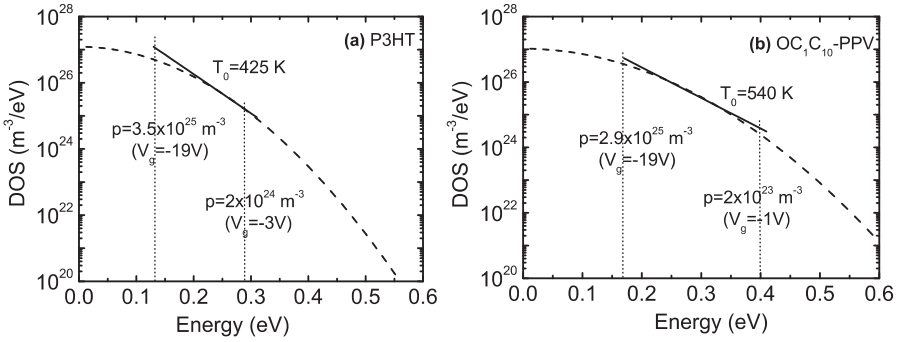

Figure 4.7: Gaussian DOS as obtained from hole-only diode analysis (Eq. 2.5) (dashed lines) and exponential DOS as obtained from FET analysis (Eq. 2.12) (solid lines) as function of energy for P3HT (a) and OC_1C_{10}-PPV (b).

The Fermi-level in the Gaussian for the charge carrier density range in which the P3HT FET operates ranges from 0.27 eV to 0.13 eV with respect to the center of the Gaussian DOS. From Figure 4.7a it appears that in this energy range the exponential distribution with $T_0 = 425$ K is a good approximation of the Gaussian DOS with $\sigma_{DOS} = 98$ meV. Similar behavior is observed for OC_1C_{10}-PPV in Figure 4.7b. The exponential distribution with $T_0 = 540$ K approximates well the Gaussian DOS with $\sigma_{DOS} = 110$ meV in the energy range from 0.4 eV to 0.16 eV. This unifies the two models, in the sense that the exponential DOS accurately describes the Gaussian DOS in the energy range in which the field-effect transistors operate. Consequently, the field, temperature and density dependence of the hole mobility in these disordered conjugated polymers are unified in one single charge transport model. An effect that we ignored in this comparison is that the density of states could be modified due to the induced charges. Recent model calculations demonstrate that an increase of the

doping level also increases the energetic disorder due to potential fluctuations caused by the Coulomb field of randomly distributed dopant ions [17]. In a FET the charge carrier density is increased by a gate field. The fact that the models for LED and FET can be unified indicates that the effect of Coulomb field of the induced charge alone, without counter ions, is less pronounced for the used gate voltage range.

In conclusion, it has been demonstrated that the large mobility differences (up to three orders of magnitude) between experimental hole mobility for one single disordered polymer-based diode and FET originates from the strong dependence of the hole mobility on the charge carrier density. The exponential density of states, which consistently describes the field-effect measurements, is shown to be a good approximation of the Gaussian density of states in the energy range where the Fermi level is varied.

4.3 Origin of the enhanced SCLC in PPV-based diodes

4.3.1 Introduction

When measured at low voltages, the current-voltage characteristics of a polymer LED shows a quadratic behavior, indicating that the current is space-charge limited (SCL) and is governed by a constant charge mobility. At high bias voltages the current is larger than the expected SCLC and this was attributed to an increase of the charge mobility with the electric field. The concept of SCLC and a field and temperature dependent mobility has been extensively applied to transport measurements in organic semiconductors. For instance, it has been used to analyze the charge carrier mobility of various PPV-derivatives [18, 19], the current and transient transport in various PPV- and polyfluorene-derivatives [20,21], and the electron transport in diodes based on small molecules of tris(8-hydroxyquinolato)aluminum [22]. The field dependent mobility (Eq. 2.11) has been incorporated in numerical simulations to model the current-voltage characteristics and the transients of PPV-based LEDs [23–25].

In a space charge-limited device an increase of the applied bias gives rise to a simultaneous increase of the electric field and charge carrier density. Consequently, at high voltages, it is difficult to distinguish between the contributions of the charge carrier density and the electric field to the mobility from the current-voltage characteristics (See Figure 4.5). For the understanding of the charge transport in polymer devices it is crucial to know whether the current is governed by the field and/or the carrier density dependence of the mobility. In the analysis of charge transport properties of polymer SCL devices the charge carrier density dependence of the mobility has not yet been taken into account. Neglecting the density dependence of hole mobility can lead to an incorrect charge carrier and field distribution in organic SCL diodes.

4.3.2 Charge carrier density dependent mobility in LEDs

To investigate the enhancement of the SCLC we try to understand if the contribution of the electric field is more important than the contribution of the charge carrier density to the mobility, or they are equally important? In *Section 4.2*, we presented a combined study on polymer diodes and FETs. It has been demonstrated that the hole mobility of OC_1C_{10}-PPV is constant for charge carrier densities typically $< 10^{22}$ m^{-3} and increases with a power law with density for carrier densities $> 10^{22}$ m^{-3}. In the analysis of charge transport properties of polymer SCL devices such dependence has not yet been taken into account. Combination of the diode and field-effect measurements shows that at room temperature the dependence of the hole mobility on charge carrier density can be described by the empirical relation:

$$\mu_{LED}(p) = \mu_{LED}(F=0) + \frac{\sigma_0}{e}\left[\frac{\left(\frac{T_0}{T}\right)^4 \sin\left(\pi\frac{T_0}{T}\right)}{(2\alpha)^3 B_C}\right]^{\frac{T_0}{T}} p^{\frac{T_0}{T}-1} \qquad (4.7)$$

It should be noted that this unification is only possible for highly disordered polymers such as OC_1C_{10}-PPV, in which the charge transport is isotropic [13]. For more ordered PPV derivatives the transport is anisotropic, depending on the ordering in the polymer film. In this situation the charge mobility is different for different directions and unification is not possible [26].

As a first step the SCL current is calculated using only the density-dependent mobility as given by Eq. 4.7. In these calculations any field-dependence of the mobility is disregarded. It should be noted that, in contrast with Eq. 2.11, where the field enhancement parameter γ is used as a fit parameter to describe the SCLC, the density dependence of the mobility as given by Eq. 4.7 does not contain any fit parameter; the mobility at low density directly follows from the quadratic part of the J–V diode characteristics, whereas the power-law dependence at high carrier densities is independently measured in the FET. The SCL current is now calculated by combining Eq. 4.7 with Eqs. 2.9 and 2.10. By numerically solving Eqs. 4.7, 2.9 and 2.10, the J-V characteristics of OC_1C_{10}-PPV are obtained, as shown in Figure 4.8 by the solid lines.

It can be observed that at $T = 275$ K and $T = 293$ K the calculated SCL current density for OC_1C_{10}-PPV at high fields is in good agreement with the experimental current densities. Surprisingly, a possible field-dependence of hole mobility, which has been used as an explanation for the SCL current enhancement at high bias [18–25], is not required to describe the experimental J–V characteristics. Therefore, the field enhancement of the mobility at room temperature has only a minor effect. As an upper limit we estimate that $\gamma(T)$ at room temperature is at least more than one order of magnitude lower than reported values [27]. Furthermore, from Figure 4.8 it appears that at temperatures lower than $T = 275$ K the carrier density dependence of the mobility alone does not explain the observed increase of the SCLC. Apparently, at low temperatures the field dependence of the mobility becomes important.

In Figure 4.9a the experimental mobility (symbols) and the dependence of the mobility on charge carrier density calculated using Eq. 4.7 (solid lines) are presented

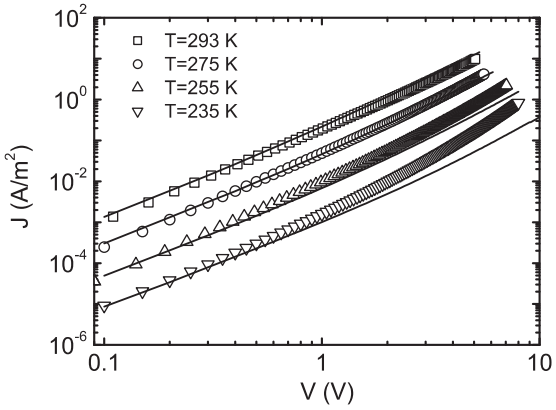

Figure 4.8: Temperature dependent J–V characteristics of the OC_1C_{10}-PPV hole-only diode. The solid lines represent the prediction from Eq. 4.7.

for various temperatures and carrier densities in the range of 3×10^{20} m^{-3} to 3×10^{25} m^{-3} for OC_1C_{10}-PPV. A good agreement between experimental and calculated data is obtained. This experimentally determined mobility dependence on carrier density now enables us to disentangle the contributions of the electric field and the carrier density to the enhancement of the SCL current at high bias.

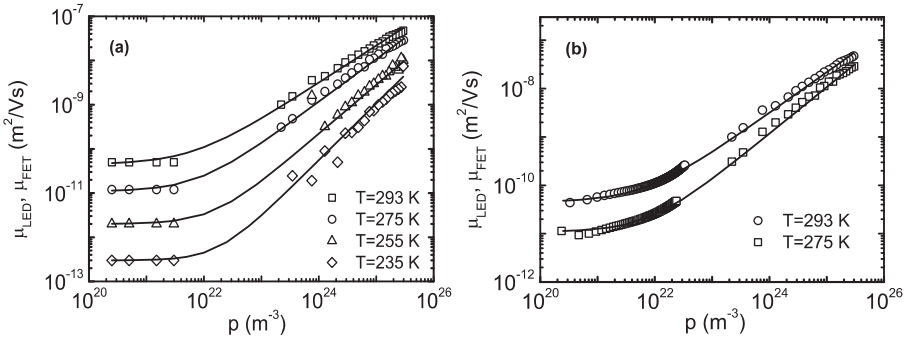

Figure 4.9: Temperature dependent mobility $\mu_{LED}(p)$, $\mu_{FET}(p)$ versus hole density p for OC_1C_{10}-PPV. The solid lines are calculated using Eq. 4.7.

A frequently asked question is: why the experimental mobility versus density plot in Figure 4.9a exhibits a gap in the 10^{22}–10^{23} m^{-3} density range? This density range is not accessible by FET measurements since it would require very small gate voltages, resulting in channel currents below the measurement accuracy. The LED data at voltages higher than 1 V (carrier densities $> 3 \times 10^{23}$ m^{-3}) were not used since the carrier density dependence of μ_{LED} can not be discriminated from the field dependence of μ_{LED}. However, the observed dominance of the density dependence of the mobility on the SCL current at $T > 255$ K now enables us to determine the

mobility-density relation directly from the J–V characteristics over the full voltage range. By comparison with numerical simulations, we obtained that the SCL current, with a density dependent mobility according to Eq. 4.7 through a device with thickness h, can be approximated by:

$$J = 0.8ep_{av}\mu_{LED}\left(p_{av}\right)F_{av} \tag{4.8}$$

with $F_{av} = V/h$, p_{av} the average density in the device given by the equation $p_{av} = 1.5(\epsilon_0\epsilon_s V/eh^2)$, and $\mu_{LED}(p_{av})$ the mobility at density p_{av}. For an experimental J–V characteristic F_{av} and p_{av} can be directly calculated for any applied voltage V and from the corresponding J the mobility $\mu_{LED}(p_{av})$ follows directly from Eq. 4.8. We tested this approximation by using the numerically simulated J–V characteristics, with $\mu_{LED}(p)$ from Eq. 4.7, as input for the above-mentioned procedure. The resulting $\mu_{LED}(p_{av})$ relation followed the analytical $\mu_{LED}(p)$ relation (Eq. 4.7) within a few percent. After this confirmation, the procedure has been used to extract the mobility/density relation directly from the experimental J–V curves (Figure 4.8) at $T = 275$ K and $T = 293$ K. The result is shown in Figure 4.9b together with the transistor data. The experimental SCLC and FET mobilities adjust very well and now nearly cover the whole density range. As a result the combination of J–V and field-effect measurements provides a consistent description of the mobility-density relation in OC_1C_{10}-PPV, and is indeed well described by Eq. 4.7 as previously assumed. In fact, since the onset of the power-law is already clearly visible from the SCLC measurement, the complete current transport in a FET can be predicted from the hole only diode measurements. The same analysis has been applied to other disordered polymers and similar consistent mobility-density dependencies have been found. Recently, a model has been proposed by Pasveer *et al.* which confirms that at room temperature it is mainly the dependence on charge density that plays an important role [31].

The fundamental question whether the increase of the mobility in a SCL device is dominated by either the carrier density or the electric field is relevant for the operation of light emitting diodes. In Figure 4.10 the distribution of the electric field $F(x)$ as a function of distance x from the ITO injecting anode is plotted in a single carrier SCL diode. For a constant mobility the electric field varies with position as $F(x) = (2Jx/\epsilon_0\epsilon_s\mu_{LED})^{1/2}$ (dotted line), and the hole concentration with $p \propto x^{-1/2}$. For a mobility that only depends on the electric field (Eq. 2.11) the charge carriers close to the injection contact will experience a low field. The charge carriers close to the Au non-injecting cathode on the other hand will experience a high field with resulting field-enhanced mobility. Since the current through the device is position independent the field close to the injecting contact will be increased, whereas the field at the collecting contact will be decreased, as shown in Figure 4.10 (solid line). However, for a mobility that is dominated by the carrier density the mobility will be large close to the injecting contact, where the charge carrier density is largest, and low at the collecting contact. Consequently, the field will be enhanced at the collecting contact and reduced at the injecting contact, in contrast to the field dependent case (Figure 4.10, dashed line).

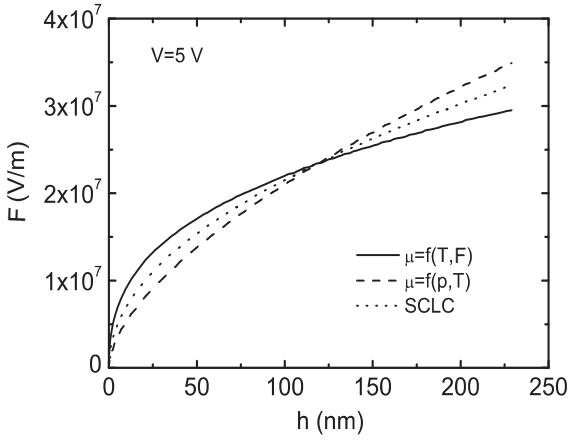

Figure 4.10: Calculated distribution of the electric field $F(x)$ in OC_1C_{10}-PPV diode at $V = 5$ V and $T = 293$ K.

Figure 4.10 shows that the electric field distribution in a polymer SCL diode is strongly dependent on the microscopic origin for the mobility enhancement. At low temperatures the distribution of the electric field becomes closer to earlier reported model calculations, because the field dependence becomes more important. This is due to the fact that at low temperatures the activated hops between neighboring sites are strongly suppressed, which means that the charge transport is also suppressed. Application of an electric field leads to a reduction of these dominant barriers for the charge transport in the field direction, resulting in strong field dependence.

4.3.3 Thickness dependence of SCLC in PPV-based LEDs

Now the charge transport in a LED based on a PPV derivative is investigated as a function of sample thickness. The thickness dependence can be used to discriminate the effect of a field from that of a density dependent mobility [32]. As a first step we check whether the experimental current at low voltages obeys the conventional Child's law (Eq. 2.8) [14]. In Figure 4.11 the current density-voltage (J–V) measurements are presented for NRS-PPV hole-only diodes with thicknesses h of 200 nm, 560 nm and 950 nm. The observed occurrence of a SCL current enables a direct determination of the hole mobility for NRS-PPV at low voltages, being 5×10^{-12} m^2/Vs. For a field dependent mobility of the form $\mu(F) = \mu_0 \exp\left(\gamma\sqrt{F}\right)$ it is demonstrated that the SCLC can be approximated by [28]:

$$J = \frac{9}{8}\epsilon_0\epsilon_s\mu_{LED}(F=0)\exp\left(0.89\gamma\sqrt{F}\right)\frac{V^2}{h^3} \tag{4.9}$$

For a large field-enhancement factor γ the exponential term will dominate the increase of the current. As a result, depending on the magnitude of γ, the SCL current at high voltages will proportional with V^2/h^3 or V/h. On the other hand, for a

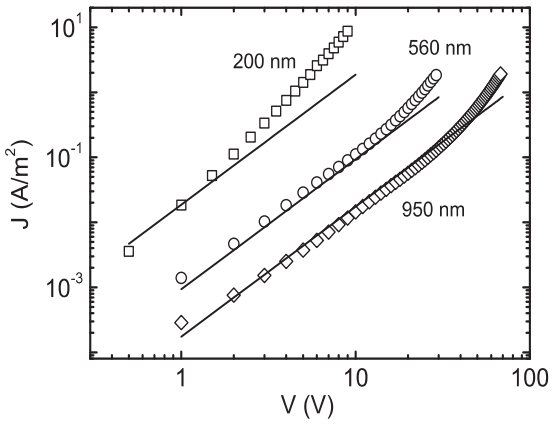

Figure 4.11: Room temperature J-V characteristics of NRS-PPV hole-only diodes with thicknesses of 200nm, 560 nm and 950 nm. The solid lines represent the prediction from the SCL model using a constant hole mobility of 5.0×10^{-12} m_2/Vs.

density dependent mobility $\mu_{LED}(p)$ (Eq. 4.7) J can be approximated by Eq. 4.8 [29]. Combining Eq. 4.7 with Eq. 4.8 leads to a thickness dependence of the form:

$$J \propto \frac{V}{h^2} \cdot \left(\frac{V}{h^2}\right)^{\frac{T_0}{T}-1} \cdot \frac{V}{h} \propto \frac{V^{\frac{T_0}{T}+1}}{h^{\frac{2T_0}{T}+1}} \tag{4.10}$$

For $T_0 = T$ this will lead to the conventional V^2/h^3 behavior and for $T_0 >> T$ the thickness dependence will approach a V/h^2 scaling. Consequently, the conventional V^2/h^3 will be weakened by a field-dependent mobility (V/h) and enhanced by a density dependent mobility (V/h^2). In this way, the thickness dependence of the SCL current at high voltages can be used to discriminate between the contributions from field and charge carrier density.

In order to model the SCL currents with either $\mu_{LED}(F)$ or $\mu_{LED}(p)$ Eqs. 2.9, 2.10, 2.11 and 4.7 are combined. In Figure 4.12a the experimental J–V characteristics are shown together with the numerical model calculations using a field-dependent mobility only. As a reference, the 200 nm device is fitted to determine the field enhancement factor $\gamma = 5 \times 10^{-4}$ $(\mathrm{m/V})^{1/2}$, in agreement with earlier results on OC_1C_{10}-PPV [27]. This γ value is then used to predict the SCL currents for the thicknesses of the 560 nm and 950 nm devices. As shown in Figure 4.12a, the predicted currents (solid lines) clearly overestimate the SCL currents at high voltages. Apparently, the calculated thickness dependence using $\mu_{LED}(F)$ is too weak. Fitting the experimental data would lead to a γ of 3×10^{-4} $(\mathrm{m/V})^{1/2}$ and 2×10^{-4} $(\mathrm{m/V})^{1/2}$ for the 560 nm and 950 nm device, respectively. A thickness dependent γ is of course not physical.

In Figure 4.12b, the predicted current (dotted lines) using $\mu_{LED}(p)$ shows better agreement for the whole thickness range studied. The calculated currents do not contain any fit parameter. This result demonstrates that the experimental J–V

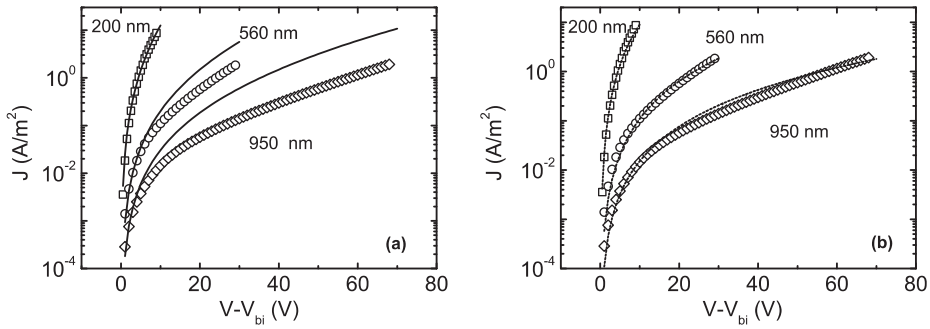

Figure 4.12: Room temperature J-V characteristics of NRS-PPV hole-only diodes with thicknesses of 200nm, 560 nm and 950 nm. The solid lines represent the prediction from the SCL model combined with a field dependent mobility (Eq. 2.11) ($\gamma = 5 \times 10^{-4}$ (m/V)$^{1/2}$. The dashed lines represent the prediction from the SCL model combined with a density dependent mobility (Eq. 4.7).

characteristics indeed exhibit the enhanced thickness dependence, as expected from the density dependent mobility. This observation is therefore a clear proof of the dominance of a density dependent mobility in the current in polymer LEDs. The injected charges will first occupy the energetically lowest localized states of the organic semiconductor. With increasing voltage the additional charges in the SCL diode fill up these lower states and therefore will need less activation energy for hops towards neighboring sites. As a result the charge carrier mobility will be enhanced at higher voltages.

4.3.4 Conclusion

It has been demonstrated that the SCL current in diodes based on the conjugated polymer OC_1C_{10}-PPV is governed by the dependence of the hole mobility on electric field and charge carrier density. At room temperature the charge carrier density dependence of the mobility is dominant, in contrast to earlier reported results, while at low temperatures the field dependence of the mobility must be taken into account. Omission of the density dependence can lead to an underestimation of the field at the collecting contact. Via the thickness dependence the contributions from the electric field and charge carrier density to the hole mobility can be disentangled. The enhanced thickness dependence of experimental SCL current in PPV is in agreement with the prediction using a density dependent mobility only.

Bibliography

[1] M. C. J. M. Vissenberg, M. Matters, *Phys. Rev. B* **57**, 12 964 (1998).

[2] A. R. Brown, C. P. Jarrett, D. M. de Leeuw, M. Matters, *Synth. Met.* **88**, 37 (1997).

[3] S. M. Sze, *Physics of semiconductor devices*, Wiley, New York (1981).

[4] M. Shur, M. Hack, J. G. Shaw, *J. Appl. Phys* **66**, 3371 (1989).

[5] C. Tanase, E. J. Meijer, P. W. M. Blom, D. M. de Leeuw, *Org. Electronics* **4**, 33 (2003).

[6] G. E. Pike, C. H. Seager, *Phys. Rev. B* **10**, 1421 (1974).

[7] P. W. M. Blom, M. C. J. M. Vissenberg, *Mat. Sc. and Engineering* **27**, 53 (2000).

[8] H. Bässler, *Phys. Stat. Sol. B* **175**, 15 (1993).

[9] S. V. Novikov, D. H. Dunlap, V. M. Kenkre, P. E. Parris, A. V. Vannikov, *Phys. Rev. Let.* **81**, 4472 (1998).

[10] A. Assadi, C. Svensson, M. Willander, O. Inganäs, *Appl. Phys. Lett.* **53**, 195 (1988).

[11] H. Sirringhaus, P. J. Brown, *Nature* **401**, 685 (1999).

[12] E. J. Meijer, C. Tanase, P. W. M. Blom, E. Van Veenendaal, B. -H. Huisman, D. M. De Leeuw, T. M. Klapwijk, *Appl. Phys. Lett.* **80**, 3838 (2002).

[13] C. Tanase, E. J. Meijer, P. W. M. Blom, D. M. de Leeuw, *Phys. Rev. Lett.* **91**, 216601 (2003).

[14] M. A. Lampert, P. Mark, *Current injection in solids*, Academic Press, New York (1970).

[15] C. M. Ramsdale, N. C. Greenham, *Adv. Mater.* **14**, 212 (2002).

[16] E. J. Meijer, M. Matters, P. T. Herwig, D. M. de Leeuw, T. M. Klapwijk, *Appl. Phys. Lett.* **76**, 3433 (2000).

[17] V. I. Arkhipov, P. Heremans, E. V. Emelianova, G. J. Adriaensses, H. Bässler, *Appl. Phys. Lett.* **82**, 3245 (2003).

[18] L. Bozano, S. A. Carter, J. C. scot, G. G. Malliaras, P. J. Brock, *Appl. Phys. Lett.* **74**, 1132 (1999).

[19] H. C. F. Martens, P. W. M. Blom, and H. F. M. Schoo, Phys. Rev. B **61**, 7489 (2000).

[20] D. J. Pinner, R. H. Friend, and N. Tessler, *J. Appl. Phys.* **86**, 5116 (1999).

[21] A. J. Campbell, D. D. C. Bradley, and H. Antoniadis, *J. Appl. Phys.* **89**, 3343 (2001).

[22] W. Brütting, S. Berleb, and A. G. Mückl, *Synth. Met.* **122**, 99 (2001).

[23] P. W. M. Blom, and M. J. M. De Jong, *IEEE J. Sel. Top. Quant. Electr.* **4**, 105 (1998).

[24] G. G. Malliaras, and J. C. Scott, *J. Appl. Phys.* **85**, 7426 (1999).

[25] D. J. Pinner, R. H. Friend, and N. Tessler, *Appl. Phys. Lett.* **76**, 1137 (2000).

[26] C. Tanase, P. W. M. Blom, E. J. Meijer, D. M. de Leeuw, *Proc. of SPIE* **5217**, 80 (2003).

[27] P. W. M. Blom, M. J. M. de Jong, M. G. van Munster, *Phys. Rev. B.* **55**, R656 (1997).

[28] P. N. Murgatroyd, *J. Phys. D* **3**, 151 (1970).

[29] C. Tanase, P. W. M. Blom, D. M. de Leeuw, *Phys. Rev. B* **70**, 1 (2004).

[30] C. Tanase, P. W. M. Blom, D. M. de Leeuw, E. J. Meijer, *Phys. Status Solidi A* **201**, 1236 (2004).

[31] W. F. Pasveer, J. Cottaar, C. Tanase, R. Coehoorn, P. A. Bobbert, P. W. M. Blom, D. M. de Leeuw, M. A. J. Michels, submited to *Phys. Rev. Lett.*.

[32] P. W. M. Blom, C. Tanase, D. M. de Leeuw, R. Coehoorn, *Appl. Phys. Lett.* **86**, 92105 (2005).

Chapter 5

Isotropic versus anisotropic charge transport in PPV-based LEDs and FETs

Summary

A systematic study on the influence of the processing conditions on the charge carrier mobility in hole-only diodes and field-effect transistors based on alkoxy substituted PPVs has been performed. It is demonstrated that by chemical modification from asymmetrically to symmetrically substituted PPVs the mobility in both types of devices can be significantly improved. Furthermore, for symmetrical PPVs the mobility is strongly dependent on processing conditions as choice of solvents and annealing conditions. The increase in mobility is accompanied by a strong enhancement of the anisotropy in the charge transport parallel and perpendicular to the substrate. Ultimately, mobilities of up to 10^{-6} m^2/Vs in FETs and 10^{-9} m^2/Vs in hole-only diodes have been achieved.

5.1 Introduction

The use of solution processable semiconductors in optoelectronic devices [1–3] and integrated circuits [4–6] is of major importance for the commercialization of low-end high-volume microelectronics. Applications are foreseen in integrated circuits for disposable smart labels and transponders, field-effect transistors in pixel engines and integrated drivers of flexible displays, electronic paper, and as an active component in sensors or in polymer solar cells [6–8].

Charge carrier mobilities of PPVs are low in LEDs, typically in the area of 10^{-11} m^2/Vs. In order to obtain highly competitive LEDs, these materials must be optimized, for example by controlling the film morphology. This can be manipulated by processing factors such as various organic solvents, solution concentrations and temperatures, spin-coating procedures, and annealing temperatures [5]. Thermal treatment of the disordered polymers can modify the film morphology and thus improve the electrical properties of the LEDs such as quantum efficiency, turn-on voltage, and electroluminescence [9, 10]. It has been suggested that when annealing PPV, e.g., poly(2-methoxy-5-(2‘-ethyl-hexyloxy)-*p*-phenylene vinylene) (MEH-PPV), at a temperature higher than the glass transition temperature (T_g) the polymer chains relax. As a result a smoother interface contact between the polymer and the cathode is formed, resulting in an increased electron injection. Other studies focused on the influence of the solvent on the polymer film properties [10–13]. It has been shown that the absorbance and the photoluminescence (PL) spectrum of MEH-PPV film obtained from chlorobenzene solution, which is an aromatic solvent, is red-shifted compared with that in tetrahydrofuran, which is a nonaromatic solvent. This shift was attributed to the formation of aggregates, which is solvent dependent. NMR studies of the polymer solution (MEH-PPV in toluene) revealed well-packed chains formed in order to minimize polymer-solvent interactions. The increase of the field-effect mobility from toluene to chlorobenzene solution in poly(2-methoxy-5-(3’,7’-dimethyloctyloxy)-*p*-phenylene vinylene) ($OC_{10}C_{10}$-PPV) FETs has also been explained on the basis of a modification of the polymer morphology [14]. Here, different classes of easily accessible alkoxy substituted PPVs are examined. The influence of the substitution pattern of the phenyl ring (asymmetrical or symmetrical), the nature of the side chain (linear or branched) and the processing of the semiconductor on the charge mobility in LEDs and FETs is investigated.

5.2 The influence of chemical modification and processing of alkoxy PPVs on charge transport

5.2.1 The influence of chemical modification of PPVs on the charge mobility

The general chemical formula of the alkoxy substituted PPVs used as active layers in field-effect transistors and hole-only diodes is presented in Figure 5.1. These polymers are symmetric or asymmetric, depending on the substitution pattern of the phenyl

ring R^1, R^2, and R^3, which are linear or branched alkyl chains (See Table 5.1). Examples are the asymmetric branched PPVs OC_1C_{10}-PPV (A), and MEH-PPV (B). In copolymers D, E and F a certain amount of asymmetrical monomer was incorporated and their side chains are branched. The random copolymers G - J consist of two symmetrically substituted monomers in a 1:1 ratio. In this case, linear alkyl chains instead of the branched alkyl chains are used. Polymerization followed a modified Gilch dehydrohalogenation procedure [15, 16] and it is explained in more details in Ref. [17]. NRS-PPV has been synthesized according to the procedure indicated in Ref. [18]. Molecular weights (Mw) have been determined by gel permeation chromatography (GPC) and they are in the range 1.3×10^5–1.4×10^6 g/mol. Despite the high molecular weights of these polymers, all (co)polymers are nicely soluble in common organic solvents (e.g. $\geq$5 mg/ml in toluene, xylene, chlorobenzene) and can therefore be processed into homogeneous thin films by standard solution-based coating processes like spin-coating or knife casting.

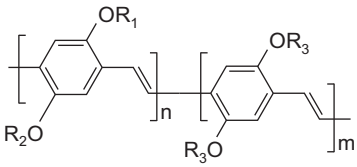

Figure 5.1: Chemical structure of alkoxy-substituted PPVs.

First, we compare the electrical transport properties of the asymmetrically and symmetrically substituted PPV derivatives in both field-effect and hole-only devices. In Table 5.1 the values of the hole mobility in the two types of devices are presented. For a direct comparison we used for all the polymers only one solvent, namely chlorobenzene.

The field-effect mobility has been determined in the linear operating regime of the FET at a gate voltage $V_g = -19$ V and a drain voltage $V_d = -2$ V, while the zero-field mobility in the hole-only diode has been determined using the space-charge limited current model (See *Chapter 4*). From Table 5.1 it can be observed that the field-effect mobility for the asymmetrically substituted PPVs is in the range of $1 - 5 \times 10^{-8}$ m^2/Vs, while for the symmetrically substituted PPVs it is in the range of $7 \times 10^{-8} - 6 \times 10^{-7}$ m^2/Vs. The same increase of the mobility from the asymmetrical PPVs to the symmetrical PPVs is observed for hole-only diodes as well, namely from $1 \times 10^{-12} - 5 \times 10^{-11}$ m^2/Vs to $2 \times 10^{-10} - 9 \times 10^{-10}$ m^2/Vs. In a PPV-based diode 9×10^{-10} m^2/Vs is the highest mobility value reported so far.

In a diode, the hole mobility determined for the symmetrically substituted PPVs is more than three times higher than for the asymmetrically substituted ones, while the field-effect mobility is at least a decade larger. This can be explained by the fact that chemical modification of PPV influences both the electronic [19, 20] and morphologic properties in terms of interchain distance, orientation and packing of the polymer chains. Using the technique of phase-imaging scanning force microscopy [21] it has been demonstrated that the symmetrical PPVs exhibit an increased regularity and a

	Polymer (n,m)	R^1	R^2	R^3	μ_{FET} (m^2/Vs)	μ_{LED} (m^2/Vs)
Asym. subst. PPVs	NRS				1×10^{-8}	1×10^{-12}
	A(1,0)	CH_3	$C_{10}H_{21}$		4×10^{-8}	5×10^{-11}
	B(1,0)	CH_3	C_8H_{17}		5×10^{-8}	5×10^{-11}
Sym. subst. PPVs	C(0,1)			C_8H_{17}	9×10^{-8}	4×10^{-10}
	D(0.5,0.5)	CH_3	$C_{10}H_{21}$	$C_{10}H_{21}$	1×10^{-7}	6×10^{-10}
	E(0.06,0.94)	CH_3	C_5H_{11}	$C_{10}H_{21}$	1×10^{-7}	2×10^{-10}
	F(0.5,0.5)	CH_3	C_8H_{17}	C_8H_{17}	7×10^{-8}	3×10^{-10}
	G(0.5,0.5)	C_8H_{17}	C_8H_{17}	$C_{18}H_{37}$	6×10^{-7}	5×10^{-10}
	H(0.5,0.5)	$C_{10}H_{21}$	$C_{10}H_{21}$	$C_{18}H_{37}$	2×10^{-7}	6×10^{-10}
	I(0.5,0.5)	$C_{11}H_{23}$	$C_{11}H_{23}$	$C_{18}H_{37}$	2×10^{-7}	9×10^{-10}
	J(0.5,0.5)	$C_{12}H_{25}$	$C_{12}H_{25}$	$C_{18}H_{37}$	2×10^{-7}	2×10^{-10}

Table 5.1: Chemical composition and charge carrier mobility of the PPVs under investigation. All measurements have been performed in polymer films obtained from chlorobenzene solution.

better ordering in the solid state. This results in a reduced energetic disorder, better interchain interaction and, as a consequence, a better charge transport. The difference in charge carrier mobilities between asymmetrically and symmetrically substituted PPVs was also reported by Martens *et al.* [20]. They found a higher zero-field mobility in hole-only diodes for the symmetrically substituted PPV and observed that the energetic disorder σ in the symmetrically substituted PPV is significantly less and the localization length larger than in the asymmetrical one. It has also been observed that by adding an asymmetrical monomer to a symmetrical one the high mobility is not affected (polymers C and F from Table 5.1).

5.2.2 The influence of processing conditions on charge mobility

It has been shown in the literature that both optimization of processing (e.g. annealing of the semiconductor [9,22]), and optimization of the transistor configuration (e.g. surface alignment layers [23], choice of gate insulator [24]) can further improve the performance of FETs. Thermal annealing of semiconductors like OC_1C_{10}-PPV (B) and MEH-PPV (C) at temperatures beyond T_g results in significant red-shift of the PL spectra, which was related to emissions from interchain species, such as aggregates or excimers [25].

Our attempts to improve the electrical performance of asymmetrical PPVs in devices by annealing in vacuum over a temperature range of 80–200°C for 5–120 minutes failed. No significant improvement of the low mobility upon annealing was observed. In contrast, the symmetrically substituted PPVs showed an increase in the

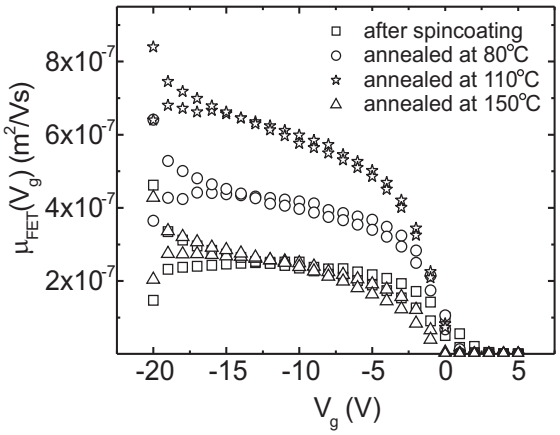

Figure 5.2: Field-effect mobility of polymer J before and after annealing ($V_d = -2$ V).

mobility for annealing temperatures lower than 110°C. Although the FETs prepared from linear alkyl chains copolymer PPVs exhibit mobilities in the range of 2×10^{-7} m^2/Vs after spin-coating and exceed those obtained for other PPVs reported so far, they were also subjected to a thermal treatment for 5-120 minutes. A typical example of such an annealing experiment is depicted in Figure 5.2 for polymer J.

As can be seen from Figure 5.2, the mobility exhibits a value of 2×10^{-7} m^2/Vs after spin-coating at 40°C. The mobility increases to 4×10^{-7} m^2/Vs after annealing the device at a temperature of 80°C, and to 7×10^{-7} m^2/Vs when the device is annealed at 110°C. It is observed that annealing temperatures higher than 110°C lower the mobility. Apparently, an annealing temperature around 110°C is optimum for these PPVs.

Figure 5.3 shows the transfer characteristics of an annealed sample of bisOC_{11}-bisOC_{18}-PPV (I). For this material the field-effect mobility increased from 2×10^{-7} m^2/Vs before annealing to 1×10^{-6} m^2/Vs after annealing. This value is the highest reported for a solution processable PPV in a FET [19].

Electronic properties of conjugated polymer films are also affected by the organic solvents from which the polymer is spin-coated. In the case of different solvents, different film morphology are obtained depending on the nature of the solvent and the solubility of the polymer. By using different solvents in hole-only diodes made from asymmetrically substituted PPVs we do not observe any difference in hole mobility. Figure 5.4 shows the current-voltage characteristics of the hole-only diode using the symmetric polymer C spin-coated from toluene and chlorobenzene as active layer. The experimental zero-field mobility determined from these measurements is 4×10^{-10} m^2/Vs for the chlorobenzene solution and 1×10^{-9} m^2/Vs for the toluene solution. Thus, the zero-field mobility in hole-only devices of symmetrical PPVs varies with solvent. This trend has been also observed for other symmetrically substituted PPVs.

In Figure 5.5 the effect of the solvent on the field-effect mobility and the UV

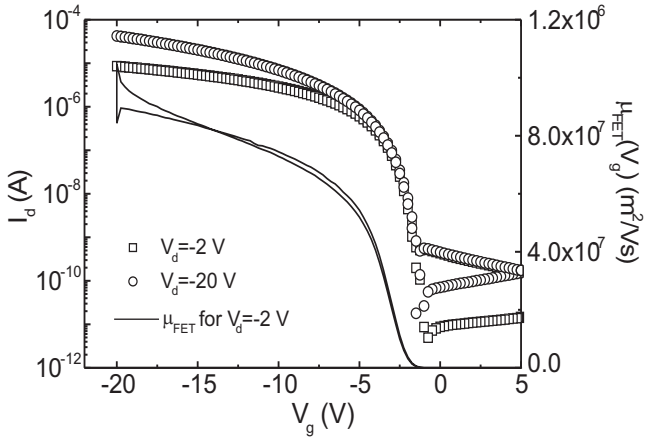

Figure 5.3: Transfer characteristics and the field-effect mobility of polymer I at 110° C.

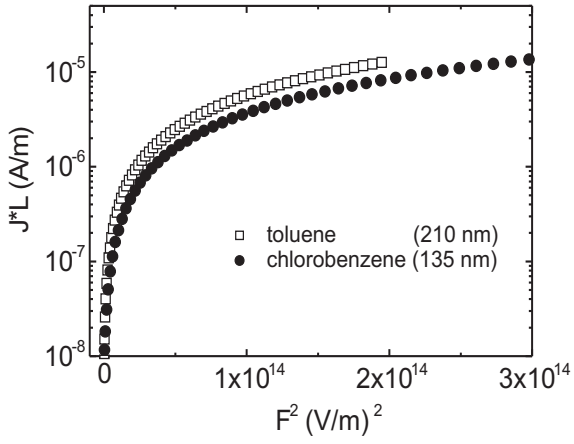

Figure 5.4: Current-voltage characteristics of polymer C spin-coated from toluene and chlorobenzene solution.

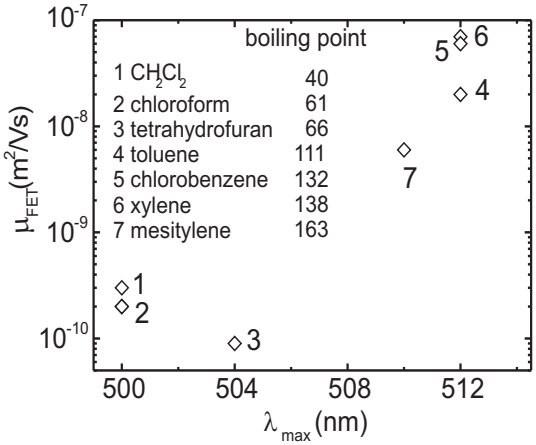

Figure 5.5: The effect of solvent on the maximum absorption peak and field-effect mobility of the spin-coated polymer F from different solvents.

absorption is presented for the symmetric polymer F. In contrast with the hole-only diodes the field-effect mobility shows a strong increase for the films spin-coated from aromatic solvents in comparison with those obtained from non-aromatic solvents, while the absorbance is red-shifted for the film obtained from aromatic solvents with respect to that spin-coated from non-aromatic solvents. This behavior can be attributed to an increased interchain interaction of the π-conjugated backbone in polymer films spin-coated from solvents such as chlorobenzene as compared to that spin-coated from tetrahydrofuran [10, 11] and is reflected in both mobility and UV spectra. When comparing the boiling point of the solvents used in this study we can conclude that solvents with low boiling points, such as chloroform, and CH_2Cl_2, tetrahydrofuran give a very low mobility, while the high boiling point solvents such as chlorobenzene or xylene give a very high mobility. This can be attributed to the fact that the chains of the polymer spin-coated from solvents like chloroform do not have time to rearrange in the polymer network as it happens for example for xylene. However, as mentioned above we do not observe the same trend in the hole-only diode.

We observed that the effects of annealing and solvent on the mobility are very weak for the heavily disordered asymmetric PPVs. For symmetric PPVs these effects are relatively large for the field-effect geometry, but small for hole-only diodes. The explanation is related to the way in which the polymer arranges itself in the film and also to the way in which the transport takes place in the two electronic devices. In hole-only diodes the transport takes place between the two electric contacts perpendicular to the polymer film, while in field-effect transistors the transport takes place in the plane of the polymer film. A possible anisotropy in the charge transport can be investigated by comparing the transport in hole-only diodes and FETs made from the same semiconductor. From Table 5.1 we observe that the field-effect mobility is

much higher than the hole-only mobility. It has been demonstrated in *Chapter 4* that this difference originates in the dependence of the hole mobility on the charge carrier density in disordered semiconducting polymers [19]. It has also been demonstrated that typically the hole mobility is constant for charge carrier densities $< 10^{22}$ m^{-3} and increases with a power law for charge carrier densities $> 10^{22}$ m^{-3}. The mobility differences of up to three orders of magnitude obtained from diodes and FETs, based on a single disordered polymer (OC_1C_{10}-PPV), originate from the different charge density regimes in these two types of devices.

We now compare the mobility results for polymer F obtained in a hole-only diode and a field-effect transistor as function of charge carrier density for two solvents: toluene and chlorobenzene. The experimental hole mobility is plotted in Figure 5.5 in the charge carrier density range of 10^{21}–10^{26} m^{-3}. The details related to the calculation of the experimental mobility as function of charge carrier density are presented in *Chapter 4*. The mobility values obtained from the toluene solution show a smooth connection between hole-only and FETs data (Figure 5.6).

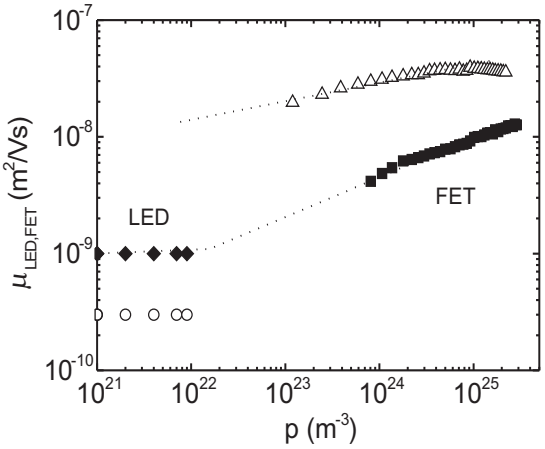

Figure 5.6: The hole mobility of field-effect transistor and hole-only diode as function of charge carrier density for polymer F spin-coated from toluene (closed symbols) and chlorobenzene (open symbols).

The width of the exponential DOS (T_0), which is an indication for the energetic disorder in the polymer, is 390 K. In contrast, for the chlorobenzene solution the mobility behavior presented in Figure 5.6 clearly shows a lack of correlation between diode and field-effect transistor measurements. Furthermore, by using chlorobenzene the width of the exponential DOS decreases to $T_0 = 340$ K. The explanation is that in the case of toluene solution the polymer is more disordered than in the chlorobenzene solution, and the charge transport approaches 3-D like behavior. The chlorobenzene on the other hand evaporates more slowly from the spin-coated film and the polymer chains at the interface with the substrate have more time to rearrange. Apparently, the packing of the polymer chains is more favorable for the charge transport

in the directions parallel than perpendicular to the substrate, leading to an increased anisotropy between hole-only diodes and FETs. Thus, depending on the solvent, the charge transport can be modified in these polymers from isotropic to anisotropic.

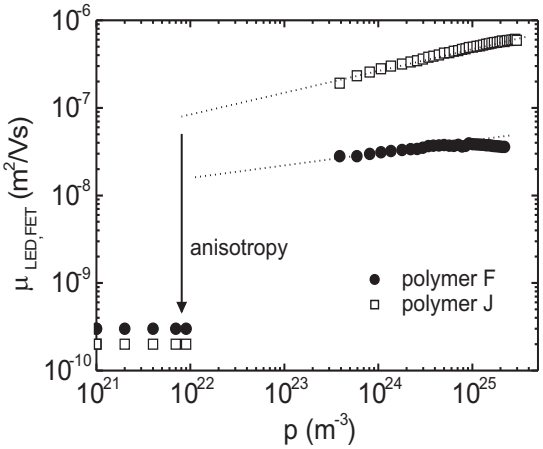

Figure 5.7: The hole mobility of field-effect transistors and hole-only diodes as function of charge carrier density for polymer F and J spin-coated from chlorobenzene.

The anisotropy of the charge transport is a characteristic of high mobility polymers. For example, Sirringhaus *et al.* demonstrated that self-organization in P3HT results in a lamella structure which can orient parallel or perpendicular to the substrate as function of processing conditions and leads to mobilities at very high fields up to 1×10^{-5} m^2/Vs [5]. As a result of this different orientation the anisotropy in mobility was found to be more than a factor of 100. We observe a similar behavior in our high mobility symmetric PPV polymers when chlorobenzene is used as a solvent. In Figure 5.7 the mobility of polymers F and J are presented for hole-only diodes and FETs. We observe that an increase of the FET mobility is accompanied by an increase of the anisotropy. This is a strong indication that the use of specific solvents and annealing procedures in the symmetric PPVs result in a better ordering of the film at the semiconductor/insulator interface, thereby enhancing the in-plane transport.

Conclusion

In conclusion, we have presented the influence of the processing and chemical structure of alkoxy substitutes PPVs on the charge carrier mobility of the field-effect transistor and hole-only diode. By changing the chemical structure of the PPVs the mobility in both types of devices increases for the symmetrically substituted PPVs in comparison with the asymmetrically substituted ones. This is attributed to the increase in the regularity and decrease of the energetic disorder of the polymers. Upon annealing of the FET the asymmetrically substituted PPVs showed little improvement, while

the field-effect mobility of symmetrically substituted PPVs can be strongly improved. The use of different solvents has shown variation in the mobility determined from both hole-only diodes and field-effect transistors for the symmetric PPVs, but not for asymmetric ones. While the transport in asymmetric polymers is isotropic, the anisotropy of charge transport in symmetric polymers is dependent on the solvent. Optimization of chemical structure, annealing, and solvent lead to high mobility of 9×10^{-10} m^2/Vs in a hole-only diode and 1×10^{-6} m^2/Vs in a FET.

5.3 Planar metal-polymer-metal diodes

5.3.1 Introduction

The light in an organic LED, typically fabricated in a sandwich configuration with the polymer layer between a hole-injecting and an electron-injecting electrode, is emitted through a transparent electrode [1,26,27]. This structure is suitable for display applications, but a disadvantage is the requirement of a transparent conductor as bottom or top electrode. In order to circumvent this problem Pei *et al.* used a different approach by developing an electrochemical light-emitting cell (LEC) [28]. They designed a planar device with two opaque electrodes deposited on top of a substrate with a separation of a few microns. An ion-conducting luminescent polymer mixed with an ionically conductive material was spin-coated on top of the device. The active layer is electrochemically p-doped near the anode side and n-doped near the cathode side; a p-n junction is formed between the doped regions. Under an applied electric field the charge carriers move toward the opposite electrode, meet within the p-n junction and recombine radiatively. The main disadvantage of LECs is that their stability is very limited, possibly due to the n- and/or p-type doping of the polymer. As an alternative to LEC, surface LEDs using planar configuration with conventional light-emitting polymers have been created by several groups [29–31]. Electroluminescence from planar metal-polymer-metal structure using LEDs materials such as PPV [29] or polythiophene derivatives [30,31] has been reported. Apart from their practical applicability, these surface-emitting devices are also interesting for basic scientific studies. From spatially resolved electroluminescence measurements the emission zone in such an in-plane device can be obtained.

The transport in the plane of the polymer film is usually investigated in the field-effect geometry. In *Chapter 4* it was demonstrated that the hole transport in sandwiched hole-only diodes and in-plane FETs can be unified for heavily disordered PPV-based semiconductors [32]. The charge carrier density in a space-charge limited diode is orders of magnitude lower as compared to the density induced in a FET. The large differences in hole mobilities obtained in diodes and FETs originates from the strong dependence of the mobility on charge carrier density [32]. A direct comparison, at low carrier density, between charge transport in the plane and perpendicular to the polymer film can be obtained from the observation of an in-plane space-charge limited current. It should be noted that such an observation is not possible in a field-effect structure with zero-gate voltage applied. Due to the relatively long distance of sev-

eral microns between the in-plane electrodes large source-drain voltages are required to obtain a measurable SCLC, which will lead to a breakdown of the gate insulator. Here the transport of holes is studied in planar structures using PPV-based polymers, namely OC_1C_{10}-PPV and NRS-PPV.

5.3.2 Electrical characterization of the in-plane diode

Figure 5.8 shows the experimental current (I) versus electric field (F) characteristics of Au/OC_1C_{10}-PPV/Au devices having a polymer thickness of 270 nm and channel length $L = 1.25$ and 20 μm, respectively. In this device configuration it is difficult to define the effective transport channel. Also included in the figure is the calculated current using Eq. 4.7 (dashed lines). Figure 5.8 demonstrates that at low electric fields the current measured for a planar device is up to six orders of magnitude higher than the expected current. Furthermore, in contrast to the SCLC [27], the experimental currents scale with the applied electric field F=V/L. In the low-field part the experimental current scales linearly with the applied field instead of quadratic as expected from a SCLC. The strongly enhanced current can not be due to a high in-plane mobility; in that case the current would still be quadratic and would not scale linearly with the applied field. Another possible explanation for the large experimental current could be a strong homogeneous doping of the polymer film. In this situation, the low-field part of the experimental current would be strongly enhanced and would scale linearly with the applied field. The current is then described by $I = qp_0\mu FA$, where q is the elementary charge, p_0 the carrier charge density due to doping, μ the hole mobility, A the area of the active channel. Using a low-field mobility of 5×10^{-11} m^2/Vs the observed current requires $p_0 = 2 \times 10^{24}$ m^{-3}. However, the presence of such a high background charge density is highly unlikely, since from LED measurements these PPV-derivatives are known to be undoped [27]. The spin casting is performed in inert nitrogen atmosphere and the measurements are performed in vacuum ($< 10^{-6}$ mbar), so there is no opportunity for the samples to get doped.

As a first test we investigate whether the observed current enhancement is specific for the OC_1C_{10}-PPV or that it also occurs for other PPV-based polymers. In Figure 5.9 we present I-V measurements on both OC_1C_{10}-PPV and NRS, processed under the same conditions (substrate, solvent, environment, device area), for a device length of 5 μm. It is observed that the current of NRS is also strongly enhanced, it is only a factor of three lower as compared to the OC_1C_{10}-PPV current. The hole mobility of NRS-PPV in a LED configuration has been previously determined and amounts to 5×10^{-12} m^2/Vs, such that the difference between hole mobility for these two polymers in hole-only diodes is about a factor of 10. Apparently, the effect of this mobility difference is strongly weakened in the in-plane measurements.

A simple test to check the presence of a large background charge carrier density in these polymers is to investigate the dependence of the in-plane current on the polymer thickness. For homogeneous doping the current is expected to be inversely proportional to the polymer layer thickness. For this purpose, we performed measurements for one polymer with different layer thicknesses in the device. All the devices were made from one single polymer solution in toluene using different rpm in order

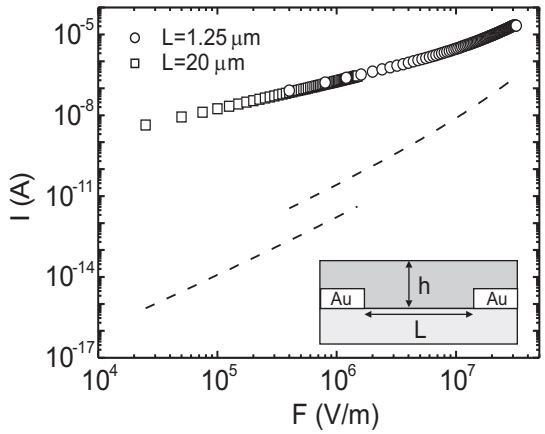

Figure 5.8: Current versus electric field for Au-OC_1C_{10}-PPV-Au structure with polymer thickness $h = 270$ nm and channel length $L = 1.25$ and 20 μm. The dashed lines represents the calculated current. The inset presents the in-plane device structure.

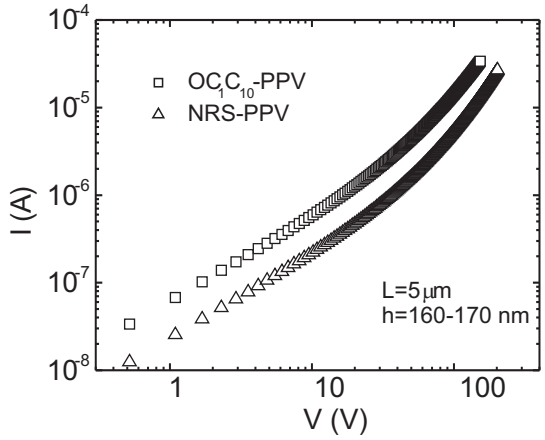

Figure 5.9: $I - V$ characteristics of OC_1C_{10}-PPV and NRS-PPV in-plane diodes with polymer thickness $h = 160 - 170$ nm and channel length $L = 5$ μm.

to obtain different polymer thickness. The results of this experiment are presented in Figure 5.10a for NRS-PPV for $L = 1.25$ μm and 20 μm. These measurements clearly demonstrate that the in-plane current is independent on the thickness of the polymer layer. From this observation doping of the polymer layer can be excluded as the origin of the enhanced in-plane current.

The absence of any scaling with the polymer film thickness suggests that the enhanced in-plane current mainly flows along the substrate/polymer or polymer/vacuum interface. In order to check whether the substrate influences the measurements, we used different substrates such as quartz, glass, Al_2O_3, SiO_2, with roughness of 0.5-1 nm. In Figure 5.10b measurements for NRS-PPV samples are presented for three different substrates. The measurements are scaled for the channel width and length of the devices. These measurements show that the current enhancement is not sensitive to the substrate used.

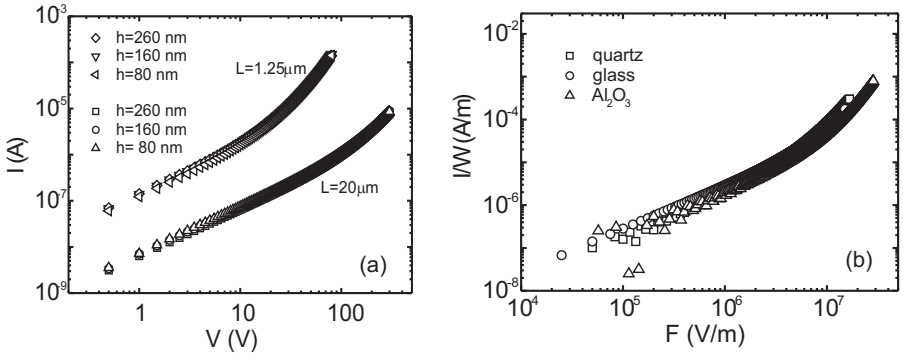

Figure 5.10: $I - V$ characteristics of NRS-PPV in-plane diodes as function of (a) polymer thickness and (b) substrate (glass: $L = 20$ μm, $h = 160$ nm, quartz: $L = 60$ μm, $h = 425$ nm, Al_2O_3: $L = 27$ μm, $h = 200$ nm.

From polymer LEDs and FETs it is known that a treatment of the substrate surface with different solvents, oxygen plasma, ultraviolet ozone, etc. strongly influences the electrical characteristics [4,33–35]. For example the SiO_2 surface of a FET treated with hexamethyldisilazane (HMDS) becomes hydrophobic and as a result enhances the attachment (wetting) of the polymer, which leads to an increased field-effect mobility [4]. We observed slight modification of the in-plane $I-V$ when the samples were treated with HMDS. But the effect of HMDS is rather small and does not significantly change the measurements.

5.3.3 In-plane diode versus field-effect transistor

The experimental study performed on planar devices did not unambiguously explain the large currents. Variations of the polymer, substrate, and chemical treatment had only a limited effect on the measured currents, and could not account for the large discrepancy between experiments and expected SCL currents of 5-6 orders of magnitude. The absence of a dependence on the polymer layer thickness suggests

that the current mainly flows across one of the interfaces in the device. In that case the current distribution in the in-plane device would be similar to that of a field-effect transistor. In a FET the current flows in the semiconductor between the source and the drain along the semiconductor/insulator interface and it consequently does not depend on the semiconductor thickness. The only difference with our in-plane device would be that a FET has a third electrode, the gate, which induces mobile charges in the conducting channel when biased. In an ideal transistor the conductance of the channel switches on at zero gate voltage [36]. However, in practice it is well known that organic FETs are far from ideal, and the switch-on voltage, V_{so} is often shifted to either positive or negative gate voltages [37–39]. In Figure 5.11 we present the transfer characteristic of an OC_1C_{10}-PPV based FET measured directly after fabrication. The field-effect transistor has a highly doped n^{++}-Si gate electrode, a 200 nm thermally-grown SiO_2 thin film used as gate-dielectric and gold electrodes evaporated onto the insulator to form the source and drain contacts. The polymer is spin coated from toluene. The channel width, W, is 2500 μm, and the channel length, L, is 10 μm. It is observed that the FET already switches on at a positive gate voltage of $V_g = 2$ V. As a result at $V_g = 0$ V the drain current is already $I_d = 1.5 \times 10^{-11}$ A. Thus, at zero gate voltage there is already a significant number of charge carriers present in the channel that participate in the transport. It has been suggested in the literature that the observed shift of V_{so} is due to the interfacial charging at the semiconductor/insulator interface [40,41]. The origin and nature of these charges are yet to be clarified.

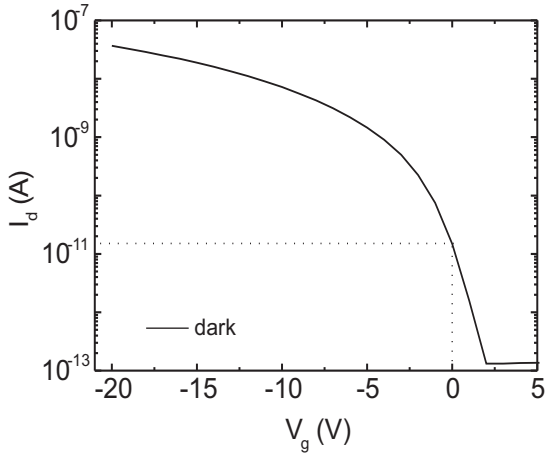

Figure 5.11: Transfer characteristics of OC_1C_{10}-PPV FET measured after preparation. The polymer was spin-coated in air.

We now investigate the possibility whether the same effect of interface charging is able to explain the large currents which we observed in the planar devices. By comparing the current of the in-plane device and the FET we can estimate the surface charge carrier density and corresponding mobility required to explain the high in-plane

currents. The product of the surface charge (Q_s) and mobility μ can be determined in the in-plane device by modeling the experimental linear data with the equation $I = W/LQ_s\mu V$ and amounts to 4×10^{-12} Fm^2/s. We calculate now the surface charge (C_iV_g) and the field-effect mobility for each gate voltage in the FET using the equation for the field-effect current $Id = W/L(C_iV_g)\mu V_d$, where $C_i = 17 \times 10^{-5}$ F/m^2 and $V_d = 0.1$ V. The same product of the surface charge × mobility corresponds in the FET to a gate voltage $V_g = -4$ V. The field-effect mobility that corresponds to $V_g = -4$ V is 6×10^{-9} m^2/Vs. Following this analysis the enhanced current can be explained by assuming that an in-plane device thus behaves like an ideal FET which is biased at -4 V. Note that the larger mobility in the in-plane device as compared to the mobility measured in the LED structure originates from the large interfacial charge carrier density [32].

An important way to check the presence of a such a channel with enhanced charge carrier density is to compare the activation energy (Δ) of the in-plane device with that of a FET. In order to determine Δ we performed temperature measurements for OC_1C_{10}-PPV in both planar devices and FETs. In Figure 5.12 the temperature scan for an OC_1C_{10}-PPV planar device is presented in a temperature range of 292 K to 206 K.

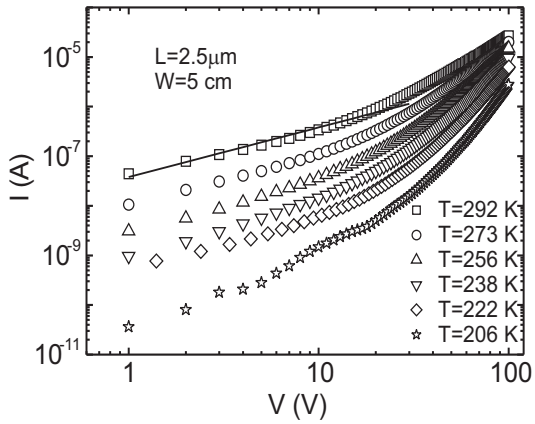

Figure 5.12: Experimental I-V characteristics of OC_1C_{10}-PPV in-plane diode.

An activation energy $\Delta = 0.39$ eV has been determined for this device (Figure 5.13a). From the FET measurements [32] the activation energy of $\Delta = 0.39$ eV corresponds exactly to the activation energy at $V_g = -4$ V (See Figure 5.13b). This identical temperature dependence confirms that the in-plane device indeed acts like a FET that is switched on with a certain gate voltage. The effective gate voltage in the in-plane device might originate from the charging of the substrate/polymer interface during processing. The temperature dependence of the NRS-based devices showed the same consistent temperature behavior.

An important question is now whether the same effects also play a role in earlier reported measurements on in-plane devices [29–31]. In case of PPV films [29] currents

of up to 1×10^{-8} A for $V = 500$ V have been measured in a Au-PPV-Au structure with $W = 600$ μm and $L = 30$ μm. These currents are typically 10^4 higher than what is expected from the SCL current. Apparently, also in these devices interface charges have significantly enhanced the current. Furthermore, on these devices also spatially resolved electroluminescence measurements have been performed. However, the presence of a conducting channel along the surface with high carrier density will modify the electroluminescence emission region. As a result such a measurement does not reflect the intrinsic in-plane transport and luminescent properties of the polymer.

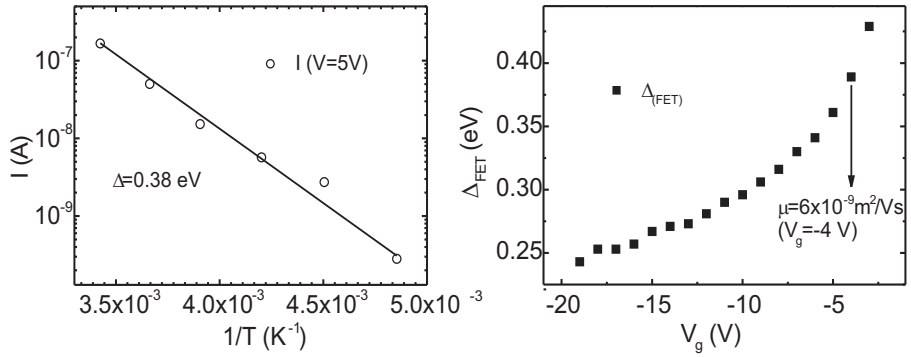

Figure 5.13: (a) The activation energy of the experimental linear current that flows in the OC_1C_{10}-PPV in-plane diode. (b) The activation energy of the drain current that flows in the accumulation channel of OC_1C_{10}-PPV FET.

5.3.4 Conclusion

In conclusion current-voltage measurements from PPV-based planar devices are analyzed. We showed that the current is proportional with the electric field and 5-6 orders of magnitude higher than the expected space-charge limited current. The current enhancement is not sensitive to the polymer or the substrate used. The treatment of the substrate with HMDS did not significantly influence the $I - V$ measurements. We did not study the influence of different electrodes on the electrical characteristics of the in-plane diode. Direct comparison of the planar devices with FETs revealed that the current which flow in the planar device is due to a charging effect on the substrate/polymer interface, which is also responsible for the shift of the threshold voltage in a FET.

Bibliography

[1] J. H. Burroughes, D. D. C. Bradley, A. R. Brown, R. N. Marks, K. Mackay, R. H. Friend, P. L. Burn, A.B. Holmes, *Nature* (London) **347**, 539 (1990).

[2] D. Braun, A. J. Heeger, *Appl. Phys. Lett.* **58**, 1982 (1991).

[3] P. W. M. Blom, M. C. J. M. Vissenberg, J. N. Huiberts, H. C. F. Martens, H. F. M. Schoo, *Appl. Phys. Lett.* **77**, 2057 (2000).

[4] H. Sirringhaus, N. Tessler, R. H. Friend, *Science* **280**, 1741 (1998).

[5] H. Sirringhaus, P. J. Brown, R. H. Friend, M. M. Nielsen, K. Beckgaard, B. M. W. Langeveld-Voss, A. J. H. Spiering, R. A. J. Janssen, E. W. Meijer, P. Herwig, D. M. de Leeuw, *Nature* **401**, 685 (1999).

[6] H. E. A. Huitema, G. H. Gelinck, J. B. P. H. van der Putten, K. E. Kuijk, C. M. Hart, E. Cantatore, P. T. Herwig, A. J. J. M. van Breemen, D. M. de Leeuw, *Nature* **414**, 599 (2001).

[7] G. H. Gelinck, T. C. T. geuns, D. M. de Leeuw, *Appl. Phys. Lett.* **77**, 1487 (2000).

[8] C. J. Brabec, V. Dyakonov, J. Parisi, N. S. Sariciftci, *Organic Photovoltaic Concepts and Realization* **60**, Springer-Verlag, London (2003).

[9] J. Liu, T.-F. Guo, Y. Yang, *J. Appl. Phys.* **91**, 1595 (2002).

[10] T.-Q Nguyen, R. C. Kwong, M. E. Thompson, B. J. Schwartz, *Appl. Phys. Lett.* **76**, 2454 (2000).

[11] T.-Q Nguyen, J. Wu, V. Doan, B. J. Schwartz, S. H. Tolbert, *Science* **288**, 652 (2000).

[12] J. Liu, Y. Shi, L. Ma, Y. Yang, *J. Appl. Phys.* **88**, 605 (2000).

[13] C. J. Collison, L. J. Rothberg, V. Treemaneekarn, Y. Li, *Macromolecules* **34**, 2346 (2001).

[14] W. Geens, S. E. Shaheen, B. Wessling, C. J. Brabec, J. Poortmans, N. S. Sariciftci, *Org. Electr.* **3**, 105 (2002).

[15] H. G. Gilch, *J. Polym. Sci.Part A: Polym. Chem.* **4**, 1337 (1966).

[16] H. Spreitzer, W. Kreuder, H. Becker, H. Schoo, R. Demandt, *PCT Patent Application* WO 98 27 136 (1996).

[17] A.J.J.M. van Breemen, P.T. Herwig, C.H.T. Chlon, J. Sweelssen, H.F.M. Schoo, D.M. de Leeuw, M.E. Mena Benito, P. W. Blom, C. Tanase, J. Wildeman, accepted in *Adv. Funct. Mat.*

[18] H. Spreitzer, H. Becker, E. Kluge, W. Kreuder, H. Schenk, R. Demandt, H. Schoo, *Adv. Mat.* **10**, 1340 (1998).

[19] C. Tanase, P. W. M. Blom, D. M. de Leeuw, E. J. Meijer, *Phys. Status Solidi A* **201**, 1236 (2004).

[20] H. C. F. Martens, P. W. M. Blom, H. F. M. Schoo, *Phys. Rev. B* **61**, 7498 (2000).

[21] M. Kemerink, J. K. J. van Duren, P. Jonkheijm, W. F. Pasveer, P. M. Koenraad, R. A. J. Janssen, H. W. M. Salemink, J. H. Wolter, *Nano Lett.* **3**, 1191 (2003).

[22] J. M. Warman, G. H. Gelinck, M. P. de Haas, *J. Phys: Cond. Matt.* **14**, 9935 (2002).

[23] H. Sirringhaus, R. J. Wilson, R. H. Friend, M. Inbasekaran, W. Wu, E. P. Woo, M. Grell, D. D. C. Bradley, *Appl. Phys. Lett.* **77**, 406 (2000).

[24] J. Veres, S. D. Ogier, S. W. Leeming, D. C. Cupertino, S. M. Khaffaf, textitAdv. Funct. Mat. bf 13, 199 (2003).

[25] T.-Q. Nguyen, I. B. Martini, J. Liu, B. J. Schwartz, *J. Phys. Chem.* **104**, 237 (2000).

[26] R. H. Friend, R. W. Gymer, A. B. Holmes, J. H. Burroughes, R. N. Marks, C. Taliani, D. D. C. Bradley, D. A. Dos Santos, J. L. Brédas, M. Lögdlund, W. R. Salaneck, *Nature* **397**, 121 (1999).

[27] P. W. M. Blom, M. C. J. M. Vissenberg, *Mat. Science and Engineering* **27**, 53 (2000).

[28] Q. Pei, G. Yu, C. Zhang, Y. Yang, A. J. Heeger, *Science* **269**, 1086 (1995).

[29] U. Lemmer, D. Vacar, D. Moses, A. J. Heeger, *Appl. Phys. Lett.* **68**, 3007 (1996).

[30] E. Smela, Y. Kaminorz, O. Inganäs, L. Brehmer, *Semicond. Sci. Technol.* **13**, 433 (1998).

[31] Y. Kaminorz, E. Smela, T. Johansson, L. Brehmer, M. R. Andersson, O. Inganäs, *Synth. Met.* **113**, 103 (2000).

[32] C. Tanase, E. J. Meijer, P. W. M. Blom, D. M. de Leeuw, *Phys. Rev. Lett.* **91**, 216601 (2003).

[33] C. C. Wu, C. I. Wu, J. C. Sturm, A. Kahn, *Appl. Phys. Lett.* **70**, 1348 (1997).

[34] S. Y. Kim, J. L. Lee, K.-B. Kim, Y.-H. Tak, *J. Appl. Phys.* **95**, 2560 (2004).

[35] A. N. Aleshin, J. Y. Lee, S. W. Chu, J. S. Kim, Y. W. Park, *Appl. Phys. Lett.* **84**, 5383 (2004).

[36] S. M. Sze, *Physics of semiconductor devices*, 2^{nd} Ed., John Wiley & Sons, New York (1981).

[37] D. Knipp, R. A. Street, A. Vlkel, J. Ho, *J. Appl. Phys.* **93**, 347 (2003).

[38] S. J. Zilker, C. Detcheverry, E. Cantatore, D. M. de Leeuw, *Appl. Phys. Lett.* **79**, 1124 (2001).

[39] G. Horowitz, R. Hajlaoui, D. Fichou, A. El Kassmi, *J. Appl. Phys.* **85**, 3202 (1999).

[40] Y.-Y. Lin, D. J. Gundlach, S. F. Nelson, T. N. Jackson, *IEEE Trans. Elec. Dev.* **44**, 1325 (1997).

[41] E. J. Meijer, C. Detcheverry, P. J. Baesjou, E. van Veenendaal, D. M. de Leeuw, T. M. Klapwijk, *J. Appl. Phys.* **93**, 4831 (2003).

Chapter 6

Dual-layer polymer LEDs

Summary

We demonstrate a new concept for an efficient dual polymer layer LED containing a polymer with high hole mobility that efficiently transports the holes towards a luminescent layer in which the light is efficiently generated. The problem of selective solvents which need to be used to spin coat the polymer layers on top of each other is solved by tuning the solubility using chemical modification of these materials. Dual-layer polymer LED exhibit an enhanced efficiency at high voltages (>10 V) and an improved robustness against electrical breakdown.

6.1 Introduction

Since the first report of electroluminescence (EL) in PPV [1,2], it has been demonstrated that the charge transport and the recombination efficiency are both governed by the charge carrier mobility [3,4]. Therefore, the control of the charge carrier mobility is crucial for optimization of polymer light-emitting diode. The ways to improve the polymer LED performances is either to increase the charge carrier mobility or to improve the balance between the transport of holes and electrons. A mobility increase is expected to be accompanied by a decrease of the operating voltage, thereby increasing the power efficiency of the polymer LED. But due to the reduced electron conduction determined mainly by the presence of traps [3,5,6], the recombination occurs in a region close to the electron-injecting metal electrode. It has been found that in polymer LEDs based on PPV-derivatives with high mobility the exciton quenching at the electron-injecting electrode is enhanced, leading to an unexpected decrease of the luminescence efficiency [7]. Consequently, the charge transport properties of the materials presently used in state-of-the-art single layer polymer LEDs, with hole mobilities of typically 10^{-11} m^2/V s, are the best compromise between these processes. Without the use of high mobility polymers low operating voltages are only achieved by keeping the active layer thickness limited to typically 80–100 nm. This approach makes the present polymer LEDs vulnerable to electrical shorts and puts strong demands on the processing conditions.

These fundamental limitations can be circumvented by using multilayer devices consisting of a number of active layers, each optimized for its own functionality. In a multilayer device electrons and holes are efficiently transported via high mobility transport layers towards a highly luminescent layer. As a result high efficiencies and low operating voltages are simultaneously achieved with relatively thick active layers. This approach has been successfully applied in small molecule based devices, in which multiple layers with various functions (charge transport, charge injection, emission), lead to highly efficient devices [8]. The technique used to fabricate these diodes is subsequent evaporation of different transporting layers. However, the fabrication of solution-processed polymer-based multilayer diodes is complicated by the fact that the spin cast layer can be dissolved in the solvent of the subsequent spin cast layer. As a first approach efficient bi-layer devices have been realized using a precursor PPV as hole transport layer [9], which is insoluble after conversion. Another approach in order to overcome the solubility problem was to crosslink the first (hole transport) layer after deposition, either by UV exposure [10] or by electron-beam irradiation [11]. The disadvantage of these methods is that the irradiation necessary for crosslinking strongly decreases the performance of LEDs fabricated from these materials [10,11].

In this chapter we focus on the development of PPV-based hole transport layers, which combine an enhanced mobility with a tunable solubility by modification of the chemical structure. Using such a hole transport layer a dual-layer polymer LED has been fabricated and compared with conventional single layer polymer LED.

6.2 High-mobility PPV hole transport layers with adjustable solubility

Chemical modification of the PPV influences the interchain distance, orientation and packing of the polymer chains and hence affects the charge carrier mobility of the polymer in devices. This has been demonstrated in *Chapter 5* for OC_1C_{10}-PPV and its derivatives in which the hole mobility could be varied over more than two orders of magnitude [12]. The highest mobility of 6×10^{-10} m^2/Vs was achieved in a symmetric $OC_{10}C_{10}$-PPV compound, due to a reduction of the energetic disorder. Following the result in OC_1C_{10}-PPV and $OC_{10}C_{10}$-PPV, we first compare the mobility of a well known polymer poly(2-methoxy,5-(2'-ethyl-hexoxy)-*p*-phenylene vinylene) (MEH-PPV) with its symmetric counterpart, namely poly[2,5-bis(2'-ethylhexyloxy)-*p*-phenylenevinylene] (BEH-PPV) (See Figure 6.1). The difference between BEH-PPV and MEH-PPV is the substitution pattern of the side chain: MeO through 2-ethylhexyloxy. Figure 6.2 presents the temperature dependence of the $J - V$ characteristics of a BEH-PPV based hole-only diode. The hole mobility of BEH-PPV amounts to 1.5×10^{-9} m^2/Vs, which is 20× higher than the hole mobility in MEH-PPV.

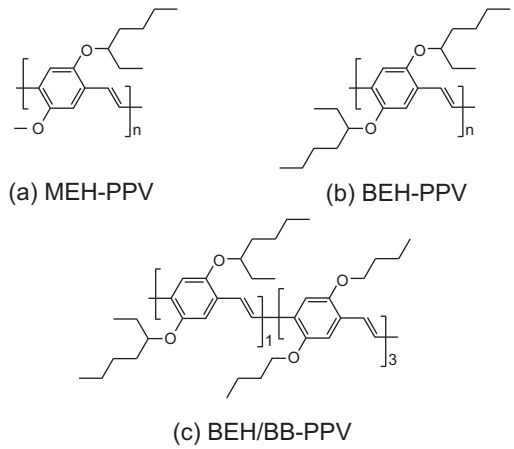

Figure 6.1: The chemical structures of (a) MEH-PPV, (b)BEH-PPV, (c) BEH/BB-PPV.

From the mobility point of view BEH-PPV seems to be a good candidate for the transport layer in a dual-layer light-emitting diode due to its enhanced hole mobility. But its long side chains makes it soluble in many common solvents such as toluene or chlorobenzene, in which many PPVs are soluble. But the solubility can be reduced by shortening of (2-ethylhexyloxy) side chains towards the butoxy side chains.

Poly[2,5-bis(butoxy)-*p*-phenylenevinylene] (BB-PPV) is only soluble in chloroform (See Table 6.1), and that in only very low concentrations. Due to its very poor solubility no diodes can be fabricated from this material. However, the combination

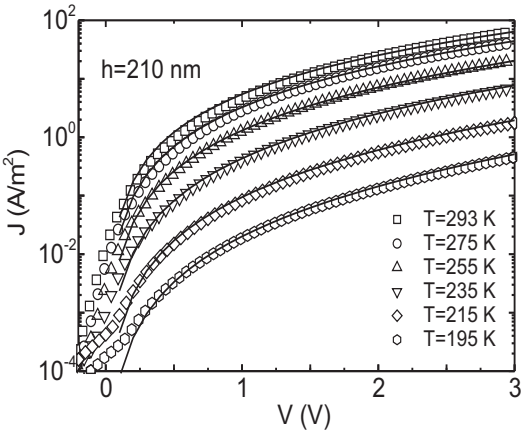

Figure 6.2: Current-voltage temperature scan of BEH-PPV hole-only diode. The solid lines represent the prediction from the SCL model including the filed dependent mobility

of BEH-PPV and BB-PPV in different ratio in copolymers can induce a variation from insoluble in toluene (BB-PPV) to highly soluble in toluene (BEH-PPV), depending on the amount of BB-PPV in the copolymer. The solubility in toluene of BEH/BB-PPV copolymer in different ratio 1/x (x=1–3) drops from 0.2 for BEH/BB-PPV 1/1 to less than 0.1 for BEH/BB-PPV 1/3. The major question is whether the incorporation of the BB-PPV monomer into the copolymer does not affect the enhanced charge transport properties of BEH-PPV. From SCL $J-V$ measurements we obtain that the hole mobility for all copolymers is equal to that of BEH-PPV, 1.5×10^{-9} m^2/Vs at room temperature. As a result BEH/BB-PPV 1/3 combines the desired properties for a hole transport layer in a polymer LED: a high mobility and a limited solubility.

In Figure 6.3 the temperature dependence of zero-field mobility is presented for some of the materials studied. The effect of side chains attached to the PV monomer is considerable. The hole mobility can be tuned over more than three orders of magnitude. Going from asymmetric (MEH-PPV) to more symmetric (BEH-PPV) polymers, the conformational freedom of individual chains is limited and results in a

Polymer	$\mu_{LED}(F=0)$ (m^2/Vs)	Mw (g/mol)	Mn (g/mol) Toluene	Solubility (wt %) Chloroform	
NRS-PPV	1.5×10^{-12}	1.0×10^{6}	1.9×10^{5}	1	1
MEH-PPV	5.0×10^{-11}	2.5×10^{5}	6.3×10^{4}	1	1
BEH-PPV	2.0×10^{-9}	5.5×10^{5}	1.3×10^{5}	1	1
BB	—	—	—	0	0.2
BEH/BB-PPV 1/3	1.2×10^{-9}	5.7×10^{5}	4.2×10^{5}	<0.1	0.6

Table 6.1: Characteristic properties of the presented polymers.

decreased energetic spread between the electronic levels of individual chain segments. Therefore the width of the Gaussian DOS is reduced from $\sigma_{MEH-PPV} = 0.105$ eV to $\sigma_{BEH-PPV} = 0.92$ eV. This reduced energetic disorder significantly enhances the hole mobility.

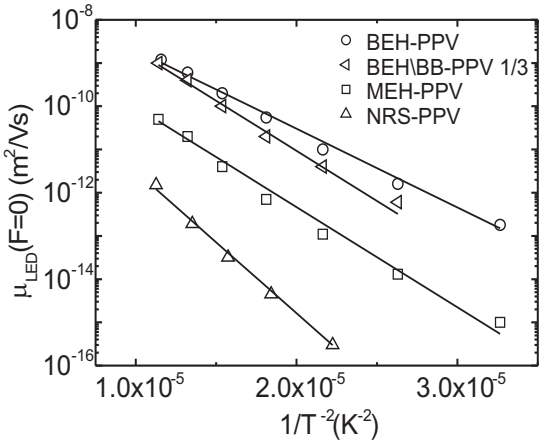

Figure 6.3: Temperature dependence of the zero-filed mobility of four PPV derivatives.

6.3 Electrical characterization of the PPV based dual layer LED

A standard material for single layer PPV-based polymer LEDs is NRS-PPV [7] which is soluble in a wide range of solvents, with a hole mobility of only 1.5×10^{-12} m^2/Vs at low electric fields at room temperature. A dual polymer layer LED can now be constructed using BEH/BB-PPV 1/3 as hole transport layer and NRS-PPV as the emissive layer. The photoluminescence efficiency of NRS-PPV amounts to 20% and that of BEH/BB-PPV 9%, both measured with an integrating sphere. In Figure 6.4 the $J-V$ characteristics of a single layer NRS-PPV LED with thickness 95 nm and a double layer of BEH/BB-PPV 1/3 and NRS-PPV based LED are presented together with the light output.

The thickness of the layers in the dual-layer diode are 160 nm for BEH/BB-PPV 1/3 and 95 nm for NRS. As a reference, the data of a single layer NRS-based LED with a thickness comparable to the dual-layer device is shown. When a bias is applied to the diode, the holes are transported efficiently through the BEH/BB-PPV 1/3 and subsequently recombine with electrons in the NRS-PPV layer. It should be noted that the holes can directly enter the NRS-PPV and are not hindered by an energy barrier at the interface, since the HOMO and LUMO levels of the two polymers align.

From Figure 6.4 it can be observed that at the same operating voltage both the current density and the light output of the double layer are significantly smaller than

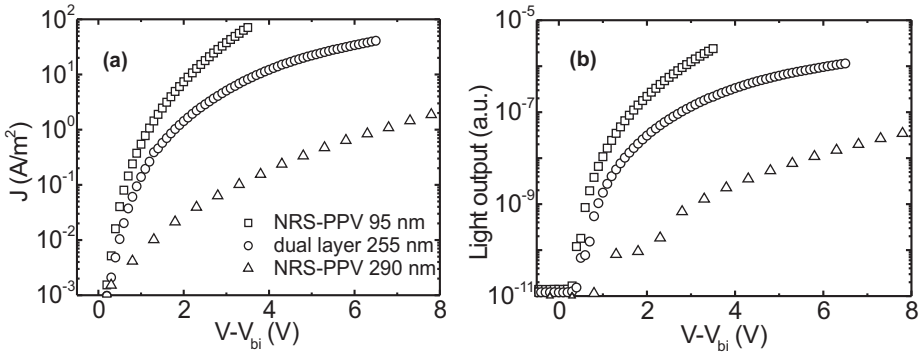

Figure 6.4: Current-voltage characteristics (a) and light output (b) of NRS-PPV and dual layer LED at room temperature

those of the single layer NRS-PPV diode of 95 nm. This seems to be in contrast with the large difference in mobility of three order of magnitude between the BEH/BB-PPV and the NRS-PPV. From device simulations, however, we obtained that the voltage distribution over the two polymers is not only governed by the mobility ratio. Since the current in the BEH/BB-PPV is also space-charge limited, a very low voltage drop across this layer directly implies that electrostatically only a small amount of charge carriers is allowed in this layer. Therefore, to make the hole transport layer highly conductive a certain voltage drop across this layer is required to fill up the layer with charge carriers. The simulations demonstrate that typically 1/3 of the voltage drops over the hole transport layer.

In Figure 6.5 the quantum efficiency (QE) (photon/charge carrier) of the double and single layer device is shown. The figure shows that the maximum efficiency of the double layer diode is slightly lower as compared to the single layer NRS-PPV diode. The main reason is that the absorbance and emission spectrum of BEH/BB-PPV 1/3 is red-shifted as compared to the NRS-PPV. Therefore, as shown in the inset of Figure 6.5, the absorption spectrum of BEH/BB-PPV slightly overlaps with the emission spectrum of NRS-PPV and part of the generated light is absorbed in the hole transport layer. However, the double layer device has a number of advantages over the single layer polymer LEDs. As shown in Figure 6.5 for $V > 7$ V the efficiency of the single layer NRS-PPV LED drops very fast, due to the strong quenching of the luminescence efficiency at high fields. Finally, the device breaks down at typically 12–13 V. The efficiency of the dual-layer device only gradually decreases from 7 V to 18 V, the device finally breaks down at 25–26 V. The reason for the more gradual decrease is that at higher voltages the field becomes more and more equally distributed over the two polymer layers. At 10 V the efficiency of the two devices is the same, at a typical light-output of 10000 cd/m^2.

Furthermore, in contrast to conventional hole transport layers our hole transport layer is emissive and its HOMO and LUMO levels align with the luminescent layer, so that electrons are not blocked at their interface. Consequently, a short-circuit in the

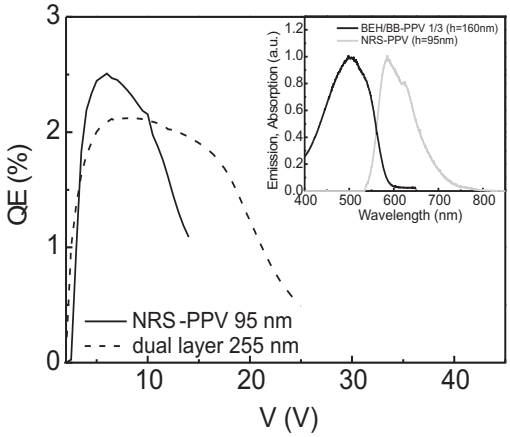

Figure 6.5: Quantum efficiency as function of applied bias for NRS-PPV and dual layer LED. The inside shows the absorption of BEH/BB-PPV 1/3 and PL of NRS-PPV.

luminescent layer does not lead to a catastrophic failure of the device. Instead, the emissive hole transport layer starts to work as a LED and, at the location of the short, only the efficiency of the LED drops since the transport layer is a less efficient emitter. Additionally, the increased layer thickness of the devices opens the process window of polymer LEDs in terms of substrate roughness and substrate cleaning. The increased efficiency and lower electric field in the luminescent layer at high voltages, combined with the prevention of catastrophic shorts, are important advantages for the use of polymer LEDs in passive matrix displays and solid-state lighting applications.

6.4 Conclusions

It has been demonstrated that the charge carrier mobility of PPV-based derivatives can be optimized by chemical modification. Copolymers with selective solubility can be achieved without loss of the enhanced charge transport properties. Dual-layer polymer LEDs in which the holes are efficiently transported via this copolymer towards the luminescent layer exhibit an enhanced efficiency at high voltages (> 10 V) and a strongly improved robustness against electrical breakdown.

Bibliography

[1] J. H. Burroughes, D. D. C. Bradley, A. R. Brown, R. N. Marks, K. Mackay, R. H. Friend, P. L. Burn, A. B. Holmes, *Nature* (London) **347**, 539 (1990).

[2] D. Braun, A. J. Heeger, *Appl. Phys. Lett.* **58**, 1982 (1991).

[3] P. W. M. Blom, M. C. J. M. Vissenberg, *Mat. Sc. and Engineering* **27**, 53 (2000).

[4] R. H. Friend, R. W. Gymer, A. B. Holmes, J. H. Burroughes, R. N. Marks, C. Taliani, D. C. C. Bradley, D. A. Dos Santos, J. L. Brdas, M. Lgdlund, W. R. Salaneck, *Nature* **397**, 121 (1999).

[5] H. Antoniadis, M. A. Abkowitz, B. R. Hsieh, *Appl. Phys. Lett.* **65**, 2030 (1994).

[6] L. Bozano, S. A. Carter, J. C. Scott, G. G. Malliaras, P. J. Brock, *Appl. Phys. Lett.* **74**, 1132 (1999).

[7] P. W. M. Blom, M. C. J. M. Vissenberg, J. N. Huiberts, H. C. F. Martens, H. F. M. Schoo, *Appl. Phys. Lett.* **77**, 2057 (2000).

[8] B.W. D'Andrade, M.A. Baldo, C. Adachi, J. Brooks, M.E. Thompson, and S.R. Forrest, *Appl. Phys. Lett.* **79**, 1045 (2001).

[9] N. C. Greenham, S. C. Moratti, D. D. C. Bradley, R. H. Friend, A. B. Holmes, *Nature* **365**, 628 (1993).

[10] B. Domercq, R. D. Hreha, Y.-D. Zhang, A. Haldi, S. Barlow, S. R. Marder, B. Kippelen, *J. Polym. Sc., Part B: Polym. Phys.* **41**, 2726 (2003).

[11] R. A. M. Hikmet, R. Thomassen, *Adv. Mater.* **15**, 115 (2003).

[12] F. C. Martens, P. W. M. Blom, H. F. M. Schoo, *Phys. Rev. B* **61**, 7489 (2000).

Chapter 7

Ambipolar FETs based on a methanofullerene

Summary

Since carrier mobility is the main limiting factor in the operating speed of FETs, the goal for highly competitive integrated circuits would be to use one active material with high mobility for both electrons and holes. Here, we report ambipolar charge transport in FETs based on methanofullerene. The charge mobility is 1×10^{-6} m^2/Vs for electrons and 8×10^{-7} m^2/Vs for holes. This results qualify methanofullerene as a potential candidate for application in solution-processed CMOS-like circuits.

7.1 Introduction

A distinct characteristic of nearly all transistors made out of small molecules, conjugated polymers and other organic semiconductors is that they transport only one type of charge, either holes [1–3] or electrons [4–6]. The simultaneous or selective transport of electrons and/or holes in a single organic layer transistor failed until the last decade, when the first organic FET employing a p/n type heterostructure of two carefully chosen materials (α-hexathienylene and C_{60}) has been reported [7, 8]. It was shown that currents of both polarities could be simultaneously injected from the source and the drain contacts under appropriate bias conditions and both electron- and hole-type transistor operation could be achieved. A major problem in achieving both electron and hole transport is determined by the occurrence of a high energy barrier for either electron or hole injection from the same metal used for the source and drain electrodes. In order to overcome this problem, Meijer *et al.* mixed a material with a low energy barrier for electron injection (PCBM), with a material with a low energy barrier for hole injection (OC_1C_{10}-PPV) and reported organic heterogeneous blend transistors [9]. However, despite promising simplification of device fabrication by using a single semiconducting layer, low carrier mobility is associated with most ambipolar organic FETs using two active materials [7–11]. Another approach to this problem is using a single organic material with a low band gap as active layer, thus reducing the energy barrier at the source and drain electrodes for both electrons and holes. The width of the injection barrier can be reduced even more by accumulating high charge carrier density in the semiconducting film [12], which will enable tunneling of charges from the electrode into the semiconductor.

Up to now, we analyzed polymers that are good hole transporters, but poor electron transporters. Since carrier mobility is the main limiting factor in the operating speed of FETs, the goal for highly competitive integrated circuits would be to use one active material with high mobility for both electrons and holes. Because relatively high electron mobility has been demonstrated for solution processable methanofullerene [6,6]-phenyl-C61-butyric acid methyl ester (PCBM) [9], we decided to further analyze this material in a FET structure. We demonstrate that the transistors based on this molecule have carrier mobilities in the order of 1×10^{-2} cm^2/Vs for electrons and 8×10^{-3} cm^2/Vs for holes [13]. This results qualify PCBM as a potential candidate for application in solution-processed CMOS-like circuits [14] and provide further supporting evidence that ambipolar charge transport is a generic property of organic semiconductors [9].

7.2 Ambipolar transistor operation

In these experiments the bottom contact ring transistor with symmetric gold source and drain contacts has been used. The conducting films were spin-coated from solution consisting of 1 wt % PCBM in chlorobenzene at 500 rpm for 1 minute. Prior to spin-coating the solution was stirred for one hour at 353 K and then filtrated. After spin-coating all transistors were annealed at 393 K for several hours under vacuum

(10^{-7} mbar). Upon annealing for several hours, the PCBM films appear microcrystalline and rough. All electrical measurements were recorded in vacuum due to instability of the devices under ambient conditions using a Keithley 4200 Semiconductor Characterization System.

When the gate is highly positively biased, a channel of accumulated electrons near the insulator/PCBM interface is formed and the transistor operates in the electron-enhanced mode. Typical transfer characteristics measured in the linear and saturation regimes and output characteristics of the PCBM transistor in the electron-accumulation mode are presented in Figure 7.1.

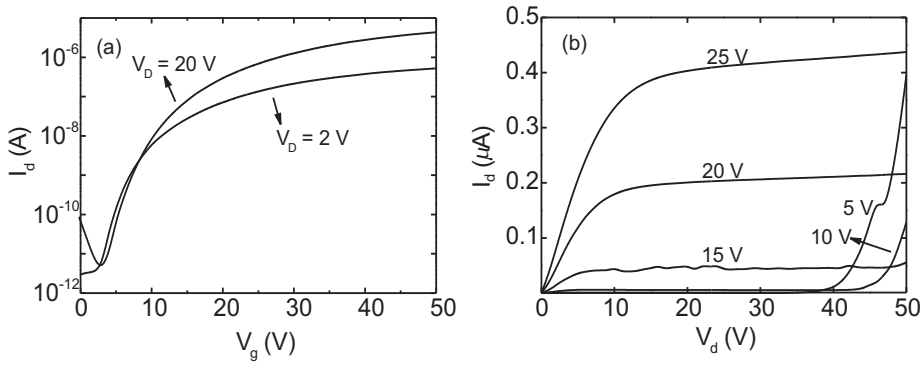

Figure 7.1: The transfer characteristics (a) and the output characteristics (b) of PCBM ambipolar transistor in the electron enhancement mode.

The electron mobility, μ_e, in the linear regime yields a maximum value of 0.009 cm^2/Vs at $V_g = 30$ V, while in the saturation regime yields a slightly higher mobility of 0.01 cm^2/Vs at $V_g = 20$ V. These values for the electron mobility exceed the mobility reported previously for PCBM based transistors employing calcium electrodes in a top contact device configuration by more than a factor of two [15]. Furthermore, they exceed the mobility calculated from the space charge limited currents in PCBM diodes by a factor of five [16]. We explain this difference by the heat treatment of the samples under high vacuum. The measurements reveal that all device characteristics are strongly dependent on the annealing process and the ambient conditions following PCBM deposition. For example, the switch-on voltage decreases from 25 V to $<$ +2 V after annealing, while the measured electron mobility increased by more than two orders of magnitude. It was also established that high vacuum, under which annealing is performed, was an essential processing parameter in order to obtain the good performance characteristics of the transistors. This drastic effect can be attributed to the doping of the PCBM layer with ambient oxygen. The dopant sites act as electron traps that lead to reduction of mobile carriers within the channel for a given gate voltage and a subsequent increase in the switch-on voltage.

By analyzing the device band diagram of PCBM in contact with gold electrodes when no bias is applied (Figure 7.2), one would expect the injection of electrons from gold into PCBM to be a difficult process due to the mismatch in the energies of

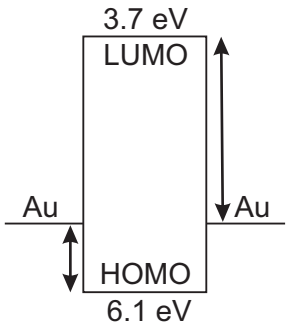

Figure 7.2: Energy band diagram of PCBM upon contact with gold electrodes.

the LUMO level of the PCBM and the work function of gold $\phi_b(e) = 1.4$ eV, but surprisingly the transistor works at a low switch-on voltage ($V_{so} < 3$ V) with the drain current saturating at $I_d = 10^{-6}$ A for an applied gate bias $V_g = 50$ V. This indicates the absence of trap states [14] at the insulator/semiconductor interface, and the presence of a rather small contact barrier between PCBM/Au. This small barrier is attributed to the formation of a strong interface dipole at the Au/PCBM interface, which lowers the barrier $\phi_b(e)$ by 0.64 eV such as the injection barrier is only 0.76 eV [17]. A similar barrier reduction has been observed for the Au/C60 interface as determined by ultraviolet photoemission spectroscopy [18].

In order to obtain some insight into the electron transport processes across the device we model the transfer characteristics using the disorder hopping model [19]. Figure 7.3 shows the experimental transfer characteristics (symbols) at T = 293 K, with the corresponding fits (solid lines) obtained using Eq. 2.20. The fitting parameters are $T_0 = 400$ K, $\sigma_0 = 8 \times 10^7$ S/m, and $\alpha^{-1} = 0.105$ nm. From Figure 7.3 it is evident that for $T = 293$ K and $V_g < 30$ V the experimental data cannot be accurately described by Eq. 2.20. The difference between the experimental and calculated current is around three orders of magnitude for V_g close to 0 V. The same difference in current has been found in the case of PCBM sandwich diodes using Au and LiF/Al contacts [17]. Au leads to strongly injection-limited current characteristics, while LiF/Al is an ohmic contact for PCBM. This discrepancy is attributed to the high contact resistance at the Au/PCBM interface, which dominates the current flow through the device at low gate voltages.

From the output characteristics (Figure 7.1) it can be observed that for low gate voltages ($V_g = 5$ V and 10 V) and high drain voltages ($V_d > 40$ V) the current shows an increase with the drain voltage. This is a characteristic of an ambipolar transistor behavior. The large increase of the drain current is a result of a hole-accumulation region induced near the drain contact when $V_d > V_g + V_{so}(p)$, where $V_{so}(p)$ is the switch-on voltage for the hole-channel operation mode. In order to further investigate this behavior, the output and the transfer characteristics in the hole-accumulation mode are measured (Figure 7.4).

As it can be observed from Figure 7.4, the transfer curves exhibit typical hole-

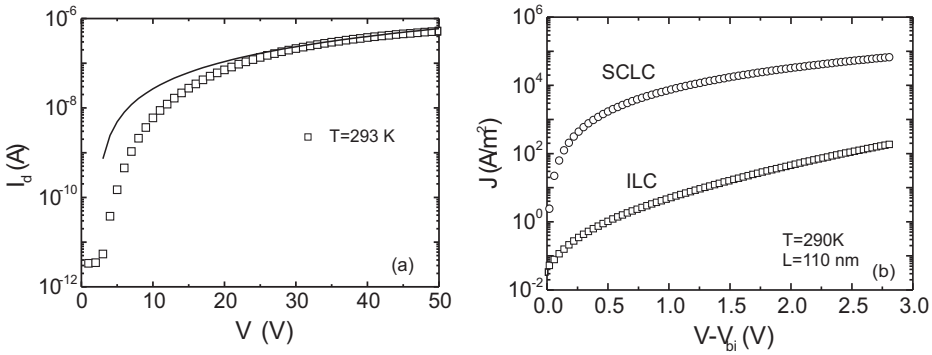

Figure 7.3: (a) The transfer characteristics of PCBM ambipolar field-effect transistor in the electron enhancement mode ($L = 40$ μm, $W = 2500$ μm). (b) $J-V$ characteristics of ITO/PEDOT-PSS/PCBM/LiF/Al (circles) and ITO/PEDOT-PSS/PCBM/Au (squares) as discussed in Ref. [17].

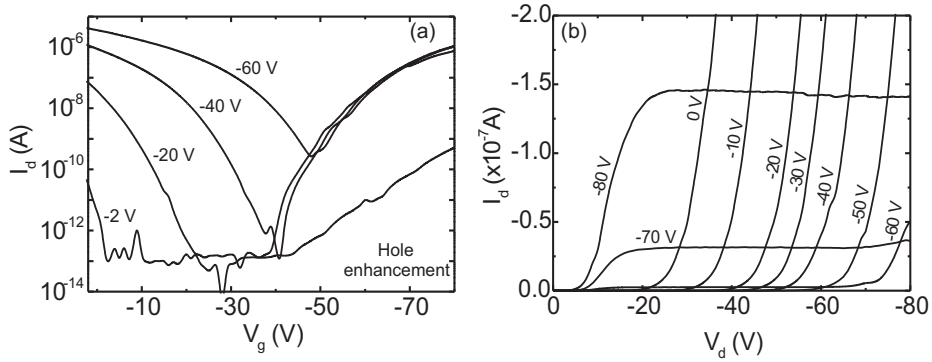

Figure 7.4: The transfer and output characteristics of PCBM ambipolar transistor in the hole enhancement mode ($L = 40$ μm, $W = 1000$ μm).

channel behavior with the creation of a hole-enhancement current when the transistor in negatively biased and for high V_g. The hole drain current increases significantly as the gate electrode is biased even more negatively and saturates at approximately 10^{-6} A for $V_g = -80$ V. The large switch-on voltage (-30 V to -40 V) needed to detect the hole-enhanced current suggests either a high density of traps for holes at the SiO_2/PCBM interface, or that the current level in the linear regime is lower than the instrument's detection limit for $0 < |V_g| < 20$ V. The low hole current is presumably due to the presence of the large injection barrier for holes of ≈1.64 eV, if the contribution from interface dipoles is included. The field-effect mobility for the holes, μ_p, in saturation regime is 0.008 cm^2/Vs, at $V_g = -75$ V, with the ON-OFF ratio in the order 10^6. In all measurements, the drain currents are more than a factor of 10 higher than the corresponding measured gate currents, emphasizing the real hole-channel operation of the PCBM based transistors. The field-effect hole mobility in the linear regime could not be reliably calculated since the contact resistance, induced by interface effects, dominates conduction across the device. From the output characteristics of the PCBM transistor the hole-channel operating mode is observed for small V_d,while for $|V_d| > |V_g| + |V_{so}(p)|$ the drain current increases abruptly. In this case the electrons are injected from the drain contact and hence contribute to the total current flowing through the device. The non-linear output characteristics observed at low V_d biases are consistent with the presence of a large injection barrier for holes $\phi_b(h+) = 1.64$ eV.

7.3 CMOS-like inverters based on methanofullerene

Silicon technology makes extensive use of complementary metal-oxide-semiconductor structures (CMOS), where an electron- and a hole-type transistor are combined to build logic circuits. They exhibit low power dissipation, small noise margin and greater operation stability. In the last years such integrated circuits have also been made from organic materials [20]. However, in this approach the fabrication proved to be difficult and expensive. Recently, an alternative approach towards organic CMOS circuits has been proposed by Meijer *et al.* [9], demonstrating that by employing identical ambipolar OFETs based on polymer-small molecule interpenetrating networks as well as narrow band-gap polymers, CMOS-like voltage inverters can be fabricated. This approach makes full use of the attractive processing properties of polymers while it simplifies device fabrication by utilizing a single semiconductor layer. Even more simple fabrication of logic voltage inverters is possible by using a single material for the semiconducting layer in combination with a single material for the electrodes.

The fact that PCBM shows ambipolar behavior in FETs, with high electron and hole mobility, qualifies it as a potential candidate for application in organic CMOS-like technology. Inverters based on two identical ambipolar PCBM transistors were designed and their schematic diagram is presented in the inset of Figure 7.5a. The channel dimensions for both FETs were identical and equal to $L = 10$ μm, $W = 1000$ μm. In the circuit the gate is common for both transistors and serves as the input

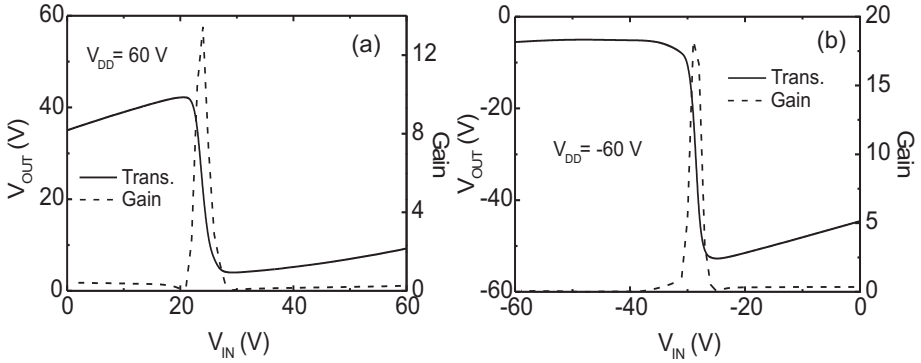

Figure 7.5: Transfer characteristics of a CMOS-like inverter with two identical PCBM-based ambipolar FETs (L = 10 μm, W = 1000 μm) when (a) V_{IN} and V_{DD} are positively biased and (b) when (a) V_{IN} and V_{DD} are negatively biased. Inset shows the inverter circuit configuration.

node (V_{IN}). When the supply voltage, V_{DD}, and the input voltage, V_{IN}, are biased positively (Figure 7.5a) the inverter works in the first quadrant and the output voltage, V_{OUT}, versus the input voltage, V_{IN}, plot exhibits a maximum gain of 13. Under these bias conditions FET 1 acts mainly like the hole-type transistor of regular CMOS inverter, while FET 2 operates as the n-type device. When V_{DD} and V_{IN} are negative, the inverter operates with electron- and hole-channel function exchanged between the two devices and exhibits a gain of 18. When the value of V_{IN} is close to that of V_{DD}, the n-channel of both transistors is on with FET 1 having a smaller overdrive than FET 2. This explains why the output node cannot be completely pulled down by FET 2 and why the output voltage slightly decreases with decreasing V_{IN}. When V_{IN} is 40 V lower than V_{DD}, the p-channel of FET 1 and FET 2 are on with a smaller overdrive on FET 2. Again this explains the incomplete pull-up and the slight reduction of the output voltage with V_{IN}. Similar considerations apply to Figure 7.5b. This ability to operate in both quadrants is a unique feature of the ambipolar transistor-based inverter since the unipolar ones operate only in the first or the third quadrant.

7.4 Conclusions

In conclusion, we have demonstrated ambipolar charge transport in field-effect transistors based on methanofullerene. The transistors are capable of operating in both the hole- and electron-channel regimes depending upon the bias conditions. However, in the hole-channel regime transistor operation is severely contact limited. We attribute this to the presence of a large injection barrier for holes at the Au/PCBM interface. Under appropriate biasing conditions the transistors exhibit electron and hole mobility in the order of 0.01 cm^2/Vs, and 0.008 cm^2/Vs, respectively. A CMOS-like inverter comprised of two identical ambipolar OFETs based on PCBM has been

demonstrated. The inverter can function at room temperature exhibiting a maximum voltage gain of 18 which is one of the highest gains reported to date for organic FET based inverters. Furthermore, the use of high mobility ambipolar organic semiconductors such as PCBM can be viewed as a significant step towards organic-based CMOS-like technology. Since the inverter represents the basic building block of most logic circuits we anticipate that other complementary-like circuits can be realized by this approach.

Bibliography

[1] A. R. Brown, C. P. Jarrett, D. M. de Leeuw, M. Matters, *Synthetic Metals* **88**, 37 (1997).

[2] H. Sirringhaus, N. Tessler, R. H. Friend, *Science* **280**, 1741 (1998).

[3] C. D. Dimitrakopoulos, S. Purushothaman, J. Kymissis, A. Callegari, J. M. Shaw, *Science* **283**, 822 (1999).

[4] R. C. Haddon, A. S. Perel, R. C. Morris, T. T. M. Palstra, A. F. Hebard, R. M. Fleming, *Appl. Phys. Lett.* **67**, 121 (1995).

[5] J. G. Laquindanum, H. E. Katz, A. Dodabalapur, A. J. Lovinger, *J. Am. Chem. Soc.* **118**, 11331 (1996).

[6] H. E. Katz, A. J. Lovinger, J. Johnson, C. Kloc, T. Siegrist, W. Li, Y. -Y. Lin, A. Dodabalapur, *Nature* **404**, 478 (2000).

[7] A. Dodabalapur, H. E. Katz, L. Torsi, R. C. Haddon, *Science* **296**, 1560 (1995).

[8] A. Dodabalapur, H. E. Katz, L. Torsi, R. C. Haddon, *Appl. Phys. Lett.* **68**, 1108 (1996).

[9] E. J. Meijer, D. M. de Leeuw, S. Setayesh, E. Van Veenendaal, B. -H. Huisman, P. W. M. Blom, J. C. Hummelen, U. Scherf, T. M. Klapwijk, *Nature Materials* **2**, 678 (2003).

[10] K. Tada, H. Harada, K. Yoshino, *Jpn. J. Appl. Phys.* **35**, L944 (1996).

[11] R. J. Chesterfield, C. R. Newman, T. M. Pappenfus, P. C. Ewbank, M. H. Haukaas, K. R. Mann, L. L. Miller, C. D. Frisbie, *Adv. Mater.* **15**, 1278 (2003).

[12] S. M. Sze, *Physics of semiconductor devices*, Wiley, New York (1981).

[13] T. D. Anthopoulos, C. Tanase, S. Setayesh, E. J. Meijer, J. C. Hummelen, P. W. M. Blom, D. M. de Leeuw, *Adv. Mater.* **16**, 2174 (2004).

[14] T. D. Anthopoulos, D. M. de Leeuw, E. Cantatore, S. Setayesh, E. J. Meijer, C. Tanase, J. C. Hummelen, P. W. M. Blom, *Appl. Phys. Lett.* **85**, 4205 (2004).

[15] C. Waldauf, P. Schilinsky, M. Perisutti, J. Hauch, C. J. Brabec, *Adv. Mater.* **15**, 2084 (2003).

[16] V. D. Mihailetchi, J. K. J. van Duren, P. W. M. Blom, J. C. Hummelen, R. A. J. Janssen, J. M. Kroon, M. T. Rispens, W.J. H. Verhees, M. M. Wienk, *Adv. Funct. Mater.* **13**, 43 (2003).

[17] J. K. J. van Duren, V. D. Mihailetchi, P. W. M. Blom, T. van Woudenbergh, J. C. Hummelen, M. T. Rispens, R. A. J. Janssen, M. M. Wienk, *J. Appl. Phys.* **94**, 4477 (2003).

[18] S. C. Veenstra, A. Heeres, G. Hadziioannou, G. A. Sawatzky, H. T. Jonkman, *Appl. Phys. A: Mater. Sci. Process.* **A75**, 661 (2002).

[19] M. C. J. M. Vissenberg, M. Matters, *Phys. Rev. B* **57**, 12 964 (1998).

[20] B. Crone, A. Dodabalapur, Y. -Y. Lin, R. W. Fillas, Z. Bao, A. LaDuca, R. Sarpeshkar, H. E. Katz and W. Li, *Nature* **403**, 521 (2000).

Summary

The discovery that plastics have the ability to function as semiconductors expanded their use beyond the familiar toys, bags or furniture, into electronic products such as flexible displays, radio-frequency identification tags, photocells, and chemical sensors. Although plastic electronics may never match the operation speed and miniaturization of silicon-based electronics, they can provide cheap, easy processable, flexible devices. Conjugated polymers are a special group of plastics, which have a framework of alternating single and double bonds. The single bonds are called σ-bonds and are associated with a highly localized electron density in the plane of the molecule. The double bonds consist of a σ-bond and a π-bond, which is the overlap between p_z orbitals of neighbouring atoms. The electric charge is delocalized along the π-conjugated segments of the polymer backbone, which have a typical length of 5-10 units. Under an applied electric field the charge carriers move by hopping between conjugated segments. The hopping of charges is strongly dependent on the energetic and structural disorder in the polymer. The influence of both types of disorder present in conjugated polymer films on the charge carrier transport is addressed by studies on polymers with symmetric and asymmetric side chains. They are used here as active materials in light-emitting diodes (LEDs) and field-effect transistors (FETs). One important parameter for the description of the performance in both types of devices is the charge carrier mobility, which is a measure of how easy the charge carriers move in the polymer film. We analyze the carrier mobility as function of temperature, electric field and charge carrier density.

In Chapter 2 the relevant charge transport models for disordered organic semiconductors are described. Using the theoretical models of hopping between sites in a Gaussian density of states for LEDs, and in an exponential density of states for FETs, the current-voltage characteristics of these devices are analyzed. The discussion is extended in Chapter 4, in which a unified picture of the hole transport in the two types of devices is presented. Apparently, the solution-processable conjugated polymers developed for LEDs and FETs have fundamentally different properties. Besides different transport models, the reported hole mobilities differ typically by more than three orders of magnitude between LEDs and FETs. In order to understand this discrepancy in the charge transport description and mobility reported for the same polymer, we determine the charge carrier density ranges in which polymer LEDs and FETs typically operate. Then we establish the dependence of the hole mobility on charge carrier density. It is demonstrated that the large differences in mobility values obtained from LEDs and FETs, based on a single semiconducting polymer, originate from the strong dependence of the mobility on the charge carrier density. The expo-

nential density of states, which consistently describes the field-effect measurements, is shown to be a good approximation of the tail states of the Gaussian in the energy range where the Fermi level is varied. This analysis is only valid for highly disordered polymers, in which the transport of charge carriers is the same in all directions.

Based on the results presented above we address the issue of the enhancement of the space-charge limited (SCL) hole current of poly(*p*-phenylene vinylene) (PPV) derivatives at high bias. In a space-charge limited device an increase of the applied bias gives rise to a simultaneous increase of the electric field and charge carrier density and their contribution to the mobility cannot be disentangled. For the understanding of the charge transport in polymer devices it is of fundamental importance to know whether the current is governed by the field- and/or the carrier density dependence of the mobility. We demonstrate that the enhancement of the current density in SCL diodes is dominated by the carrier density dependence of the hole mobility at room temperature and, contrary to numerous reports, the dependence of the mobility on the electric field is only observed at low temperatures. Via the thickness dependence the contributions from the electric field and charge carrier density to the mobility in SCL diodes can be disentangled. It is demonstrated that a field-dependent mobility weakens the thickness dependence of the SCL current, whereas a carrier density dependent mobility gives rise to an enhanced thickness dependence. The enhanced thickness dependence of the experimental SCL current in PPV is in agreement with the predictions using a density-dependent mobility only.

To relate the transport characteristics to the morphological and energetic disorder present in the polymer film, in Chapter 5 the charge transport for PPV derivatives is studied as function of the chemical modification and processing conditions. It is demonstrated that by chemical modification from asymmetrically to fully symmetrically substituted PPVs the mobility in both type of devices can be significantly improved. Furthermore, for symmetrical PPVs the mobility is strongly dependent on processing conditions as choice of solvents and annealing conditions. It was also observed that the increase in mobility is accompanied by a strong enhancement of the anisotropy in the charge transport. In the second part of Chapter 5, the electrical measurements in planar metal-polymer-metal devices are compared with those in field-effect transistors. It is demonstrated that the enhanced current measured in planar devices originates from a high surface charge carrier density at the polymer/substrate interface. The presence of such a conducting channel due to charging of the surface obscures the intrinsic in-plane conducting properties of PPV.

In Chapter 6 a new concept for an efficient dual polymer layer LED is demonstrated. This LED contains a polymer with high hole mobility that efficiently transports the holes towards a highly luminescent layer. As a result high light efficiency and low operating voltage are simultaneously achieved. Furthermore, the hole transport layer is emissive and its HOMO and LUMO levels align with the luminescent layer, so that electrons are not blocked at their interface. Consequently, a short-circuit in the luminescent layer does not lead to a catastrophic failure of the device. Instead, the emissive hole transport layer starts to work as a LED and, at the location of the short, only the efficiency of the LED drops since the transport layer is a less efficient emitter.

Since carrier mobility is the main limiting factor in the operating speed of FETs, the goal for highly competitive integrated circuits would be to use one active material with high mobility for both electrons and holes. In Chapter 7 we report ambipolar FETs based on a solution processable methanofullerene derivative. The transistors are capable of operating in both the p- and n-channel regimes depending upon the bias conditions and high carrier mobilities are determined for both electrons and holes. Furthermore, the use of this high mobility ambipolar organic semiconductor simplify the fabrication of organic-based CMOS-like voltage inverters.

Samenvatting

De ontdekking dat plastics zich als halfgeleiders kunnen gedragen heeft hun toepassingsgebied verruimd van speelgoed, tassen of meubilair naar elektronische producten zoals flexibele beeldschermen, radiofrequentie identificatie labels, fotocellen and chemische sensoren. Hoewel plastic elektronica nooit de snelheid and miniaturisatie van op silicium gebaseerde elektronica zal kunnen evenaren, kunnen ze wel gebruikt worden voor eenvoudige elektronische circuits die goedkoop, makkelijk produceerbaar en flexibele moeten zijn. Geconjugeerde polymeren vormen een speciale groep plastics, waarvan de hoofdketen uit alternerende enkele en dubbele bindingen bestaat. De enkele bindingen heten σ-bindingen en corresponderen met een sterk gelokaliseerde elektronen dichtheid in het vlak van het molecuul. De dubbele bindingen bestaan uit een σ-binding en een π-binding, een overlap tussen p_z orbitalen van naburige atomen. De elektrische lading is gedelokaliseerd langs de π-geconjugeerde segmenten van de hoofdketen van het polymeer, die een typische lengte van 5-10 eenheden hebben. Onder invloed van een aangelegd elektrisch veld springen de ladingsdragers het ene geconjugeerde element naar het andere, dit proces wordt ook wel *hoppen* genoemd. Het hoppen van ladingen hangt sterk af van de energetische en ruimtelijke wanorde in het polymeer. De invloed van beide vormen van wanorde op het ladingstransport wordt onderzocht door polymeren met symmetrische zijketens te vergelijken met polymeren met asymmetrische zijketens. In dit proefschrift worden deze materialen bestudeerd onder de omstandigheden zoals ze in licht emitterende diodes (LEDs) en veldeffect transistoren (FETs) gebruikt worden. Een belangrijke parameter voor de beschrijving van de prestatie van deze applicaties is de mobiliteit van de ladingsdragers, hetgeen een maat is voor de snelheid waarmee de ladingsdragers door de polymeerfilm bewegen. Wij analyseren de mobiliteit van ladingsdragers als functie van temperatuur, elektrisch veld en ladingsdragerdichtheid.

In hoofdstuk 2 worden de relevante modellen voor ladingstransport in wanordelijke organische halfgeleiders beschreven. Gebruik makend van de theoretische modellen voor het op hoppen gebaseerde ladingstransport in een Gaussische toestandsdichtheid voor LEDs, en in een exponentiele toestandsdichtheid voor FETs, worden de stroomspanning karakteristieken geanalyseerd. In hoofdstuk 4 wordt vervolgens het gatentransport in LEDs en FETs aan elkaar gekoppeld. Ogenschijnlijk hebben de specifieke polymeren zoals die voor LEDs en FETs ontwikkeld zijn fundamenteel andere eigenschappen. Naast het feit dat er voor beide toepassingen verschillende transportmodellen worden gebruikt, verschillen de voor LEDs en FETs gerapporteerde experimentele gatenmobiliteiten typisch meer dan drie ordes van grootte. Om deze theoretische en experimentele verschillen te begrijpen, bepalen we als eerste stap de

ladingsdragerdichtheden in LEDs en FETs onder typische gebruiksomstandigheden. Vervolgens tonen we aan dat de gatenmobiliteit sterk van de ladingsdichtheid afhangt en dat het grote verschil in mobiliteit, zoals gemeten in FETs en LEDs gebaseerd op een enkel halfgeleidend polymeer, wordt veroorzaakt door het feit dat de ladingsdragersdichtheid in beide applicaties sterk verschillen. Verder wordt aangetoond dat de exponentiele toestandsdichtheid, die de veldeffect metingen consistent beschrijft, een goede benadering is van de staart van de Gaussische toestandsdichtheid in het energie gebied waarbinnen het Fermi niveau van de FET wordt gevarieerd. Echter, deze analyse is alleen geldig voor sterk wanordelijke polymeren, waarin het transport van ladingsdragers in alle richtingen hetzelfde is.

Deze resultaten worden vervolgens gebruikt om de oorzaak van de sterke toename van de ruimteladingsbegrensde gatenstroom in poly(*p*-phenylene vinylene) (PPV)-achtige polymeren bij hoge aangelegde spanningen te onderzoeken. In een ruimteladingsbegrensde diode veroorzaakt een verhoging van de aangelegde spanning tegelijkertijd een verhoging van het elektrisch veld en een toename van de ladingsdragerdichtheid, en kan hun afzonderlijke bijdrage aan de mobiliteit niet gescheiden worden. Voor het begrip van het ladingstransport in deze polymeren is het van fundamenteel belang om te weten of de stroom bepaald wordt door de veld- en/of dichtheidsafhankelijkheid van de mobiliteit. We tonen aan dat de toename van de stroomdichtheid in ruimteladingsbegrensde diodes bij kamertemperatuur gedomineerd wordt door de dichtheidsafhankelijkheid van de gatenmobiliteit. Dit is in tegenspraak met de in de literatuur algemeen geaccepteerde aanname dat de bijdrage van het elektrische veld overheerst. Onze studie laat zien dat de afhankelijkheid van de mobiliteit van het elektrisch veld alleen bij lage temperaturen waargenomen wordt. Verder blijkt dat de afzonderlijke bijdrages van het veld en de ladingsdragersdichtheid aan de mobiliteit ook middels de stroomafhankelijkheid van de polymeerfilm dikte kunnen worden gescheiden. Een veldafhankelijke mobiliteit verzwakt de dikte afhankelijkheid van de ruimteladingsbegrensde stroom, een ladingsdragerdichtheid-afhankelijke mobiliteit daarentegen geeft aanleiding tot een sterkere dikte afhankelijkheid. De sterke dikte afhankelijkheid van de experimentele ruimteladingsbegrensde stroom zoals gemeten in PPV is consistent met een dichtheidsafhankelijke mobiliteit.

Om de transporteigenschappen te relateren aan morfologische en energetische wanorde in het polymeer, wordt in hoofdstuk 5 het ladingstransport van verschillende PPV derivaten bestudeerd als functie van de chemische structuur en proces condities. Er wordt aangetoond dat d.m.v. chemische modificatie van asymmetrische naar volledig symmetrische gesubstitueerde PPVs de mobiliteit in zowel LEDs als FETs significant verbeterd kan worden. Bovendien is de mobiliteit van symmetrische PPVs sterk afhankelijk van de proces condities zoals de gebruikte oplosmiddelen en thermische behandeling. Er wordt ook waargenomen dat de verhoging van de mobiliteit gepaard gaat met een sterke toename van de anisotropie van het ladingstransport. In het tweede deel van hoofdstuk 5 worden elektrische metingen aan metaal-polymeer-metaal diodes, waarin het transport in het vlak van de polymeerfilm plaatsvindt, vergeleken met metingen aan veldeffect transistoren. Het blijkt dat de verhoogde stroomsterkte in deze in-vlak diodes haar oorsprong vindt in een hoge oppervlakteladingsdichtheid op het polymeer/substraat grensvlak. De aanwezigheid van een

dergelijk geleidend kanaal t.g.v. het opladen van het oppervlak maskeert de intrinsieke in-vlak geleidingseigenschappen van PPV.

In hoofdstuk 6 wordt een nieuw concept voor efficiente dubbellaag polymeren LEDs gedemonstreerd. Een dergelijke LED bevat een polymeer met een hoge gatenmobiliteit, die de gaten efficient naar een sterk luminescerende laag transporteert. Dit resulteert in een hogere licht opbrengst en een lagere werkspanning. Bovendien kan de gatentransportlaag licht uitzenden en komen de HOMO en LUMO overeen met die van de luminescerende laag, zodat de ladingsdragers niet geblokkeerd worden bij de overgang tussen de twee materialen. Dientengevolge leidt een kortsluiting in de luminescerende laag niet tot een catastrofale uitval van de LED. In plaats daarvan functioneert de gatentransportlaag nu als een LED en neemt op de plek van de kortsluiting alleen de efficientie van de LED af, omdat de transportlaag minder efficient licht emitteert.

Aangezien de mobiliteit de belangrijkste limiterende factor is voor de schakelsnelheid van FETs, is het streven om voor polymeer geintegreerde circuits een actief materiaal met een hoge mobiliteit voor zowel elektronen als gaten te gebruiken. In hoofdstuk 7 rapporteren we over ambipolaire FETs gebaseerd op een vanuit oplossing verwerkbaar methanofullereen. Deze transistoren kunnen zowel in het p- als n-kanaal regime functioneren, afhankelijk van de aangelegde spanning, en een hoge mobiliteit wordt gevonden voor zowel de elektronen als de gaten. Het gebruik van deze ambipolaire organische halfgeleider met een hoge mobiliteit vereenvoudigt de fabricage van complementaire logische schakelingen.

List of Publications

1. *Switch-on voltage in disordered organic field-effect transistors*
   E. J. Meijer, C. Tanase, P. W. M. Blom, E. Van Veenendaal, B. -H. Huisman, D. M. De Leeuw, T. M. Klapwijk, Appl. Phys. Lett. **80**, 3838 (2002).

2. *Charge transport in disordered organic field-effect transistors*
   C. Tanase, P. W. M. Blom, E. J. Meijer, D. M. de Leeuw, Mat. Res. Soc. Symp. Proc. **725**, P10.9.1 (2002).

3. *Local charge carrier mobility in disordered organic field-effect transistors*
   C. Tanase, E. J. Meijer, P. W. M. Blom, D. M. de Leeuw, Org. Electronics **4**, 33 (2003).

4. *Unification of the hole transport in polymeric field-effect transistors and light-emitting diodes*
   C. Tanase, E. J. Meijer, P. W. M. Blom, D. M. de Leeuw, Phys. Rev. Lett. **91**, 216601 (2003).

5. *Charge transport in polymeric opto-electronic devices*
   P. W. M. Blom, T. van Woudenberg, C. Tanase, V. Mihailetchi, B. de Boer, Polymer Preprint **44**(2), 342 (2003).

6. *Hole transport in polymeric field-effect transistors and light-emitting diodes*
   C. Tanase, P. W. M. Blom, E. J. Meijer, D. M. de Leeuw, Proc. of SPIE **5217**, 80 (2003).

7. *Charge carrier density dependence of the hole mobility in poly(p-phenylene vinylene)*
   C. Tanase, P. W. M. Blom, D. M. de Leeuw, E. J. Meijer, Phys. Status Solidi A **201**, 1236 (2004).

8. *Origin of the enhanced space-charge-limited current in poly(p-phenylene vinylene)*
   C. Tanase, P. W. M. Blom, D. M. de Leeuw, Phys. Rev. B **70**, 193202 (2004).

9. *Ambipolar organic field-effect transistors based on a solution processed methanofullerene*
   T. D. Anthopoulos, C. Tanase, S. Setayesh, E. J. Meijer, J. C. Hummelen, P. W. M. Blom, D. M. de Leeuw, Adv. Mat. **16**, 2174 (2004).

10. *Organic complementary-like inverters employing methanofullerene based ambipolar field-effect transistors*
T. D. Anthopoulos, D. M. de Leeuw, E. Cantatore, S. Setayesh, E. J. Meijer, C. Tanase, J. C. Hummelen, P. W. M. Blom, Appl. Phys. Lett. **85**, 4205 (2004).

11. *Thickness dependence of the space-charge limited current in poly(p-phenylene vinylene)*
P. W. M. Blom, C. Tanase, D.M. de Leeuw, R. Coehoorn, Appl. Phys. Lett. **86**, 92105 (2005).

12. *High-performance solution-processed polymer ferroelectric field-effect transistors*
R. C. G. Naber, C. Tanase, P. W. M. Blom, G. H. Gelinck, A. W. Marsman, F. J. Touwslager, S. Setayesh, D. M. de Leeuw, Nature Mat. **4**, 243 (2005).

13. *Enhancement of the hole transport in poly(p-phenylene vinylene) based light-emitting diodes*
C. Tanase, J. Wildeman, P. W. M. Blom, Proc. of SPIE **5464**, 351 (2004).

14. *Hole transport in poly(p-phenylene vinylene) based light-emitting diodes revisited*
C. Tanase, P. W. M. Blom, D. M. de Leeuw, Proc. of SPIE **5519**, 120 (2004).

15. *High performance solution processable PPVs for air-stable organic field-effect transistors*
A.J.J.M. van Breemen, P.T. Herwig, C.H.T. Chlon, J. Sweelssen, H.F.M. Schoo, M.E. Mena Benito, D.M. de Leeuw, C. Tanase, J. Wildeman, P.W.M. Blom, accepted Adv. Func. Mat.

16. *Luminescent poly(p-phenylene vinylene) hole transport layers with adjustable solubility*
C. Tanase, Jurjen Wildeman, Paul W. M. Blom, submitted to Adv. Mat.

17. *Optimization of the charge transport in poly(phenylene vinylene)-derivatives by processing and chemical modification*
C. Tanase, J. Wildeman, P. W. M. Blom, M. E. Mena Benito, D. M. de Leeuw, A. J. J. M. van Breemen, P. T. Herwig, C. H. T. Chlon, J. Sweelssen, H. F. M. Schoo, submitted to J. Appl. Phys.

18. *Thin-film field-effect transistors, inverters and ring-oscillators from vitreous, solution-processed rubrene hypereutectics*
N. Stutzmann, E. Smits, H. Wondergem, C. Tanase, P. W. M. Blom, P. Smith, D. M. de Leeuw, Nature Mat. in print.

19. *Unified description of charge-carrier mobilities in disordered semiconducting polymers*
W. F. Pasveer, J. Cottaar, C. Tanase, R. Coehoorn, P. A. Bobbert, P. W. M. Blom, D. M. de Leeuw, M. A. J. Michels, Phys. Rev. Lett. in print.

20. *Simultaneous enhancement of the charge transport and exciton diffusion in poly-(p-phenylene vinylene) derivatives*
D. E. Markov, C. Tanase, P. W.M. Blom, J. Wildeman, submitted to Phys. Rev. B.

To my son *or*
In lieu of acknowledgments

My dearest Tudor,

I will tell you a story with no magic carpets, genies or talking creatures. It is a story about people you may not know but whom I value and hold dear. It is also about (re)search, knowledge and science. Nevertheless it does have magic – hidden in all little, often unmentioned things which make life so wonderful. Like all good old fairy tales, my story begins with...

Once upon a time, about seven-times-your-age ago, I came from far away to this land of windmills, cheese and tulips to get a doctor's degree.

I was lucky to be among the first members of the Physics of Organic Semiconductors group. There is something special about being in a small group in which it is easy to communicate and get to know each other. Although the group kept growing, Paul always had time to point me to the right direction in my research and lead me to the best scientific solutions; from him I have learned to work with efficiency and effectiveness, as he always has the goal in mind. I appreciate him as a scientist and as a person, he knows when you need a boss and when you need a friend.

The other 'cohesive element' in the group, our warm-hearted, nature-loving technician Minte, was always there to help. Every time I needed him he had a technical solution for my setup and a word of wisdom.

It is difficult and it would never do to try to summarize a four years' interaction with all the members of the group in just a few lines: each cup of coffee drunk together, each exchange of knowledge and opinions was unique and would be worth mentioning. Bert's and Jurjen's polymers, Teunis' useful tips, Ronald's article, Jan-Anton's help with my presentation at SPIE, Afshin's tiramisu, Vali's IT support, Magda's company or Hilke's clear explanations on photolithography are a mere fraction of what it meant to me to be their colleague for all these years. Renate and Margriet helped me disentangle the maze of bureaucracy.

All along my project, Dago had a significant influence on my development. To begin with, he provided me with samples which I could start measuring very early in my research; besides, he offered valuable guidance and support. From him I have learned that basic scientific truths are not trivial. The fruitful collaboration with his group members, Eduard, Thomas, Estrella and Natalie, resulted in a series of articles.

The regular DPI meetings were just as many opportunities for very useful discussions. I am particularly grateful to Reinder Coehoorn, Eric Meulenkamp, Herman Schoo, Peter Bobbert, Albert van Breemen, John van Haare and Thijs Michels.

My stay in Groningen did not mean only work. For my social life I am indebted to all my friends. Denis always had a fancy for a relaxing chat in the lunch break or for a drink in the weekend. I have Gerard to thank for the interactive *inburgeringscursus* and his help on various occasions. Dan and Irina's parties insured social contacts I wouldn't have had otherwise. Mirko and Nico were a comfortable and cheering presence whenever I needed it.

Living far from one's country is sometimes trying. I was blessed with the close presence of some family members. Gabi, Mihaela and Violeta encouraged and heartened me constantly. Mihaela's demanding way of being helped me to keep my standards up. My parents' unconditional credit and support have sustained me throughout my life.

My precious, the past few months I was very busy writing this book. Most of this time your daddy took care of everything in the house, including you and me. And he never ceased to understand, support and love me. The two of you made me realize how beautiful life is.

Cristina